First year report
RAL-UCL
Jan 2001
Supervisors:
Dr.Jon M. Butterworth[2]
Dr.Michael H. Seymour[1]

Multiparton interactions as part of Underlying Event in Hard Scattering Processes

Ivan Borozan

Theoretical Particle Physics
[1]*Rutherford Appleton Laboratory*
and
Department of Physics and Astronomy
[2]*University College London*

Abstract

The energy contribution due to multiparton interactions to the total jet energy was determined using HERWIG a Monte Carlo Event Generator running in conjunction with JIMMY the Monte Carlo Multiparton Event Generator. The Dijet Mass Distributions and the Inclusive Jet distribution at $\sqrt{s}$=1.8 TeV, simulated using both HERWIG + JIMMY and HERWIG + Soft Underlying Model were compared to CDF and DØ measurements. No significant deviation from the values used by the two collaborations to correct the jet energies for the underlying event activity was found. The two underlying event models running in conjunction with HERWIG were used to simulate the entire proton-antiproton event structure which growth and structure was measured and analysed by Rick Field and David Stuart at CDF. We show that for a suitably tuned set of parameters HERWIG + Multiparton model describe reasonably well the experimental data. Of course, it will be essential to test this set of chosen parameters with a different experimental data for exemple at HERA.

Contents

List of Figures

1 Introduction

In this report we will be concerned with the proton-antiproton collisions at 1.8 TeV of center of mass energy at the Tevatron Collider at Fermilab. At such high energies the proton and the antiproton may undergo an inelastic hard core collision where a "hard" and "soft" processes may occur. A "soft" inelastic collisions correspond to events in which no "hard" scattering interaction has occurred. A "hard" scattering collision is the inelastic collision between two hadrons (here proton-antiproton), where a two-to-two parton-parton subprocess has occurred. (we present in more detail the hadron-hadron collision in appendix B). As the center-of-mass energy of a proton-antiproton collisions increases the "hard" scattering becomes larger and larger fraction of the total inelastic cross section. In such a "hard scattering" jets of hadrons with large transverse momentum P_T are produced from large transverse momentum outgoing partons coming from the hard subprocess (see Fig.1). In addition to hadrons coming from the hard two-to-two parton-parton subprocess hadrons may also originate from the break-up of the proton and antiproton called **beam-beam remnants** (see Fig.1). We will define as "Underlying Event" processes, all the ambient processes which surround the "hard" two-to-two parton-parton subprocess. We will also consider multiparton interactions in beam-beam remnants as part of the "Underlying Event"(see Fig.1). Because of it's complex nature the Underlying Event is an interesting object that is not very well understood. To be able to compare effectively the experimental distributions with the QCD NLO calculated ones, the contribution from the underlying event need to be determined and then subtracted from the measured jet energy. Since this value is not well known it is the largest source of systematic error for the inclusive cross section at low E_T (for the CDF collaboration this uncertainty is of 30%). In Sec.4 we investigate the values of the underlying event determined and used by DØ and CDF collaborations. We found that in both collaborations the underlying event is considered **as the average energy level found in "active" minimum bias inelastic proton-antiproton collisions** and that it's value is considered as constant over the whole range of jet energies. To test their assumptions we produce Monte-Carlo simulations for the inclusive and dijet distributions measured at DØ and CDF. In Sec.5.1 we simulate the same distributions with HERWIG running in conjunction with either the Soft model or the Multiparton Interaction model. We show that the simulated distributions reproduce well the experimental distributions (within a given scaling factor). In Sec.5.2 we determine the average transverse energy generated by multiparton interaction model in jets and we show that up to 70 GeV of jet transverse energy this contribution might not be constant. Finally we show that the simulated contribution from the two models to the simulated distributions (for the cuts applied) is well within the correction range used by both collaborations. In the " Run 2 Workshop on QCD and Weak Boson Physics" Ref.[14](by Rick Field and David Stuart February 01/2000) it was observed that "none of the QCD Monte-Carlo models (with their default parameters) describe correctly all the properties of the Underlying Event". It was also shown, in the same paper Ref.[14] that the Underlying Event in "hard" scattering is not the same as a "soft" hard-core proton-antiproton interaction. The underlying event in "hard" scattering shows more "activity", (in the sense that it produces higher charged particle multiplicity and higher average scalar P_{Tsum} of charged particles) than the "soft" scattering. In Sec.5.3, using the same definition of the jet algorithm, we reproduce Field and Stuart simulated data from their study of the growth and structure of the underlying event in hard scattering. Using HERWIG + Multiparton Model (see Ref.[1]) we show that the underlying event "activity" might be enhanced by including multiparton interactions as part of the beam-beam remnant collisions. We determine the optimum values for the parameters used in this model which produce the best agreement between simulated and experimental data. We finally show (see Sec.5.5) that with a suitably tuned set of parameters, using HERWIG + Multiparton Model, it is possible to simulate the entire proton-antiproton event structure in agreement with the experimental data presented in Ref.[14].

1.1 Kinematics and jet definition.

When the energy (see Ref.[7]) of scattering of two incoming partons (see appendix B and C for more details) is high enough to produce two outgoing partons with high enough p_T then this outgoing partons will be observed as jets of particles. The center of mass of the parton-parton scattering is usually boosted with respect to that of the two incoming hadrons. Thus we need to express final state in terms of variables such as the rapidity y, the transverse momentum p_T and the azimuthal angle ϕ (see Fig.2) which transform simply under longitudinal boosts. The four-momenta of a particle of mass m is given in eq.1.

$$P^{\mu} = (E, p_x, p_y, p_Z) = (m_T coshy, p_T sin(\phi), p_T cos(\phi), m_T sinhy) \quad (1)$$

where the transverse mass is defined as $m_T = \sqrt{p_T^2 + m^2}$. The rapidity of the particle is defined in eq.2 and is additive under the restricted class of Lorentz transformation corresponding to a boost along the z direction. Rapidity differences are boost invariant.

$$y = \frac{1}{2} ln(\frac{E + p_z}{E - p_z}) \quad (2)$$

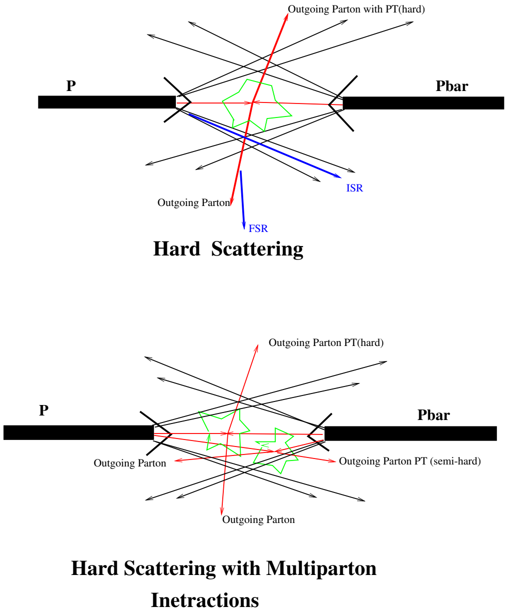

Figure 1: In "Hard Scattering" we illustrate a proton-antiproton collision in which a "hard" 2-to-2 parton scattering with transverse momentum, P_T(hard), has occurred. The event contains particles that originate from the two outgoing partons (plus initial and final state radiation) and particles that comes from the breakup of proton and antiproton. The "underlying event" consists of the beam-beam remnants interaction. In "Multiple Parton Interactions" we illustrate a proton-antiproton collision in which a multiple parton interaction has occurred. In addition to the "hard" 2-to-2 parton scattering with transverse momentum, P_T(hard), there is an additional "semi-hard" parton-parton scattering that contribute particles to the "underlying event".

The pseudorapidity of the particle is defined in eq.3.

$$\eta = -ln tan(\theta/2) \tag{3}$$

The pseudorapidity is equal to rapidity in the limit where m $\rightarrow$0. This is a more convenient variable experimentally, since the angle θ from the beam direction is measured directly in the detector. Also transverse energy E_T (see eq.4) of a particle is used rather then the transverse momentum ($p_T = \sqrt{p_x^2 + p_y^2}$) because it is E_T which is measured directly in the detector. The transverse energy is defined in eq.4.

$$E_T = E sin\theta \tag{4}$$

To define the jet of hadrons we use the **cone algorithm** which is based on energy deposited inside the angular region or "cone" of radius R (in η, ϕ

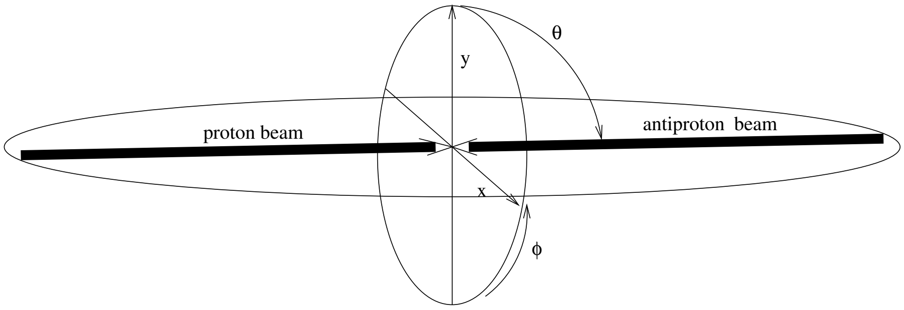

Figure 2: Set of coordinate system used in the measurement.

space) (see eq.5).

$$R = \sqrt{(\Delta\eta)^2 + (\Delta\phi)^2)} \tag{5}$$

In two dimensional η, ϕ plane, curves of constant R are circles around the axis of the jet. The cone jet algorithm build a jet from it's constituent particles according to the Snowmass accord (see Ref.[9]). The transverse energy, E_T, pseudorapidity, η, and azimuth, ϕ of the jet are defined respectevely in eq.6, eq.7 and eq.8 :

$$E_{Tjet} = \sum_i E_{Ti} \tag{6}$$

$$\eta_{jet} = \sum_i \frac{E_{Ti}\eta_i}{E_{Tjet}} \tag{7}$$

$$\phi_{jet} = \sum_i \frac{E_{Ti}\phi_i}{E_{Tjet}} \tag{8}$$

where i runs over all the particles in the jet. We define then as "angle" the Lorentz-invariant opening angle $R_{ij} = \sqrt{(\eta_i - \eta_j)^2 + (\phi_i - \phi_j)^2}$.

1.2 The DØ algorithm.

The particles are clustered into jets according to the following steps (see Ref.[6]):

1. The particles are passed trough a calorimeter with cell size $d_0 \times d_0$ in $\eta \times \phi$ (in DØ, $d_0 = 0.1$).

2. Every calorimeter cell (cluster) with energy above E_0, is considered as a 'seed cell' for the following step (in DØ, E_0 = 1GeV).

3. A jet is defined by summing all cells within an angle R of the seed cell according to eq.6, eq.7 and eq.8.

4. If the jet direction does not coincide with the seed cell, step 3 is reiterated, replacing the seed cell by the current jet direction, until a stable jet direction is achieved.

5. We now have a long list of jets, one for each seed cell. Many are duplicates: these are thrown away.

6. Some jets may be overlapping. Any jet that has more than 50% of it's energy in common with the higher-energy jet is merged with that jet: all the cells in the lower-energy jet are considered part of the higher energy jet, whose direction is again recalculated according to eq.6, eq.7 and eq.8.

7. Any jet that has less than 50% of its energy in common with a higher-energy jet is split from that jet: each cell is considered part only of the jet to which it is nearest.

This is essentially the algorithm used by ZEUS(PUCELL), except that their merging/splitting threshold is 75% instead of 50%.

1.3 The CDF algorithm

Same as DØ except for

6. Any jet that has more than 75% of it's energy in common with the higher-energy jet is merged with that jet: all the cells in the lower-energy jet are considered part of the higher energy jet, whose direction is again recalculated according to the eq.6, eq.7 and eq.8.

7. Any jet that has less than 50% of its energy in common with a higher-energy jet is split from that jet: each cell is considered part only of the jet to which it is nearest.The directions of the two jets are then recalculated by iterating step 3.

2 HERWIG

HERWIG Ref.[16] which stand for Hardon Emission Reactions With Interfering Gluons is a Monte Carlo event generator. The Monte Carlo methods Ref.[8] are used for integration of the total cross section and the full QCD event generation. The core of the Monte Carlo methods is the random number generator and the possibility to produce random numbers distributed according to any probability distribution function using appropriate techniques.[1] To calculate an integral we first observe that the integral can be seen as the average of the integrand,

$$I = \int_{x_1}^{x_2} f(x)dx = (x_2 - x_1)\langle f(x)\rangle. \tag{9}$$

[1] The one used in the event generator is the Rejection method.

Taking a value of x distributed uniformly on (x_1,x_2), then the average value of $f(x)$ will be a reasonable estimator of I.

$$I = (x_1 - x_2)\frac{1}{N}\sum_{i=1}^{N} f(x_i) \tag{10}$$

If N is sufficiently large using the Central Limit Theorem the distribution of $f(x_i)$ will tend to a Gaussian with standard deviation $\sigma_{MC} = \sigma/\sqrt{N}$ where σ is the standard deviation of $f(x_i)$. Thus the inaccuracy on the value of the integral decreases as $1/\sqrt{N}$.

2.1 Rejection method

The distribution $f(x)$ can be obtained Ref.[8] by choosing x which is uniformly distributed on the range (0,1), and rejecting it's choice if

$$p > \frac{f(x)}{f_{max}} \tag{11}$$

where p is another uniformly distributed number on the range (0,1) and f_{max} is the largest value of $f(x)$ within the integration region. If the choice is rejected the new ones are made until one is found which does satisfy eq.11. x will then be distributed according to $f(x)$.

2.2 The Unweighted Events and the Event Generator.

The event generaton (see Ref.[8]) is a program which simulate an event of a given physical process (in our case two-to-two parton parton scattering) which is of random or stochastic nature. A set of phase space point (events) is generated using Monte Carlo methods at random with their weights. The weights of each event in the integral correspond to the probability of each event occurring. To obtain a maximum efficiency in the event generation and not waist time on the events with the low weight in the integral the unweighted events are being produced with the exactly the same weight by the rejection method. The unweighting of events is done by keeping only a fraction of events according to their weights. This is done by finding the maximum weight which occurs anywhere in the integration region by Monte Carlo search of the phase-space. Then we choose whether to keep or reject each event with probability $f(x)/f_{max}$. The event generation may be divided in following steps (see Ref.[8]),

1. **Initialization**. Initialization parameters are checked and parameter-dependent values are calculated. Number of phase points are generated, to search for maximum weight. Initial estimate of the cross section is performed.

2. **Hard process generation**. For each hard process and in this report particularly for two-to-two parton parton scattering **LO QCD** matrix element are used, there is two calls to the same subroutine. In the first call a phase-space point is generated and the corresponding weight in the integral calculated. Then if the event was accepted a second call sets the particle momenta corresponding to the phase space point, together with the various pointers, spin vectors and other variables needed by later stages of processing. A cut on the hard scale Q ($\sim E_T^{jet}$), p_T^{min} is the lowest transverse momentum for outgoing partons coming from the perturbative "hard" scattering. Also Q_0 (infrared cutoff defining the resolvability of the partons) is introduced as to prevent the cross section becoming divergent in the limit $Q_0 \Rightarrow 0$. In order to fully describe the final state, Q_0 is required to be around the typical hadronic scale, $Q_0 \sim$ 1GeV. The scale Q of interaction calculated by HERWIG in two-to-two paron parton scattering is given bellow in eq.12, we can require that μ^2 the factorization scale be equal to Q^2. Thus μ^2 in the limit of massless partons and scattering perpendicular to the beam axis is the same as $\frac{4}{3}P_T^2$ where P_T is the transverse momentum of the outgoing partons.

$$Q^2 = EMACST^2 = \frac{2\hat{s}\hat{t}\hat{u}}{\hat{s}^2 + \hat{t}^2 + \hat{u}^2} \tag{12}$$

3. **Parton Evolution**. The final state partons are evolved iteratively trough the perturbative branchings q$\rightarrow$qg, g$\rightarrow$gg, g$\rightarrow$q$\overline{q}$. Initial state partons are evolved "backwards" away from the hard process into the incoming hadrons. This gives more incoming hadrons which are in turn evolved. The cross section for additional partons to be radiated is enhanced by powers of log(Q/Q_0) since these terms are large they need to be summed to all orders in α_s. This summation can be implemented as a probabilistic evolution of the external (both incoming and outgoing) partons. For collinear emissions the summation is done over single logarithmic terms but to fully model the final state single and double logarithmic terms associated with soft emission must be summed to all orders. This is done by *coherent parton shower algorithms* Ref.[5].

4. **Hadronisation**. The least understood physically due to the softness of the scale it is essentially the conversion of the emitted partons into outgoing hadrons.

5. **Particle decays**. The hadrons which are instable undergo secondary decays.

6. **Underlying Event**. The model used for the underlying event is based on the minimum-bias $p\overline{p}$ event generator of the UA5 Collaboration, modified to make use of the cluster fragmantetion algorithm. The model starts from

a parametrisation of the $p\overline{p}$ inelastic charged multiplicity distribuiton.

3 Multiparton Interactions in the $p\overline{p}$ environment.

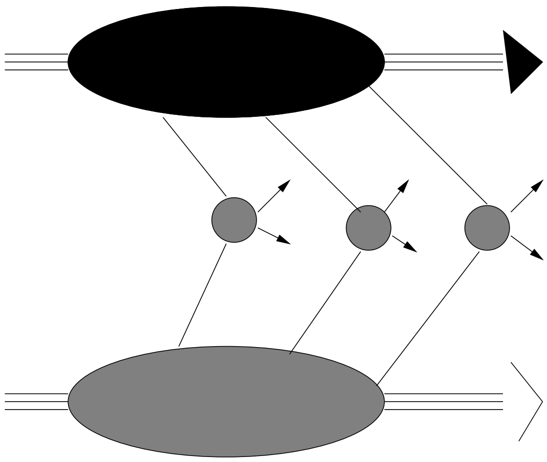

Figure 3: Example of a multiparton scattering in $p\overline{p}$ collision

The model developed for multiple parton interactions in Photo-production (see Ref.[1]) can be applied to $p\overline{p}$ collisions with some minor change to the whole. First the P_{res} which is the probability that a photon is resolved will be set to one since both of the particles are hadrons. The form factor G_γ for the photon will be replaced by the form factor of the antiproton $G_{\overline{p}}$. As it was mentioned in the introduction the multiparton interactions are additional 2-to-2 parton parton hard scattering (the main one being the one involving the largest transverse momentum exchange Q) of partons contained in the two proton antiproton remnants. In the CM frame partons can be pictured as Lorentz contracted 'parton pancakes' colliding at some impact parameter, b. The mean number of jets pairs produced in this interaction is then :

$$\langle n(b,s)\rangle = \mathcal{L}_{partons} \otimes \hat{\sigma}_H \tag{13}$$

where $\mathcal{L}_{partons}$ is the parton luminosity and $\hat{\sigma}_H$ is the cross section for a pair of partons to produce a pair of jets (i.e. partons with $p_T > p_T^{min}$). The convolution is because the parton cross section depends upon the parton energies. More specifically,

$$d\mathcal{L}_{partons} = A(b) n_p(x_p) n_{\overline{p}}(x_{\overline{p}})\, dx_p\, dx_{\overline{p}} \tag{14}$$

where $n_i(x_i)$ is the number density of partons in hadron i which carry a fraction x_i of the hadron energy. There is no distinction between parton types and the scale dependence of the number densities is being ignored. $A(b)$ is a function which specifies the distribution of partons in impact parameter.It must satisfy

$$\int \pi \, db^2 A(b) = 1 \tag{15}$$

in order that the parton luminosity integrated over all space is simply the product of the parton number densities. Factorizing the b dependence like this is an assumption. In particular we do not contemplate QCD effects which would spoils this, e.g. perhaps leading to 'hot spots' of partons. The number density for proton and antiparton are $n_p(x_p) \equiv f_p(x_p)$ and $n_{\overline{p}}(x_{\overline{p}}) \equiv f_{\overline{p}}(x_{\overline{p}})$. Thus, after performing the convolution we can write:

$$\langle n(b, s_{p\overline{p}}) \rangle = A(b) \sigma_H^{inc}(s_{p\overline{p}}) \tag{16}$$

where $\sigma_H^{inc}(s_{p\overline{p}})$ is the inclusive cross section for $p\overline{p} \rightarrow$ jets. Restoring the parton indices, it is given by

$$\begin{aligned} \sigma_H^{inc}(s_{p\overline{p}}) &= \int_{p_T^{min\,2}}^{s_{p\overline{p}}/4} dp_T^2 \int_{4p_T^2/s_{p\overline{p}}}^{1} dx_p \int_{4p_T^2/x_p s_{p\overline{p}}}^{1} dx_{\overline{p}} \sum_{i,j} f_i(x_p,\ p_T^2) f_j(x_{\overline{p}},\ p_T^2) \\ &\quad \times \frac{\hat{\sigma_{ij}}(x_p x_{\overline{p}} s_{p\overline{p}}, p_T)}{dp_T^2} \end{aligned} \tag{17}$$

The probability distribution for having m and only m scatters in a given p-$\overline{p}$ is P_m. In order to determine this value it is assumed that the separate scatters are uncorrelated, i.e. they obey Poissonian statistics.

$$P_m = \frac{(\langle n(b, s_{p\overline{p}}) \rangle)^m}{m!} \exp\left(-\langle n(b, s_{p\overline{p}}) \rangle\right) \tag{18}$$

This formula is central to the Monte Carlo implementation in HERWIG. We can now ask for the total cross section for $p\overline{p} \rightarrow$partons with $p_T > p_T^{min}$.

$$\begin{aligned} \sigma_H(s_{p\overline{p}}) &= \pi \int db^2 \sum_{m=1}^{\infty} P_m \\ &= \pi \int db^2 [1 - \exp(-\langle n(b, s_{p\overline{p}}) \rangle)] \end{aligned} \tag{19}$$

Since the total inclusive cross section (σ_H^{inc}) counts all jet pairs (even ones which occur in the same event) it is expect it to be larger than σ_H by a factor equal to the mean number of multiple interactions per event (i.e. averaged over impact parameter). Let $\langle n(s_{p\overline{p}})\rangle$ be the average number of jet pairs produced in $p\overline{p}$ events which contain at least one pair of jets, then

$$\begin{aligned}\langle n(s_{p\overline{p}})\rangle &= \frac{\int db^2 \sum_{m=1}^{\infty} mP_m}{\int db^2 \sum_{m=1}^{\infty} P_m} \\ &= \frac{\int db^2 \langle n(b, s_{p\overline{p}})\rangle}{\int db^2 [1 - exp(-\langle n(b, sp\overline{p})\rangle)]} \\ &= \frac{\sigma_H^{inc}(s_{p\overline{p}})}{\sigma_H(s_{p\overline{p}})} \end{aligned} \tag{20}$$

Note that σ_H must always be less than the total $p\overline{p}$ cross section, whereas σ_H^{inc} need not be. Now we must specify how the partons are distributed in impact parameter space. In first approximation pQCD effects are ignored and it is assumed that $A(b)$ can be written as a convolution of proton and antiproton form factors.

$$G_p(\mathbf{b}) = G_{\overline{p}}(\mathbf{b}) = \int \frac{d^2\mathbf{k}}{(2\pi)} \frac{exp(\mathbf{k} \cdot \mathbf{b})}{(1 + \mathbf{k}^2/\mu^2)^2} \tag{21}$$

then

$$A(b) = \int d^2\mathbf{b'} G_p(\mathbf{b'}) G_{\overline{p}}(\mathbf{b} - \mathbf{b'}) \tag{22}$$

The integral then yields:

$$A(b) = \frac{\mu^2}{96\pi} (\mu b)^3 K_3(\mu b) \tag{23}$$

To have a more detailed properties of the final state this eikonal model should be implemented as part of a HARWIG Monte Carlo package.

3.1 Implementing MI in HERWIG

In incorporating (see Ref.[1]) the multiple interactions model into the Monte Carlo event generator several additional problems arise from the fact that the model assumes that different scattering are uncorrelated, while in the event generator this is not possible. The first is that of energy conservation. In the analytical model, there is a non-zero (though small) cross section for events in which the total energy participating in hard scatters is greater than the energy of the incoming particles. This is exacerbated by the backward evolution, since additional energy is radiated away in the additional partons. A global energy-momentum conservation is imposed by adding the simplest possible correlation between scatters: a Θ-function in the cross section to produce m and only m scatters requiring their total energy to be less than the available energy. This will reduce the amount of eikonalisation of the cross section relative to the analytical model. When generating events, this is implemented by calculating the total cross section and probabilities for exactly m scatters using the analytical model, and generating hard scatters according to this probabilities. Scatters in which energy-momentum cannot be conserved are then vetoed (although the event itself is kept, with all the other scatters). At the end of the event generation, the number of vetoed scatters is used to make a revised estimate of the total cross section.

The simple model used in HERWIG for hadrons remnants is no longer appropriate when there is more than one scatter. This is because once the incoming colorless hadron has been replaced by an outgoing colored remnant by the first interaction, the same procedure cannot be iterated for subsequent interactions. Instead, the remnant is labeled as a new kind of the incoming hadron for the other interactions, which has identical properties to the original hadron, except that gluons are labelled as its valence partons. Thus, if the backward evolution does not result in a gluon, an additional emission is forced to produce one. The outgoing colored remnant from this interaction is the same as that from the first,but with reduced momentum. This procedure can then be iterated as many times as required for all subsequent interactions. By modifying only the part of the model that connects the hard processes to the incoming hadron, and not the backward evolution itself, we ensure the predictivity of the model, using the parameters fixed to other reactions.

3.2 The effect of MI on the Hadronic Final State

The multiple parton scattering is expected to affect jet rates in two ways (see Ref.[1]). First the average number of jets per event should be increased when partons from secondary hard scatters are of sufficient high p_T to give jets in their own right. The second effect where lower p_T secondary scatters produce extra transverse energy in the event which can contribute to the pedestal energy underneath other jets in the event. In this way, the inclusion of multiple scattering can be thought of as an attempt to extend perturbative QCD in order to calculate some part of the "soft underlying event", which is included in many simulations as a parameterized extrapolation of existing data. The first effect will increase multi-jet cross sections and leave the inclusive jet cross section unchanged. The second effect will increase both inclusive and multi-jet cross section. It was also determined that the effect of multiple interactions is more significant for the dijet cross section than the inclusive jet cross section. In all cases the effect is more significant at lower

E_T^{jet}. For multiple jet events the cross section for m jets is defined as the production cross section of events containing m and only m jets and there is an enhancement in all jet rates above the single jet rate and the significance rises with increasing jet multiplicity.Without considering the extra transverse energy generated by multiple scattering, it is expected that the sum of the jet cross sections obtained including multiple scattering to be lower than the corresponding sum obtained without multiple scattering (and the latter should be concentrated more at lower jet rates), by a factor equal to the mean multiplicity of jet pairs. The parameter in the model which has the strongest effect on the cross section is the value of the p_T^{min} (i.e. the value of the lowest possible transverse momentum for an outgoing parton). Lowering the value of p_T^{min} increases the effect of multiple interactions.

4 DØ and CDF data

4.1 DØ inclusive jet cross section.

A precise measurement (see Ref.[2]) of the central inclusive jet cross section at $\sqrt{s} = 1.8$ TeV was completed by the DØ collaboration. The measurement is based on an integrated luminosity of 92 pb^{-1} collected at the Fermilab Tevatron $p\overline{p}$ Collider with the DØ detector. The cross section reported as a function of jet transverse energy ($E_T \geq 60$ GeV) in the pseudorapidity interval $\mid \eta \mid \leq 0.5$. The corrected inclusive jet cross section has been averaged over each E_T bin (ΔE_T) and over the central unit of rapidity ($\Delta\eta$=1). This bin-averaged double differential cross section,$\langle d^2\sigma/(dE_T d\eta)\rangle$, was calculated as N$/(\Delta E_T \Delta\eta\, \epsilon \mathcal{L})$ where N is the total number of jets observed in the bin, ϵ is the selection efficiency as a function of E_T, and $\mathcal{L}$ the integrated luminosity associated with the trigger set. Jet candidates were reconstructed online with a cone algorithm of opening angle R=0.7 in the $\eta - \varphi$ space (see Ref.[13]), and the event was recorded if any jet E_T exceeded a specified threshold. The transverse energy of each jet was corrected for the underlying event, additional interactions, calorimeter noise, the fraction of particle energy that showered hadronically outside of the cone, and for the hadronic response.

4.2 DØ dijet mass spectrum.

The inclusive dijet mass (see Ref.[3]) spectrum was measured in the central pseudorapidity region $\mid \eta_{jet} \mid < 1$ for dijet masses greater than 200 GeV/c^2. The dijet mass spectrum was calculated using

$$d^3\sigma/dMd\eta_1 d\eta_2 = (N_i C_i)/(\mathcal{L}_i \epsilon \Delta M \Delta\eta_1 \Delta\eta_2)$$

where N_i is the number of events in the mass bin i, $\mathcal{L}_i$ is the integrated luminosity for that bin, ϵ is the efficiency of the vertex selection and jet quality cuts, ΔM is the width of the mass bin, and $\Delta\eta_{1,2}$ is the width of the η bin for jets 1 and 2 (both jets are required to satisfy the η requirement).

4.3 DØ correction to data.

The *particle* level jet energy is defined as the energy of a jet found from final state particles using a similar cone algorithm to that used at the calorimeter level. The particle jet is never observed in data because it gets distorted when it interacts with the calorimeter material. But it can be clearly defined in a Monte Carlo sample by clustering together the final state particles, instead of calorimeter cells, into a fixed cone size. The particle jet includes only particles arising from partons participating in the hard scatter. **The purpose of the jet energy scale calibration is to correct observed jets to the particle level**(see Ref.[12]).

4.4 Physics of the Underlying Event in DØ measurement.

The $p\overline{p}$ inelastic collisions (see Ref.[12]) are classified as non-diffractive, single diffractive and double diffractive. An inelastic non-diffractive collisions, also sometimes called hard core interactions, is an event in which both the proton and the anti-proton break up. **A particular case of a hard core interaction is high-p_T or hard parton scattering.** The offset correction is determined for non-diffractive events. It subtract energy which is not associated with the high-p_T interaction. This excess energy includes the contributions of uranium noise, pile-up, and additional $p\overline{p}$ interactions. Pile-up is the residual energy from previous $p\overline{p}$ crossings, which results from the long shaping times of the electronic signals in the calorimeter readout cells. Pile-up depends on the number of interactions in the previous beam crossings, and is therefore luminosity dependent. The underlying event includes soft interactions between spectator partons that constituted the colliding proton and anti-proton. This energy can be subtracted or not, depending on the characteristics of each particular physics measurement. A crossing selected by a high-p_T trigger can be modeled as the sum of a hard parton scattering overlaid with a zero bias (ZB) event at the same luminosity. The ZB trigger accepts every $p\overline{p}$ crossing, regardless of whether or not it contains an actual collision. The average number of hard interactions in a high-p_T event $\langle N\rangle$, may be written as :

$$\langle N\rangle = 1 + \langle N_{ZB}\rangle \tag{24}$$

Here, $\langle N_{ZB}\rangle$ is the average number of hard interactions in a ZB event can be expressed as :

$$\langle N_{ZB}\rangle = \sum_{n=0}^{\infty} nP(n) \tag{25}$$

where the probability of having n hard core collisions at a given luminosity, $P(n)$, follows a Poisson distribution. The total offset correction, E_0, can be presented as the sum:

$$E_0 = (1 + \langle N_{ZB}\rangle)E_{ue} + E_{noise} + Epile \tag{26}$$

where E_{ue} is the energy associated with the physics underlying event, $\langle N_{ZB}\rangle Eue$ is the contribution to the underlying event from additional $p\overline{p}$ interactions, $Enoise$ is the energy from uranium decay, and E_{pile} is the pile-up energy. For the actual correction, the last three terms may be combined, yielding :

$$E_0 = E_{ue} + E_{\Theta} \tag{27}$$

The energy from spectator partons is measured using low luminosity minimum bias (MB) data ($\mathcal{L} = 0.1 \times 10^{30} cm^{-2} sec^{-1}$). The MB trigger requires an inelastic collision in which both the proton and anti-proton break up. MB events are, therefore dominated by hard core interactions. The E_T density per increment $\Delta\eta \times \Delta\varphi$ in MB events, D_{MB}, is a measure of the transverse $E_{ue} + Enoise + Epile$ density. The contribution of uranium noise and pile-up, D_{ZB}^{noHC}, is measured in a low luminosity ZB sample with the requirement that there is no hard interaction. D_{ue} is then :

$$D_{ue} = D_{MB} - D_{ZB}^{noHC} \tag{28}$$

It depends both on the center-of-mass energy and pseudorapidity. The energy to be subtracted from the jet, E_{ue} is $D_{ue} \times A_{\eta,\varphi}$ where $A_{\eta,\varphi}$ is the area of the jet in $\eta - \varphi$ space. Fig.4 shows the dependence of D_{ue} on physics η for both $\sqrt{s} = 1800$ GeV and $\sqrt{s} = 630$ GeV collisions. The uneven shape results from imperfect calibration of the intercryostat detector and loss of EM coverage in the intercryostat region. Because the physics underlying event is associated with the soft interactions in a single $p\overline{p}$ collision, it is independent of luminosity and of the number of $p\overline{p}$ interactions in the event.

4.5 CDF Measurement of the Differential Dijet Mass Cross Section in $p\overline{p}$ Collisions at $\sqrt{s}$=1.8 TeV

A measurement of the cross section (see Ref.[4]) for production of two or more jets as function of dijet mass, based on an integrated luminosity of 86 pb^{-1} was completed by the CDF collaboration. The dijet system is defined as the two jets with the highest transverse momentum in an event (leading jets) with the dijet mass defined as :

$$M = \sqrt{(E_1 + E_2)^2 - (\mathbf{P_1} + \mathbf{P_2})^2}$$

The events selected was required to have two or more jets with two leading jets having pseudorapidities of $\mid \eta_1 \mid < 2$ and $\mid \eta_2 \mid < 2$ and satisfying

$$\mid cos\theta^* \mid = \mid tanh[(\eta_1 - \eta_2)/2] \mid < 2/3$$

where θ^* is the scattering angle in the dijet center-of-mass frame. The corrected cross section as a function of dijet mass is given by :

$$d\sigma/dM = N_i/(K_i \mathcal{L} \epsilon_i \Delta M)$$

where from each mass bin i, N_i is the number of events, $\mathcal{L}$ is the integrated luminosity, ϵ_i is the efficiency of the trigger and z-vertex selections, and ΔM is the width of the mass bin.

4.5.1 Correction to CDF data

The energy due to the underlying event is the ambient energy produced in hadrons collisions associated with the soft interactions of spectator partons. The energy from the underlying event will increase the effective energy found in the jet cone but is not associated with the hard scattering process. Thus when comparing the experimental data with the simulated data at the particle level this energy need to be subtracted from the jet energy. The energy that falls outside the clustering cone is associated with fragmantetion effects and gluon radiation. This energy normaly needs to be added to the jet energy. For this set of data no correction was applyed for the energy lost outside the clustering cone since a similar loss is present in NLO calculation in which an extra gluon can be radiated outside the jet clustering cone. Full details of jet reconstruction and jet energy corrections at CDF can be found elsewhere Ref.[11].

5 Results

5.1 Simulations of DØ and CDF distributions using HERWIG + Multiparton model (JIMMY).

Our first goal in this work was to simulate the experimental distributions measured at CDF (the dijet mass distribution) and DØ (the dijet mass distribution and the inclusive jet distribution) using HERWIG. Our next step was to look whether the inclusion of the multiparton interaction model (JIMMY) was going to alter in a significant way the overall shape and normalization of the simulated distributions. The cuts on the simulated events obey the same constraint as the one, set in the measurements (see Sec.4). The correction applied by CDF and DØ were done in such way as to permit a direct comparison between the corrected experimental data and the simulated distributions at the particle level. In the case where simulations included either the Underlying Soft event model or the Multiparton Interactions model we have corrected , for the underlying energy activity our simulated data by the same amount as in the experiments. For DØ the energy subtracted from each jet is calculated as $D_{ue} \times A_{\eta,\varphi}$, A being the area of the jet, $A = \pi R^2$ and the values of D_{ue} were taken from Fig.4 for $\mid \eta \mid< 1$ and $\mid \eta \mid< 0.5$ (see Sec.4.4). These values were 1.39 GeV for the dijet distribution and 0.90 GeV for the inclusive jet distribution. For the CDF dijet distribution we subtracted 0.5 GeV. For all distributions simulated with the multiparton model a minimum P_{Tmin} (see Sec2.2) for the outgoing partons was set to 2.0 GeV. The choice of the value for the P_{Tmin} is constrained by two conditions first condition is to have a sufficiently low value for this parameter so to have a high sensitivity to partons and ultimately particles with low P_T produced in multiparton interactions, the second condition is to have it sufficiently high enough as to stay within the perturbative QCD calculable region. The jet algorithm used in all our simulations was PUCELL (see Sec.1) cone algorithm with it's merging/splitting jets threshold set accordingly to the values used by $D\emptyset$ and CDF algorithms. This kind of algorithm is generally used in $p\overline{p}$ experiments such as (UA1/CDF) and the version used corresponds to the "Snowmass convention"(see Sec.1.2). The GRV set was used as the structure function of the proton Ref.[15] and antiproton.

5.1.1 The effect of multiple interactions on hadronic distributions.

Two sets of distributions was simulated for each experimental distribution with two different underlying event models. One set was simulated with the Multiple Interaction model (IPROC=11500) turned on and the second with the Soft Underlying model (IPROC=1500) turned on (see Sec.2.2). Each simulated distribution was corrected for the underlying event activity by subtracting the same amount of energy from jets as in the experiments (described in the Sec.4). In Fig.5 and Fig.10 for DØ and Fig.13 for CDF we show that the shapes between the corrected simulated and experimental distributions are very similar. However to have an accurate match between the two, HERWIG distributions need to be scaled up by factors given in table.1. The overall match then, between the scaled up HERWIG corrected distributions and the experimental ones are given in table.2 and shown in Fig.8, Fig.9, Fig.11, Fig.12 for DØ and Fig.14 and Fig.15 for CDF. In table.3 we show how the average number of multiple interactions per event increases as the value of P_{Tmin} is lowered to 2 GeV where the model produces the highest number of secondary scatters and consequently the highest activity. The difference in normalization values between the experimental data and HERWIG, observed in both dijet and inclusive distributions occurs because HERWIG uses only LO calculations for the hard scattering processes. It is expected that the inclusion of NLO corrections to the LO processes could increase the overall distributions by a factor up to 2 thus compensating for the difference in scale observed here. In the next section we will see whether it is possible to determine one of the important effects of the multiple scattering on the overall distribution, namely the value of the pedestal energy (see Sec.3.1).

5.1.2 Determining the pedestal energy using the $D\emptyset$ inclusive distribution.

As discussed in Sec.3.2 we expect that the effect of multiparton interactions on the inclusive distribution would increase the inclusive jet cross section by adding extra energy to jets in an event. This increase in jets energy should shift the overall distribution by some constant value. To determine whether we observe such a shift at this energies, we have simulated three distributions. One with Multiparton interactions model switched on (IPROC=11500 + JIMMY , P_{Tmin}=2.0 GeV) one with Multiparton interactions model switched off (IPROC=11500) and Underlying Soft model switched on and one with both Soft and Multiparton Interactions switched off (IPROC=11500) (see Fig.6 and Fig.7). We fitted all the distributions using PAW (in the E_T range 110 - 350 GeV) with parametrized exponential functions of the form

$$y = exp(par(1) + par(2)E_T)$$

or formulated differently as

$$\sigma_{MI-offandUE-off} = C_1 e^{\lambda_1 E_t}$$

simulation	*MI-off IPROC(11500) scaling factors*	*MI-on (IPROC11500) scaling factors*	*SOFT (IPROC=1500) scaling factors*
DØ dijet mass Xsec	1.80±0.044	2.01±0.04	1.85± 0.04
non corrected	1.80±0.044	1.91±0.04	1.72± 0.03
DØ inclusive jet Xsec	1.89±0.026	2.12±0.03	1.94± 0.02
non corrected	1.89±0.026	2.01±0.03	1.84± 0.02
CDF dijet mass Xsec	1.95±0.048	2.15±0.06	1.97± 0.04
non corrected	1.95±0.048	2.03±0.05	1.89± 0.04

Table 1: Scaling factors.

simulation	*(Data-Theory)/Theory MIon*	*(Data-Theory)/Theory SOFT*
DØ dijet mass Xsec	0.042± 0.022	0.033 ± 0.022
DØ inclusive jet Xsec	0.0089± 0.013	0.0025 ± 0.013
CDF dajet mass Xsec	0.075± 0.03	0.018 ± 0.03

Table 2: (Data-Theory)/Theory for the MI and the Soft model.

P_{Tmin}	*NO.OF MULTI.SCATTERS*	$\langle n_{multi} \rangle / event$
2.0	321211	2.070
2.25	239619	1.796
2.5	176225	1.591
3.0	98711	1.336
4.0	36107	1.120
15.0	194	1.001
50.0	0	1.000

Table 3: Number of multiparton interactions simulated for CDF and D0 in 3.10^5 events.

and

$$\sigma_{MI-on/Soft-on} = C_{2/3} e^{\lambda_2 E_t}$$

and obtained following values for the above coefficients.

$$C_{1(MIoffandUEoff)} = 15.234 \pm 0.040$$
$$\lambda_1 = \text{-}0.0360 \pm 0.0002$$
$$C_{2(MIon)} = 15.443 \pm 0.077$$
$$\lambda_2 = \text{-}0.0368 \pm 0.0004$$
$$C_{3(UEon)} = 15.390 \pm 0.04$$
$$\lambda_3 = \text{-}0.0363 \pm 0.0002$$

From the values of λ's we could have determined

$$\lambda = \frac{1}{2}(\lambda_1 + \lambda_{2/3})$$

an average slope for the two distributions and could have calculated the pedestal shift under jets by defining the MI-on distribution as

$$\begin{aligned} \sigma_{MI-on/UE-on} &= C_{2/3} e^{\lambda E_t} = C_1 e^{\lambda (E_t - \Delta)} \\ \frac{\sigma_{MI-on/UE-on}}{\sigma_{MIoff}} &= \frac{C_{2/3}}{C_1} = e^{-\lambda \Delta} \end{aligned}$$

giving finally

$$\ln\left(\frac{C_{2/3}}{C_1}\right)\frac{1}{\lambda} = \Delta$$

where Δ is the pedestal shift. However due to the difference in values between the two slopes (see Fig.6 and (λ_1 and λ_2)) it was not possible to determine the pedestal shift for the MI model using the above method. For the Underlying Soft model we found Δ=0.2818 $\pm$ 0.2 GeV (see Fig.7 and (λ_1 and λ_3)). Because of the "roughness" of the method used in the next section we will show how to determine this pedestal value for the multiparton model using a different approach.

5.2 Determining the average amount of transverse energy generated by secondary scatters part of the total transverse energy of the jet.

Because our first method in Sec.5.1 had failed to give us some quantitative results about the pedestal value undernith the jets a program in Fortran was written in order to determine it directly by looking at the amount of energy generated from multiparton interaction in a given jet. Events were simulated using HERWIG v6.1 ((IPROC=11500) running in conjunction with JIMMY, $P_{Tmin} = 2.0$ GeV). We used PUCELL jet algorithm with the merging/splitting threshold set to 50% . Once the jet algorithm had produced a list of jets we searched for the origin of each particle composing each jet. Particles can originate from two separate process in an event, either from the main hard scatter (usually with the highest P_T) or from the secondary hard scatters (usually with lower P_T) occurring in beam-beam remnant interaction. We define the total transverse energy of a given process as a scalar sum of all particles transverse energies coming from that process. We call the main hard scattering process the one with the highest total transverse energy. All other particles, not part of the main process were considered as originating from the multiparton interactions. In Fig.16 we present the distribution of E_T generated by secondary scatters versus the total transverse jet energy. We notice that the transverse energy generated by multiparton model varies with the total transverse energy of the jets. The distribution in jet E_T of the transverse energy generated by the secondary scatters produces a “bump” in the low jet E_T region with a maximum of “activity” in jets with E_T between 10 and 20 GeV. It is only for jets with transverse energy greater then 70 GeV that the contribution from the multiple scattering becomes roughly independent of the total jet energy producing a “plateau”. It is the hight of this “plateau” which will produce the pedestal shift in jet energies. For jets with transverse energy greater then 70 GeV the amount of average energy generated by multiple scattering was estimated to be 0.628 $\pm$ 0.22 GeV (see Fig.16). This value is well within the correction for the Underlying event activity applied by the two collaborations (see Sec.5.1).

5.3 The Underlying event in hard Scattering Processes

In the work (see Ref.[14]) a study of the growth and structure of the underlying event was measured at the CDF detector. The experimental data was then compared to the QCD Monte-Carlo simulations. Next we will summarize the most important points of this work, which also will be used in our own analysis.

The overall CDF data are composed of two sets: the minimum bias set for which the minimum bias trigger selects predominantly the "hard core" component of the inelastic cross section and the JET20 (Calorimeter Tower cluster with $E_T > 20$GeV) set. To remain in region where the charged particle tracks are found with high efficiency only the particles with ($P_T > 0.5$ GeV and $|\eta| < 1$) were considered.“The data was not corrected for the central tracking chamber (CTC) track finding efficiency but instead the theoretical

Monte-Carlo model predictions were corrected." Although the Monte-Carlo models used in the Field and Stuart analysis were HERWIG 5.9, ISAJET 7.32, PYTHIA 6.115, PYTHIA 6.125 and PYTHIA No MS (without Multiple Scattering), in this report we will be concerned only with HERWIG v5.9 data. For the theoretical simulations all the parameters in HERWIG were set to their defaults values (IPROC=1500), except for the P_{Tmin} which was set to 3 GeV. The P_{Tmin} was set large enough for perturbative QCD calculation to be applicable. The particles were divided into two categories: particles arising from the beam-beam remnants (those described as composing the underlying event) and particles originating from the hard scattering component (particles that result from the outgoing hard scattering jets plus initial and final-state radiation). The theoretical Monte-Carlo prediction was corrected for the track finding efficiency, this correction amount to 8% and correspond in removing 8 out of 100 charged particles on average from the theoretical prediction. It was also required that the Monte-Carlo events satisfy the CDF min-bias trigger. Finally the data presented in Field and Stuart work had an error of about 5%. The error on the experimental data included both statistical and correlated systematic uncertainties.

5.3.1 The jet definition

Below we give the definition of the charged particle jet algorithm Ref.[14] used by Field and Stuart, which we will use in our own work.

The charged particles form "jets" of radius $R = 0.7$ in η-ϕ space which contain particles from both underlying event and hard scattering. **"Every charged particle is assigned to a jet with a possibility that some "jets" might consist of just one charged particle. Since the standard jet algorithm based on calorimeter clustering is not applicable at low transverse momentum of charged particles,"** a very simple jet definition is given below :

- Charged particles are first ordered according to their P_T.
- Starting with the highest P_T particle, all the particles within the "radius" $R = 0.7$ are included to form a jet.
- Then proceed to the next highest P_T particle (not already included in a "jet") all the particles within the "radius" $R = 0.7$ (not already included in a "jet") are included to form a new jet.
- This is continued until all charged particles are part of one of the jets.

All charged particles with ($P_T > 0.5$ GeV and $|\eta| < 1$) are considered and the jet is allowed to extend outside $|\eta| < 1$. The transverse momentum of the jet is defined as the scalar P_T sum of all particles within the jet. Once all jets had been produced the one with the highest P_T(jet#1) is selected to be the leading jet. We calculated the ϕ of the leading jet following the definition given in Sec.1.1, where instead of using E_T we used the P_T of the particles.

$$\phi_{jet} = \sum_i \frac{P_{Ti}\phi_i}{P_{Tjet}} \tag{29}$$

5.3.2 The particle distribution as function of the P_T of the leading jet

Our first goal was to reproduce the simulated data presented in the Field and Stuart paper(see Ref.[14]). By applying the same jet definition as the one given above (see Sec.5.3.1) and by using the same default parameters in HERWIG v5.9 as the one presented in Ref.[14] we simulate our own set of data. In the same way as in (see Ref.[14]) our data are studied over three different regions away in ϕ from the leading jet(jet#1) as illustrated in Fig.17. The angle $\Delta\phi = \phi$ - $\phi_{jet\#1}$ is the relative azimuthal angle between charged particles and the direction of jet#1. The three regions are as follows; the toward region from the leading jet (jet#1) defined over the range $|\Delta\phi| < 60°$ (this region includes the particles of the leading jet#1), the away region from the leading jet#1 defined over the range $|\Delta\phi| < 120°$ and the transverse region from the leading jet#1 defined over the range $60° < |\Delta\phi| < 120°$. Each region, toward, transverse, and away covers the same range $|\Delta\eta|\times|\Delta\phi|=2\times120°$.

Fig.18 show the agreement between our simulated data and those of Field and Stuart (theory corrected) for the overall charged multiplicity (the overall charge multiplicity is the sum of charged particles in the toward, away and transverse region) versus P_T of the leading jet. Fig.19 to Fig.22 show the agreement between our plots and those of Field and Stuart for the toward, away and transverse regions.

5.4 Toward, away and transverse region

For our simulated distributions (as in Field and Stuart paper) we will separate charged particles in two group, those arising from the beam-beam remnant and those which are part of the outgoing "hard" scattering jets originating from two-to-two parton parton subprocess (including initial and final state radiation). For the toward region Fig.30 show how for charged jets with P_T > 5 GeV (leading jet#1 P_T) the dominant contribution comes from charged particles, part of the outgoing "hard" jets. In the away region Fig.31 show how for charged jets with P_T > 5 GeV the dominant contribution comes from the "away-part" of the charged particles, part of the outgoing "hard" jets.

It is in the transverse region that the proportion of the beam-beam remnants contribution to the overall values studied (average number of charged particles and average scalar P_{Tsum} of charged particles) becomes most pronounced. Fig.32 show how the dominant contribution to the average number of charged particles until up to 15 GeV of the leading charged jet P_T is due to particles originating from the beam-beam remnants (for the average scalar P_{Tsum} vs leading jet#1 P_T (see Fig.33)). In all three regions studied, HERWIG + Soft Underlying model produce a characteristic "bump" (the "bump" in the beam-beam remnant contribution at low P_T(jet#1) is caused by leading jets composed almost entirely from the remnants in low P_T (leading charged jet#1) region) followed by a flat distribution. In Fig.34 to Fig.37 we show the simulations of HERWIG + Soft Underlying model in the three different regions with two different values of P_{Tmin}, 3.0 GeV and 2.0 GeV, as the value of P_{Tmin} is lowered the "bump" due to beam-beam remnants in the low P_T (leading jet#1) region increases while the "plateau" and the contribution from the outgoing "hard" scattering jets stays roughly the same (see Fig.36, Fig.37). If we consider particularly the transverse region (see Fig.37), the "bump" reaches the maximum value in both cases for jets with P_T (leading charged jet#1) between 4-5 GeV. Thus lowering the P_{Tmin} induce HERWIG + Soft Underlying model to produce particles with low P_T enhancing only the soft model activity (in all three regions (see Fig.34 to Fig.37) away in ϕ from the leading jet) in the low P_T (leading charged jet#1) region. To try to change the hight of the plateau region we would have to change the value of ENSOF (enhancement factor used in choosing the multiplicity of the underlying soft event) input parameter in HERWIG. If we now compare our simulated data (ENSOF=1) with the experimental data measured at CDF (see Ref.[14]), we observe that they do agree in the toward and in the away region, although not exactly (see Fig.23 to Fig.25 and Fig.27 and Fig.28). It is in the transverse region that the discrepancy between the simulated and the experimental data is the biggest. The default HERWIG + Soft Underlying model produces a too steep P_T distribution for the $<P_{Tsum}>$ (see Fig.29) and does not produce enough $<P_{Tsum}>$. If we try to enhance the soft model by lowering the value of P_{Tmin} we produce a too steep rise in the low P_T (leading charged jet#1) region for <Nchrg>, for $<P_{Tsum}>$ distribution we produce more $<P_{Tsum}>$ and a steeper rise in low P_T (leading charged jet#1) region however since the "plateau" do not change in hight the rise is then followed by a slight decrease and then again a too steep rise in P_T distribution (see Fig.38) and still not enough $<P_{Tsum}>$. Thus we come to the same conclusion as the one presented in the introduction (see Ref.[14]) namely that HERWIG + Underlying Soft model (with default ENSOF) do not have enough activity in the underlying model and predict too steep P_T distribution in the transverse region. In the next section we will replace the Underlying Soft model by the Multiparton Interaction model and see whether it describes better the experimental data.

5.5 The effect of the Multiparton Interaction model on charged particle distributions

Using the same jet algorithm for charged particles as the one defined in Sec.5.3.1 we have simulated a new set of data using multiparton interaction model running in conjunction with HERWIG and soft underlying event model turned off IPROC(11500). In Fig.39 to Fig.46 we present the ensemble of simulated distributions for the set of parameters presented in table.5.

PDF	P_{Tmin}	$\langle n(b, s_{p\overline{p}})\rangle$
GRV	2.2	2.18
CTEQ4L	2.0	2.14
	3.0	1.37
DO(set 1)	2.0	1.36

Table 4: Parameters

We notice that the shapes of the distributions do not depend so much on the PDF's as on the mean number of secondary scatters, $\langle n(b, s_{p\overline{p}})\rangle$ (see eq.16). As the mean number of secondary scatters increases, the distribution of the total average number of charged particles in the event $< Nchg >$ (see Fig.40) tend to rise too fast in the low P_T (leading charged jet) region producing a shoulder not observed in the experimental data as the P_T of the leading charged jet increases, the $< Nchg >$ then doesn't continue to rise fast enough. We notice for distributions simulated with lower $\langle n(b, s_{p\overline{p}})\rangle$ that although their shapes are more similar to the experimental distributions, their overall scales are too low (see Fig.41,Fig.44 and Fig.46). In the transverse region the Multiparton model produce a steep rise in the low P_T (leading charged jet) region followed by a roughly flat P_T distribution in agreement with the experimental data (see Fig.45 and Fig.46). The overall "enhancement" of the simulated data by a certain factor may be produced by decreasing the proton radius (see eq.16 and eq.23). We chose to decrease the proton radius by a factor of 1.731 and simulate the ensemble of distributions with $P_{Tmin} = 3.0$ GeV (to avoid the shoulder in the low P_T (leading charged jet) region). In Fig.47 to Fig.53 we show that for this set of parameters HERWIG + Multiparton model produce distributions which are in good agreement with the experimental data in all three regions away in ϕ from the leading jet.

6 Conclusion

The purpose of this work was twofold : first to evaluate the effect of the underlying event models on simulated distributions and compare them to distributions measured at CDF and DØ, second to evaluate and simulate (with models at hand) the underlying event structure in $p\overline{p}$ collisions at the Tevatron. We have simulated the inclusive jet distribution and dijet distributions measured at DØ and CDF using HERWIG with two different underlying event models, JIMMY (the Monte Carlo Event Generator) and HERWIG Soft Underlying event model. We've found that for the cuts applied in those measurements (see Sec.4) the contribution due to the simulated underlying event "activity" was not significant and well within the correction applied by the two collaborations. We have studied the amount of transverse energy generated by the multiparton model as function of the total transverse jet energy. We found that the amount of transverse energy generated by multiparton interactions model **varies** with the total transverse jet energy. It is only for jets with transverse energy greater then 70 GeV that the multiparton interactions contribution becomes roughly constant with a value equal to 0.675 ± 0.22 GeV. We've shown that in both CDF and DØ collaboration the underlying event in hard scattering is considered as the average energy level found in $p\overline{p}$ minimum bias collisions. According to data taken and analyzed at CDF by David Stuart and Rick Field Ref.[14] the underlying "hard scattering" event is not the same as a "soft" minimum-bias proton - antiproton collision. Thus the underlying event in "hard" collisions is considerably more active (i.e higher charge particle density and more transverse momentum).

We have used HERWIG + Soft Underlying model and HERWIG + Multiparton model to describe the entire proton-antiproton event structure. In order to test our implementation of the Jet definition and Jet algorithm given in Field and Stuart paper (and used in their experimental analysis) we have reproduced their simulated data. By using the same Jet algorithm we have simulated also a new set of data using HERWIG + Multiparton model. Finally we've shown that by allowing the proton radius in the multiparton model to decrease by a factor of 1.731, we are able to obtain a good agreement between simulated and CDF experimental data. Following this work it would be essential to test whether the same set of parameters will agree with different experimental data measured at HERA for example.

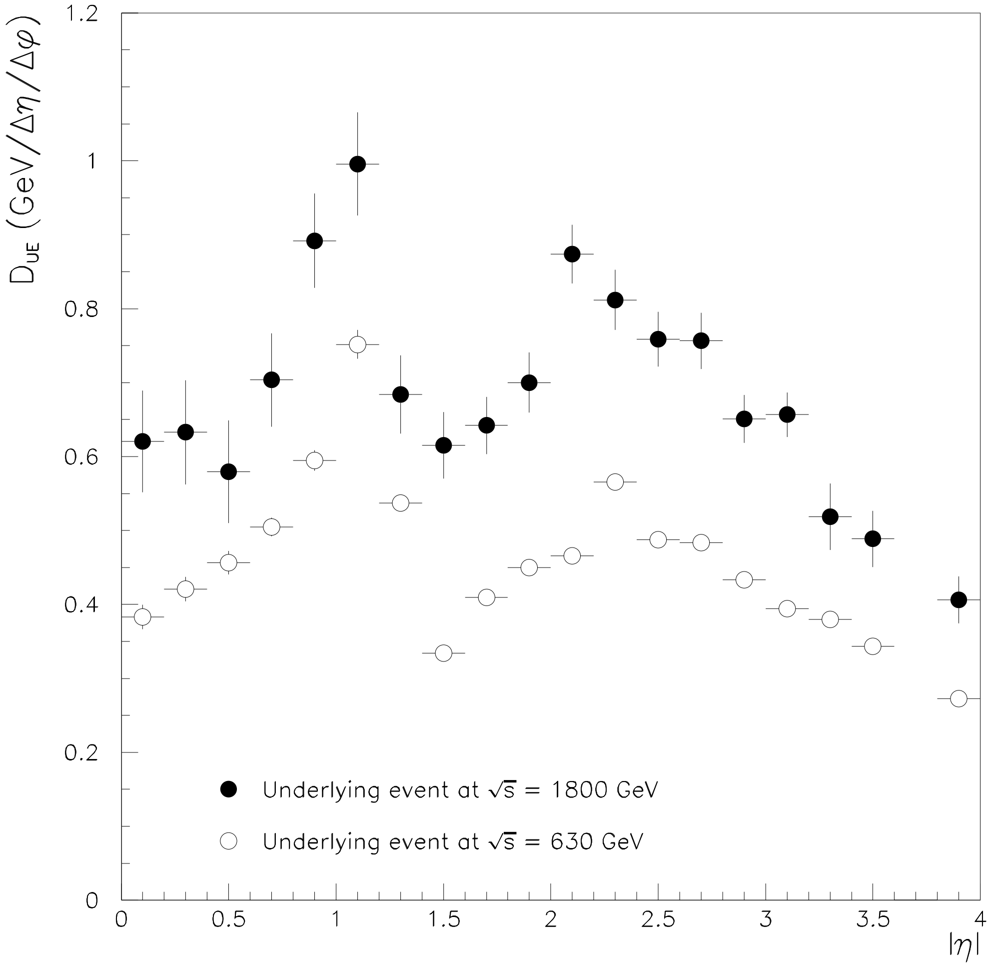

Figure 4: Physics underlying event E_T density, D_{ue} ($\sqrt{s}$=1800 and 630 GeV).The larger samples available for the low center-of-mass energy measurement explain the smaller statistical errors.

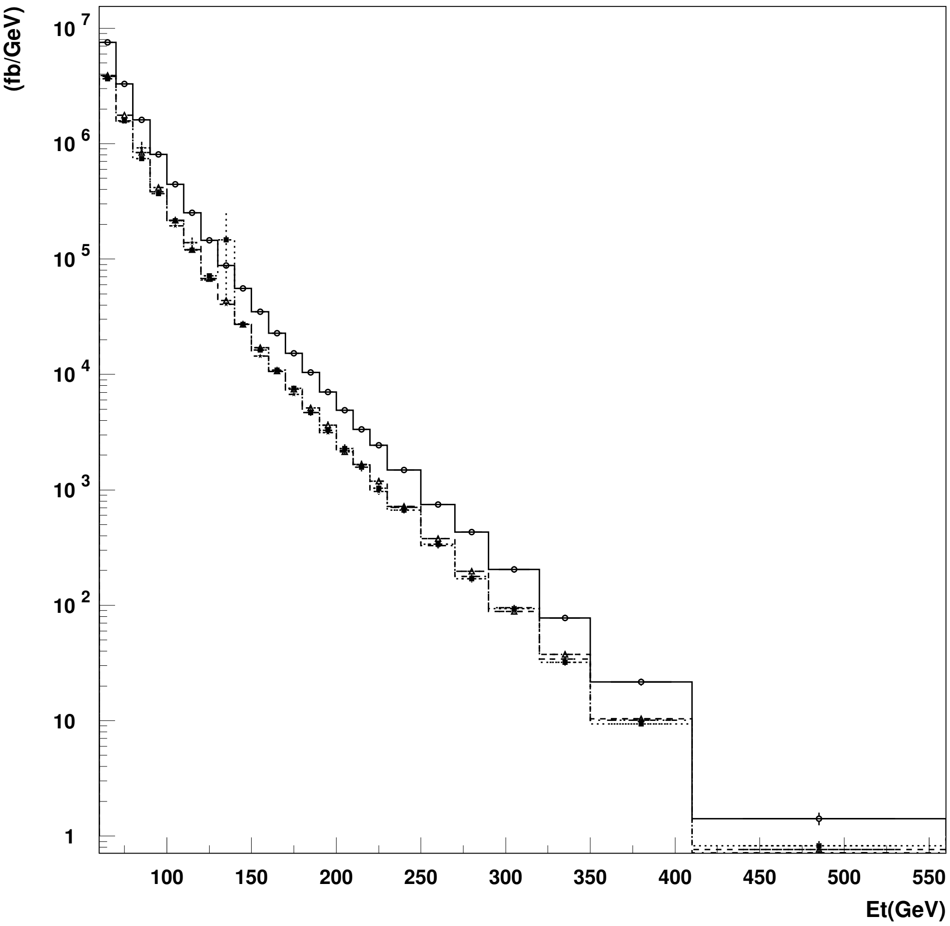

Figure 5: Plots show the the DØ inclusive jet distribution as function of ET(jet) (PDF=GRV, PTmin=2.0 GeV), solid circles (experimental data), solid squares simulated data (HERWIG + Multiparton interactions), triangles (HERWIG + Underlying Soft model), dashed line simulated data (HERWIG IPROC=11500, MI-off). All the simulated distributions including any of the underlying event models were corrected for the underlying event activity.

MI-off MI-on D0 inclusive

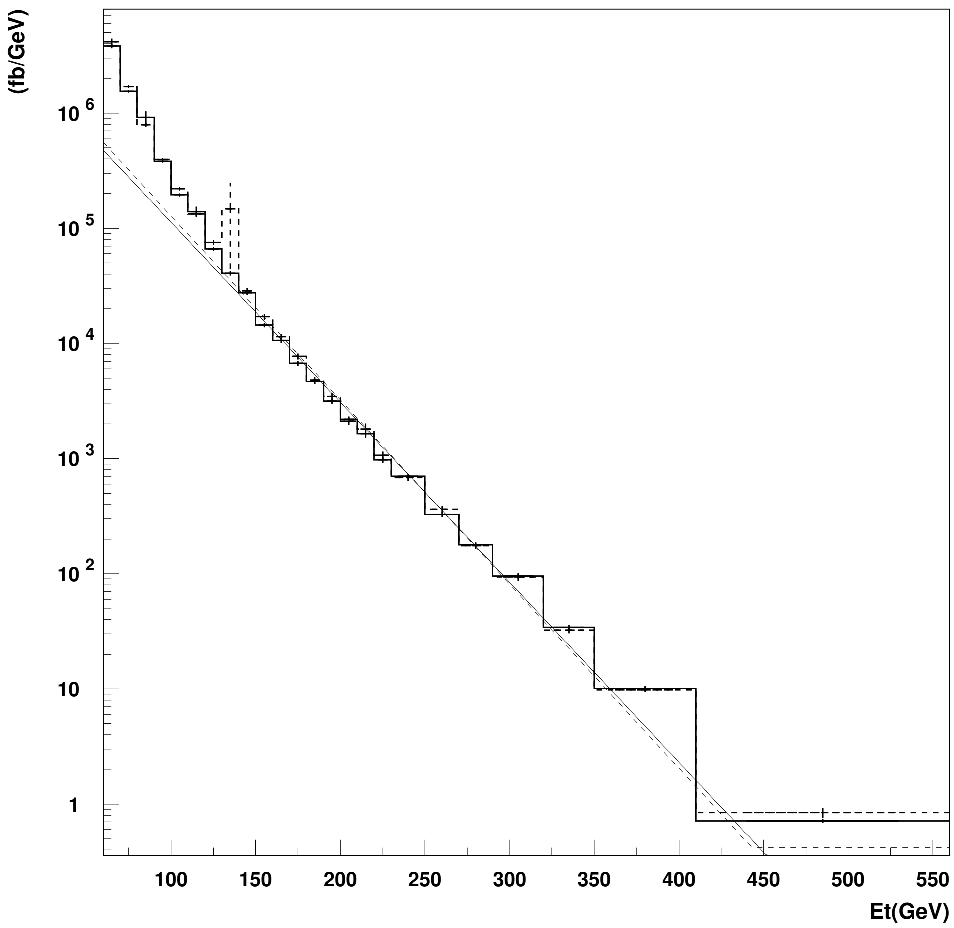

Figure 6: Plots show simulated DØ inclusive jet distribution as function of ET(jet) (PDF=GRV, PTmin=2.0 GeV), dashed line (HERWIG + Multi-parton interactions without correction), solid line HERWIG(IPROC=11500, MI-off).

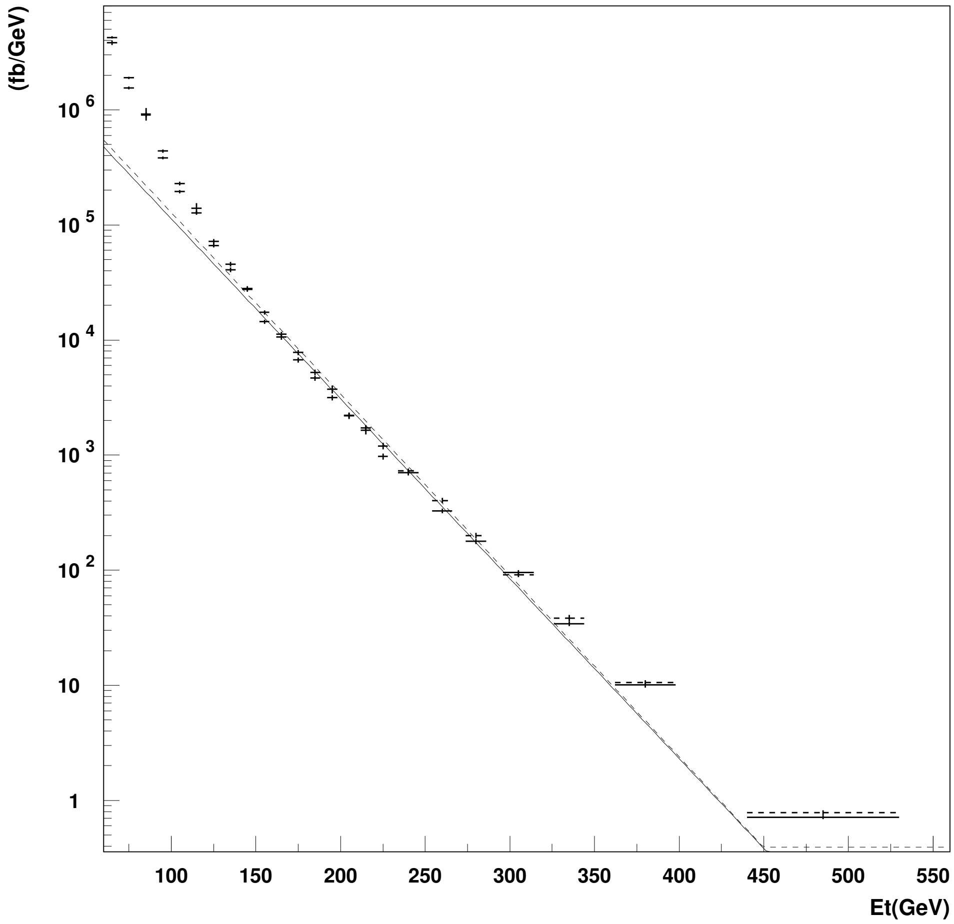

Figure 7: Plots show simulated DØ inclusive jet distribution as function of ET(jet) (PDF=GRV, PTmin=2.0 GeV), dashed line (HERWIG + Underlaying Soft model(IPROC=1500) without correction), solid line HERWIG (IPROC=11500, MI-off).

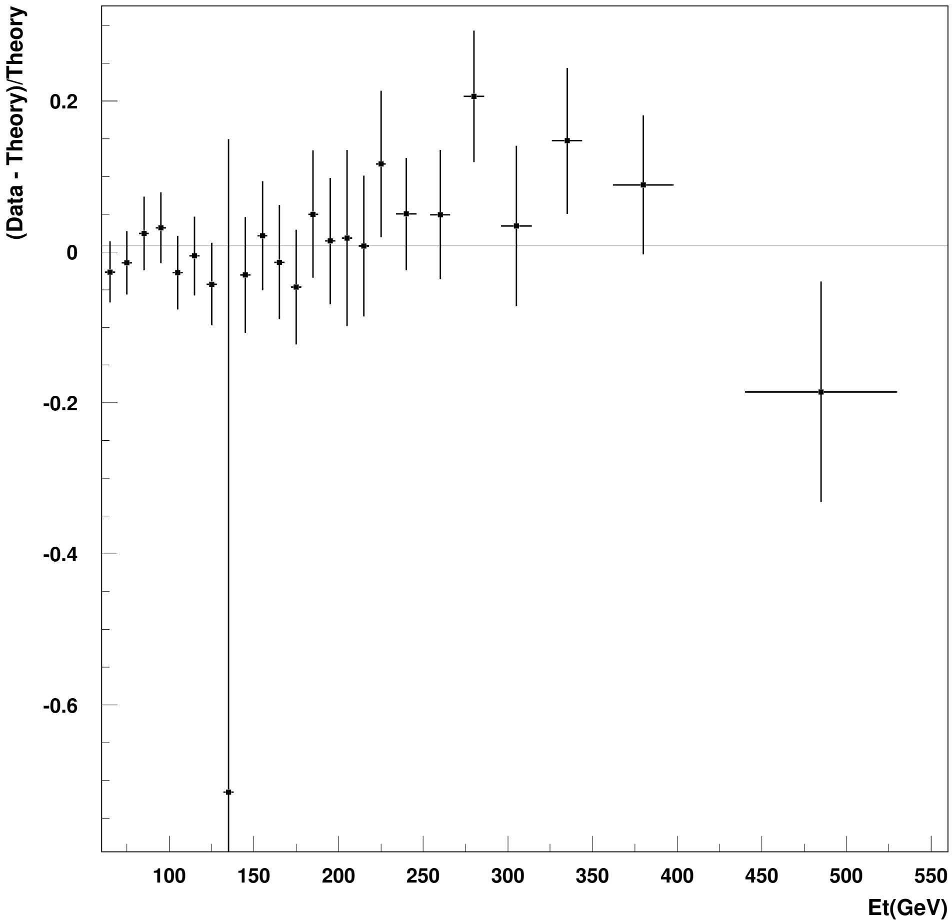

Figure 8: Plot show DØ inclusive jet distribution as function of ET(jet) (PDF=GRV, PTmin=2.0 GeV), fractional difference between the measured distribution and the simulated HERWIG + MI-on (corrected and multiplied by 2.12).

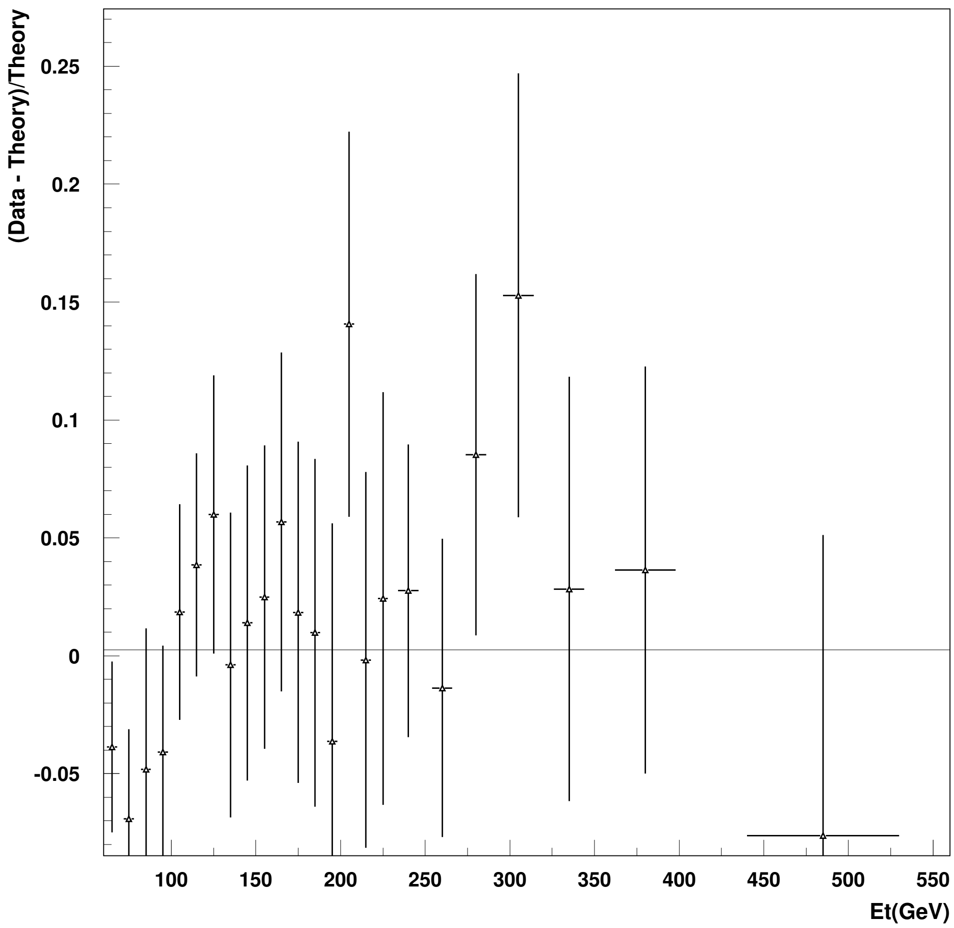

Figure 9: Plot show DØ inclusive jet distribution as function of ET(jet) (PDF=GRV, PTmin=2.0 GeV), fractional difference between the measured distribution and the simulated HERWIG + Underlying Soft model (corrected and multiplied by 1.94).

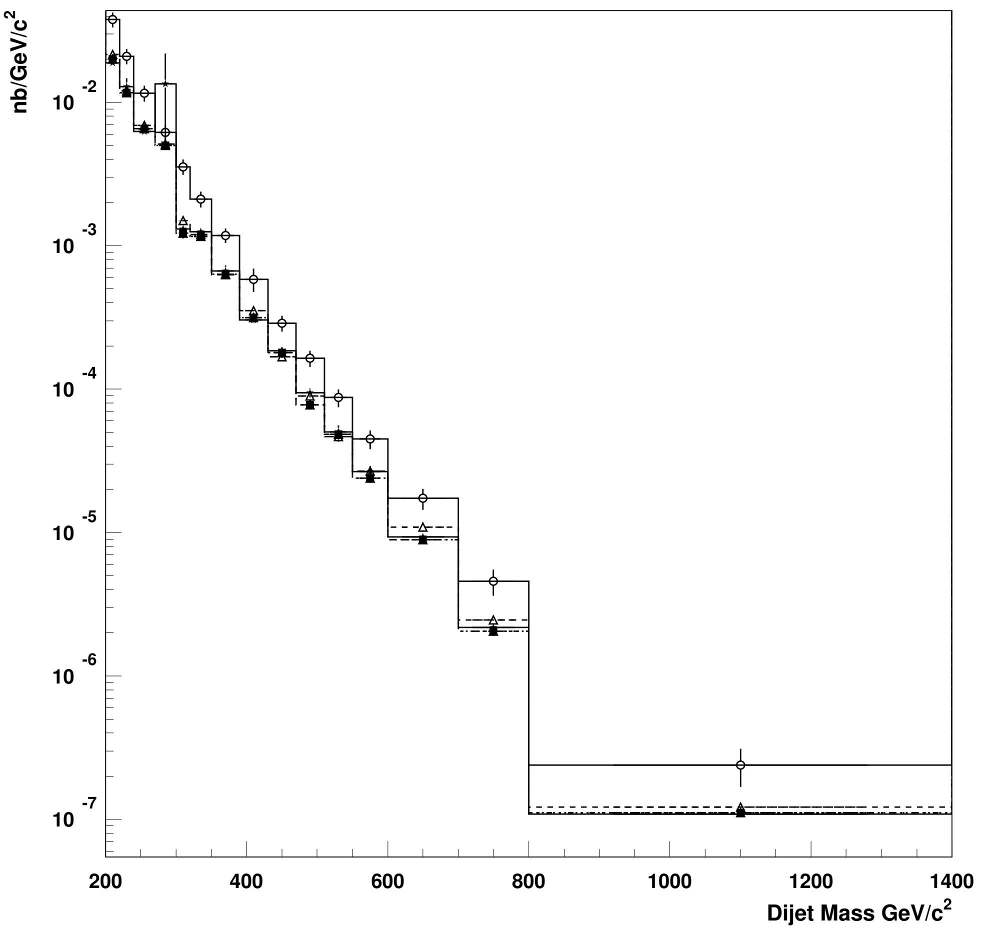

Figure 10: Plot show DØ dijet mass simulated distribution as function of dijet mass (PDF=GRV, PTmin=2.0 GeV), hollow circles (experimental data), solid squares simulated data (HERWIG + MI-on), dashed line simulated data (HERWIG IPROC=11500, MI-off), triangles simulated data HERWIG + Underlying Soft model. All the simulated distributions including any of the underlying event models were corrected for the underlying event activity.

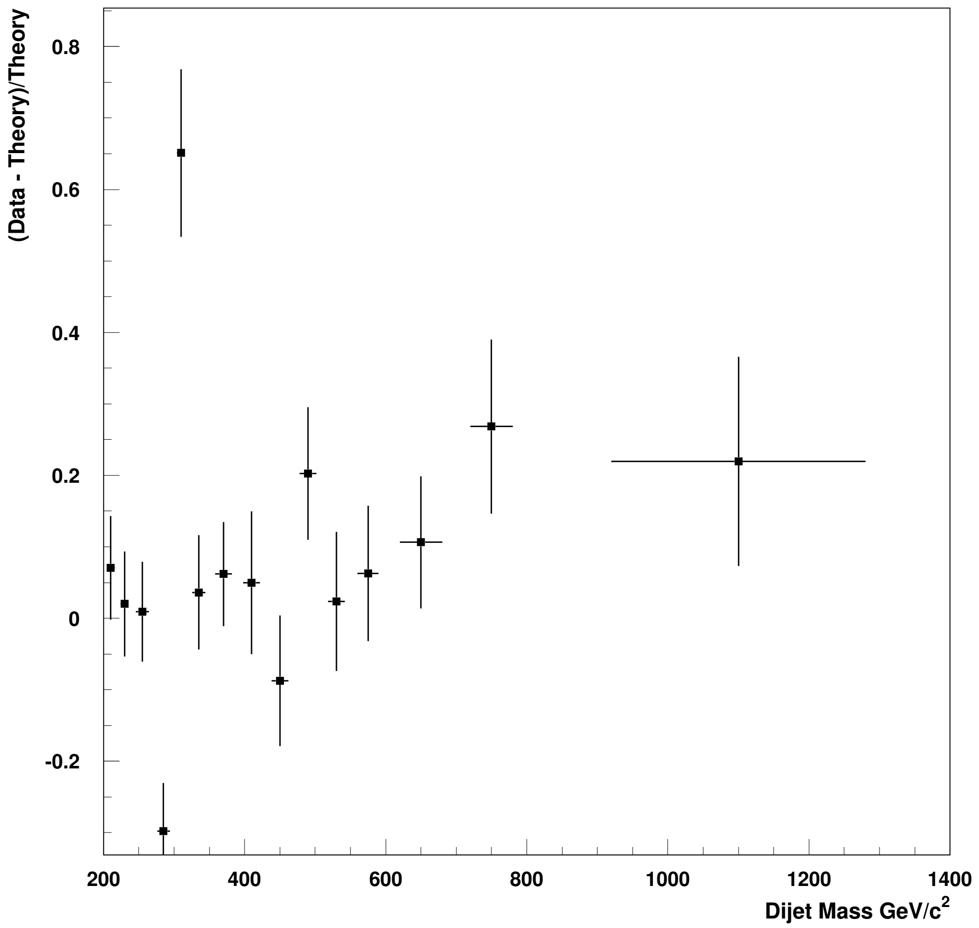

Figure 11: Plot show the fractional difference between the measured DØ differential cross section and the simulated HERWIG + MI-on (corrected and multiplied by 2.01).

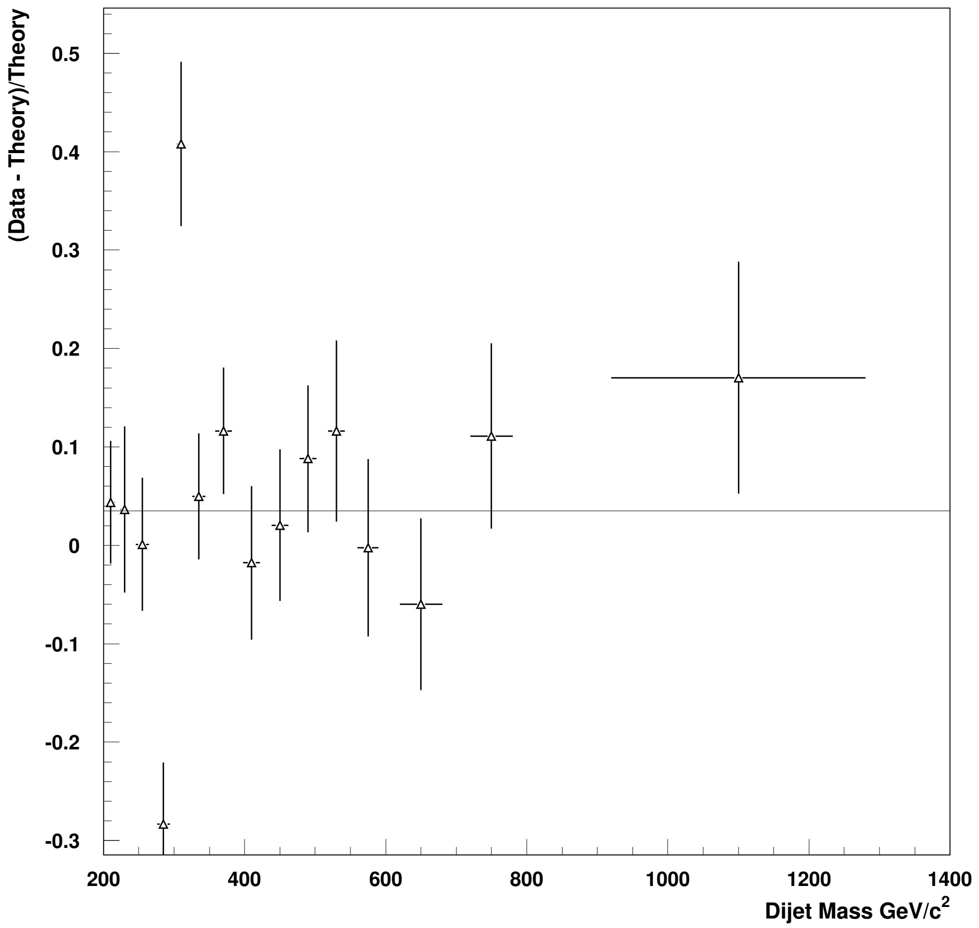

Figure 12: Plot show the fractional difference between the measured DØ differential dijet mass cross section and the simulated HERWIG + Underlying Soft model (corrected and multiplied by 1.85).

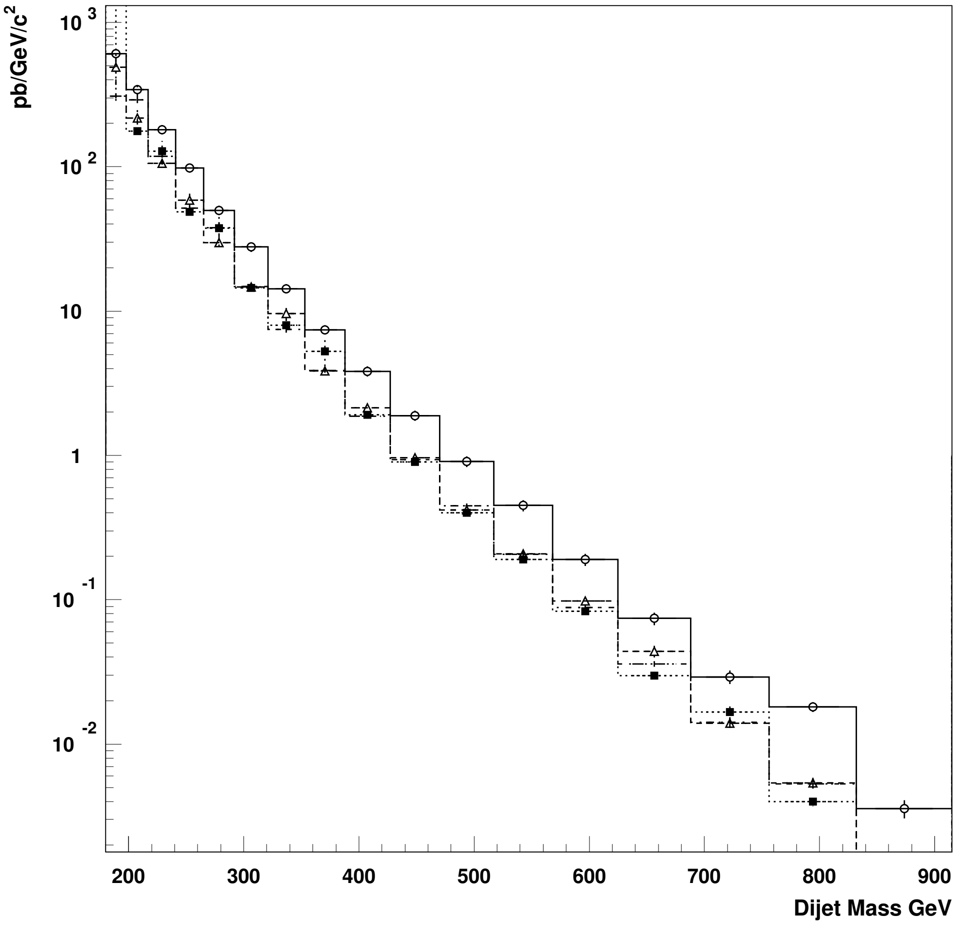

Figure 13: Plot show CDF dijet mass distribution as function of dijet mass (PDF=GRV, PTmin=2.0 GeV), hollow circles (experimental data), solid squares simulated data (HERWIG + MIon), dashed line simulated data (HERWIG IPROC=11500, MI-off), triangles simulated data HERWIG + Underlying Soft model. All the simulated distributions including any of the underlying event models were corrected for the underlying event activity.

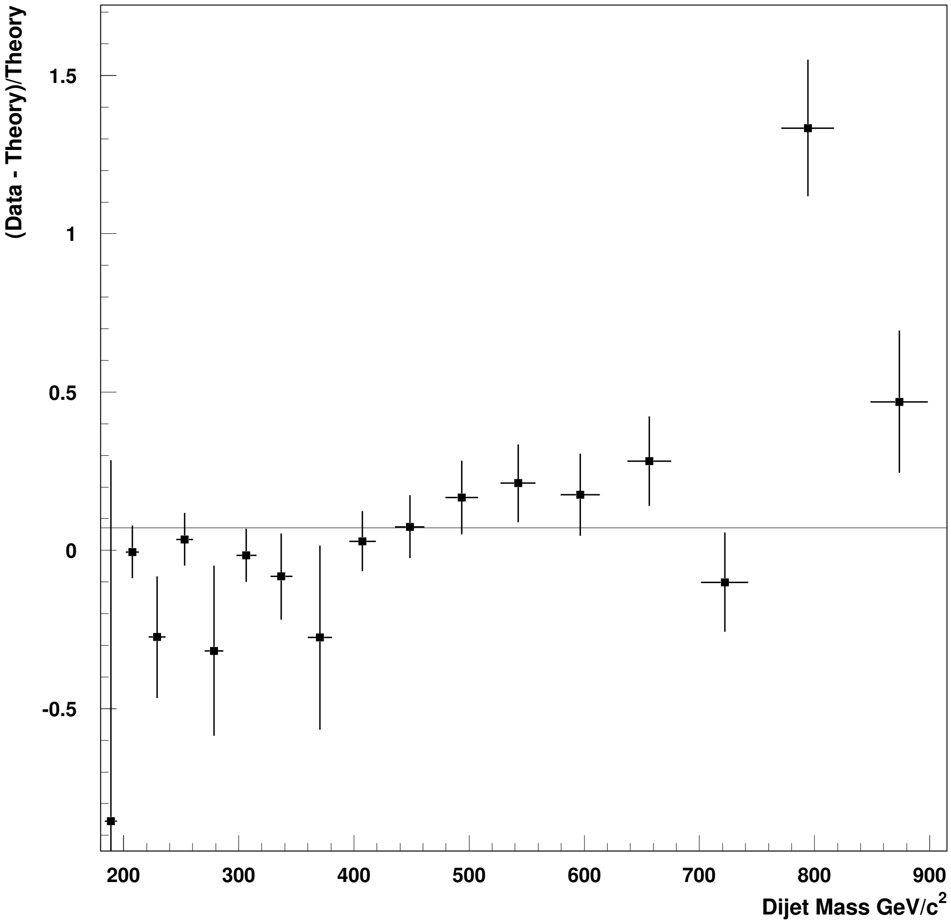

Figure 14: Plot show the fractional difference between the measured CDF differential dijet mass cross section and the simulated HERWIG + MI-on (corrected and multiplied by 2.15).

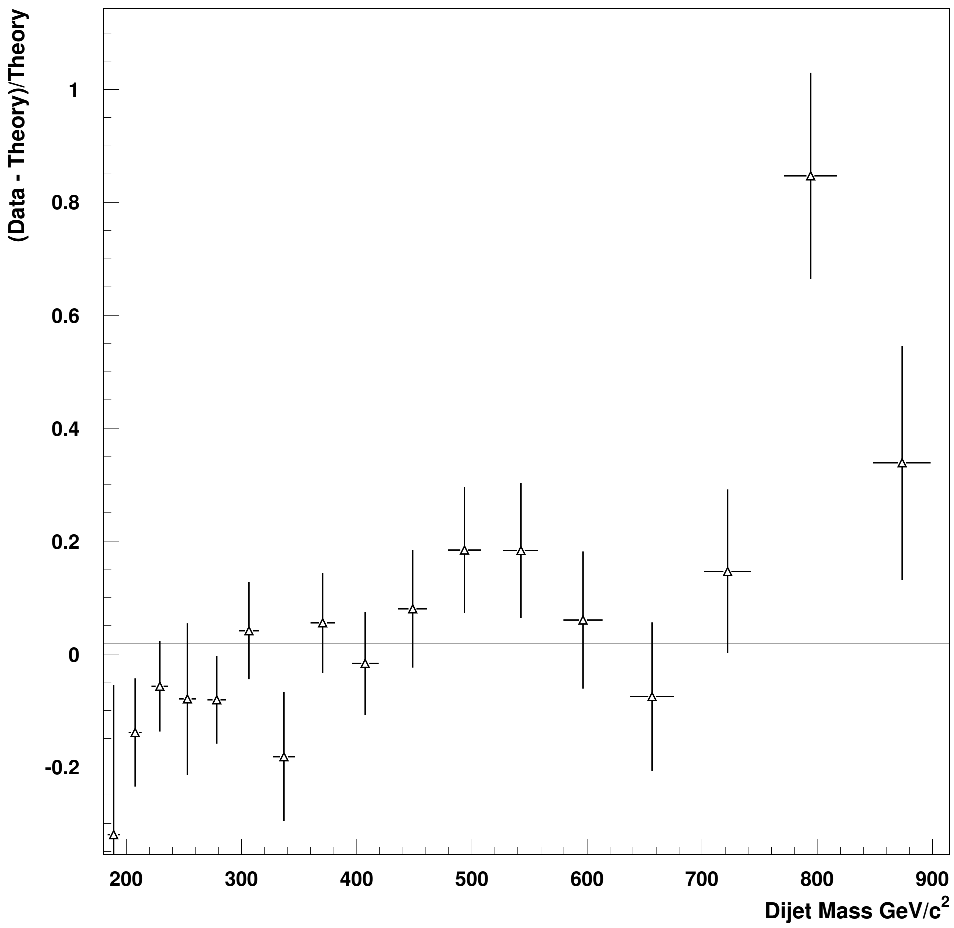

Figure 15: Plot show the fractional difference between the measured CDF differential dijet mass cross section and the simulated HERWIG + Underlying Soft model (corrected and multiplied by 1.97).

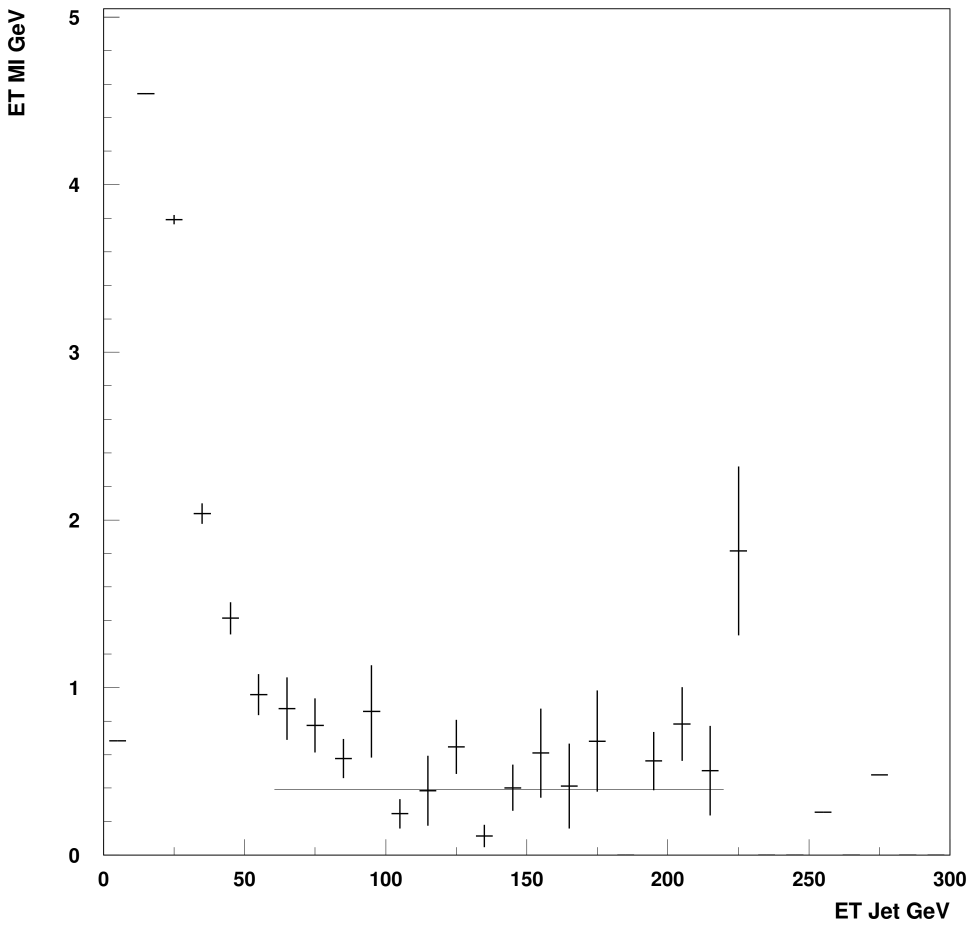

Figure 16: Plot show the transverse energy generated by multiple interactions as function of the total transverse jet energy.

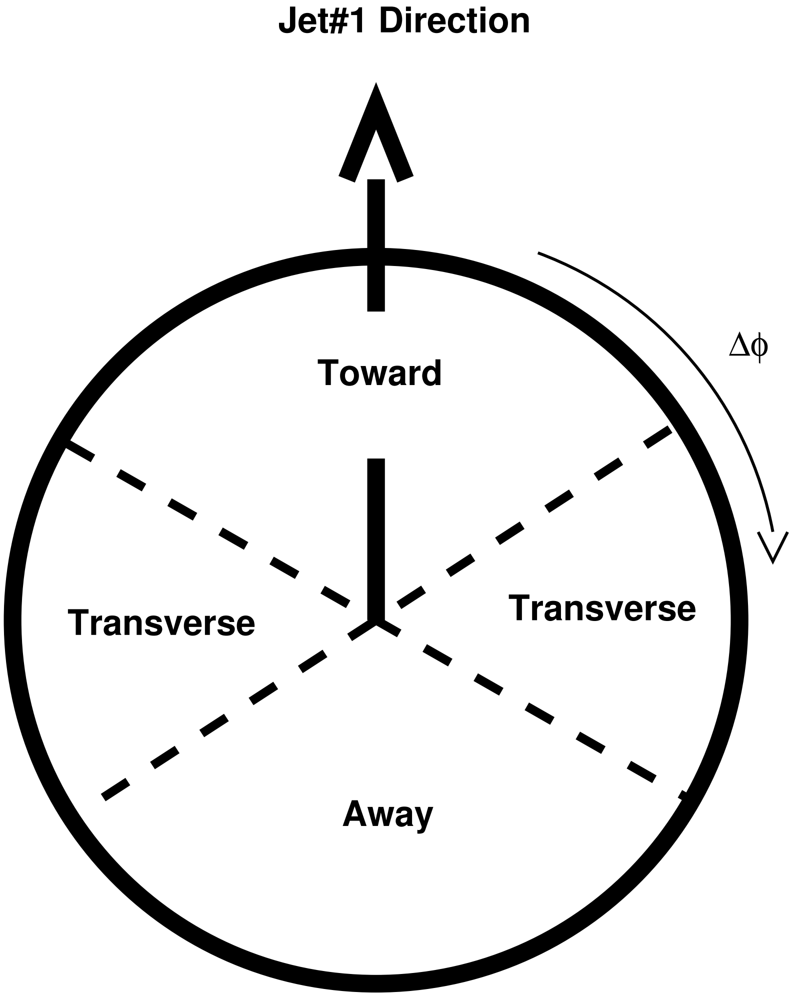

Figure 17: Toward, away and transverse regions from P_T leading jet.

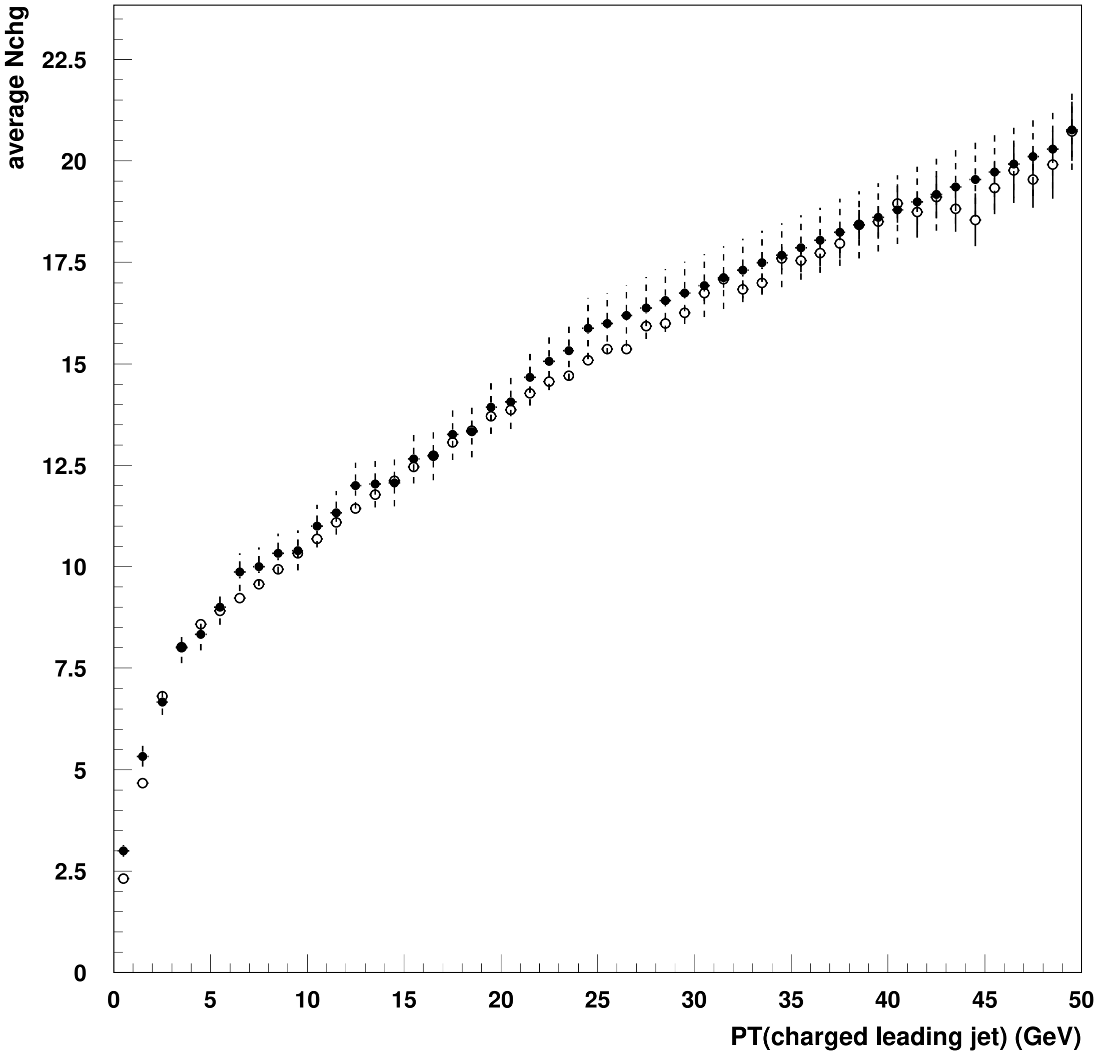

Figure 18: Plots shows the average total number of charged particles in the event (PT> 0.5 GeV and $|\eta|$<1 including leading charged jet) as a function of the transverse momentum of the leading charged jet. The solid circles Field and Stuart (corrected) simulated data, hollow circles our (reproduced and corrected) simulated data.

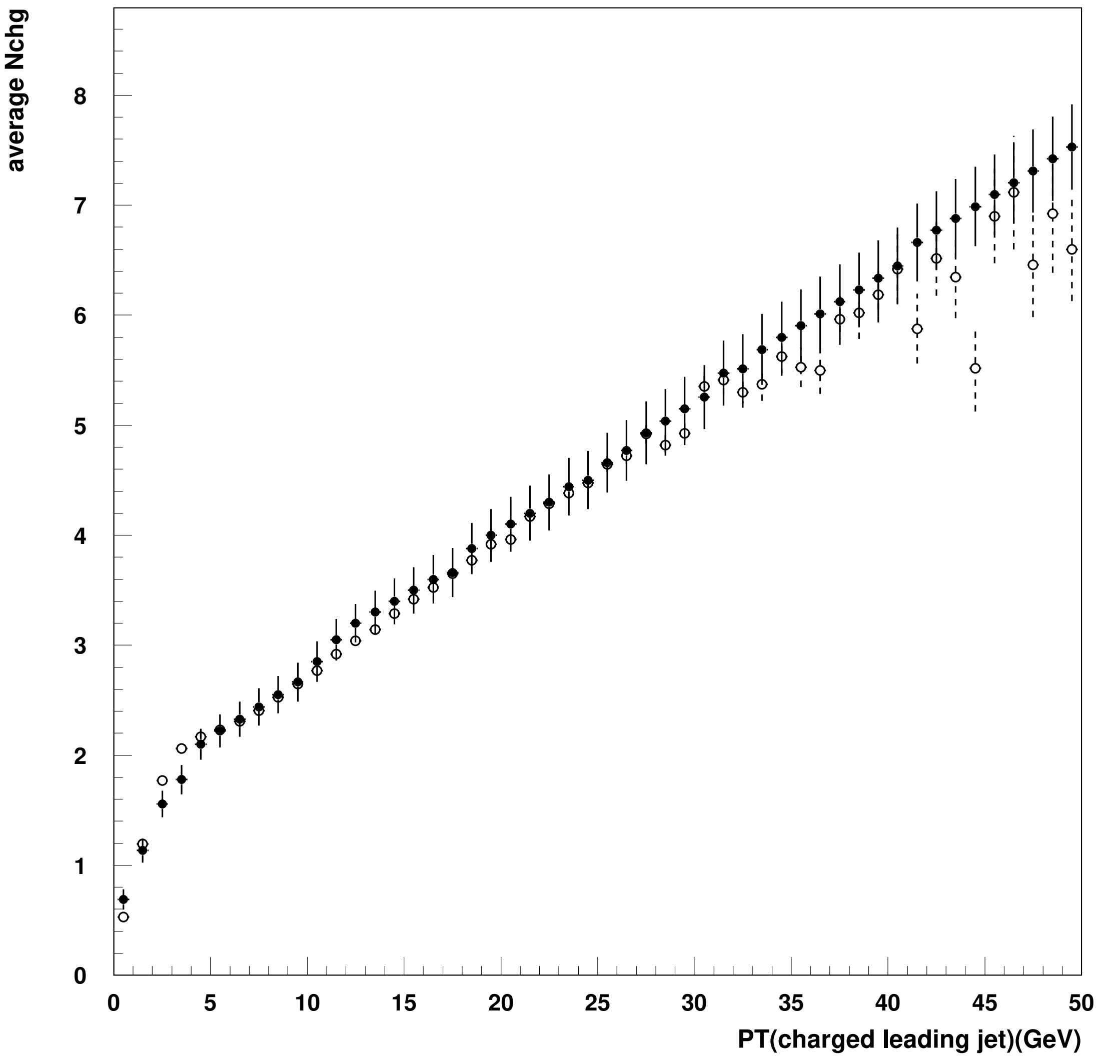

Figure 19: Plots shows the average number of charged particles (PT> 0.5 GeV and $|\eta|$<1) as function of PT(leading charged jet) for the away region. The solid circles Field and Stuart (corrected) simulated data, hollow circles our (reproduced and corrected) simulated data.

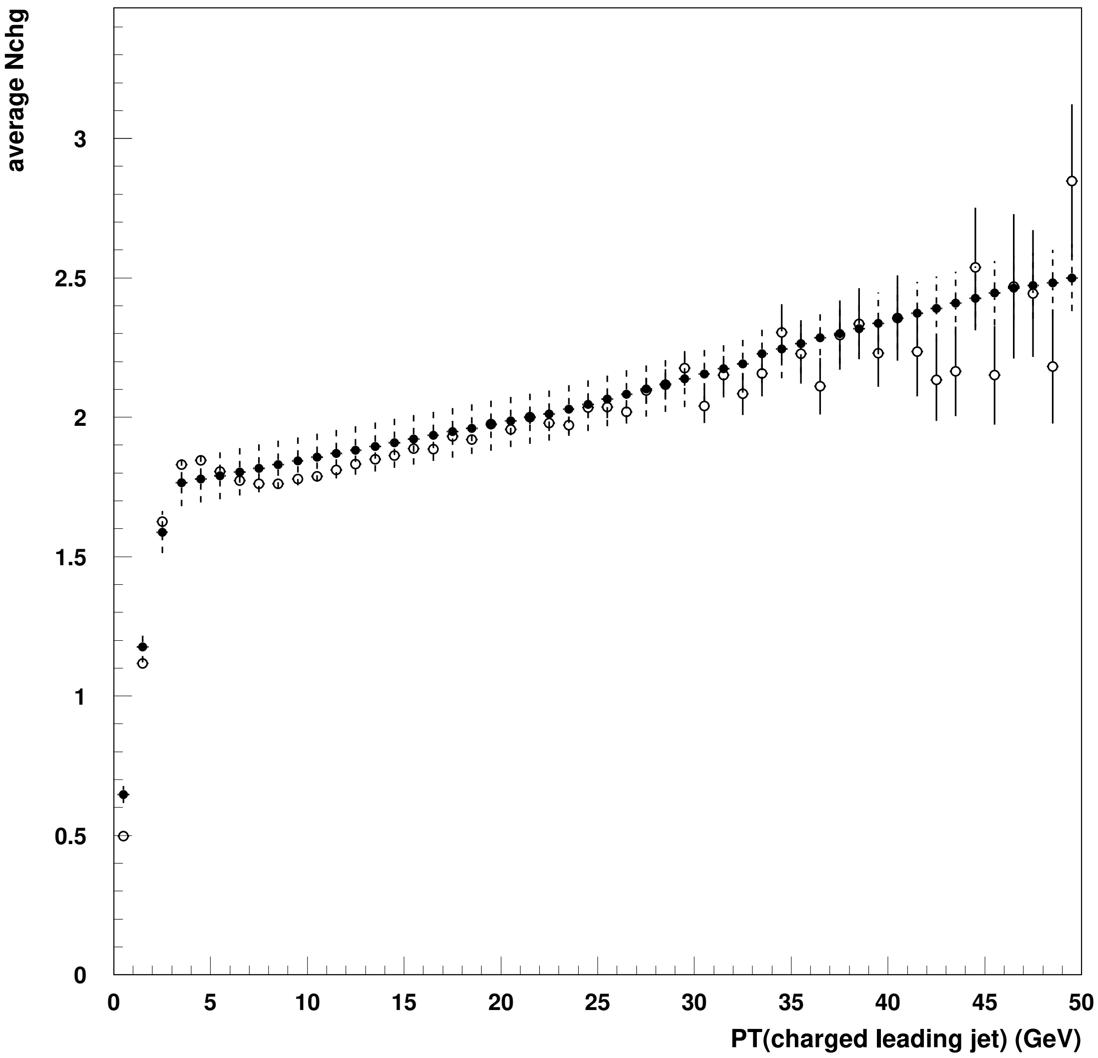

Figure 20: Plots shows the average number of charged particles (PT> 0.5 GeV and $|\eta|$<1) as function of PT(leading charged jet) for the transverse region. The solid circles Field and Stuart (corrected) simulated data, hollow circles our (reproduced and corrected) simulated data.

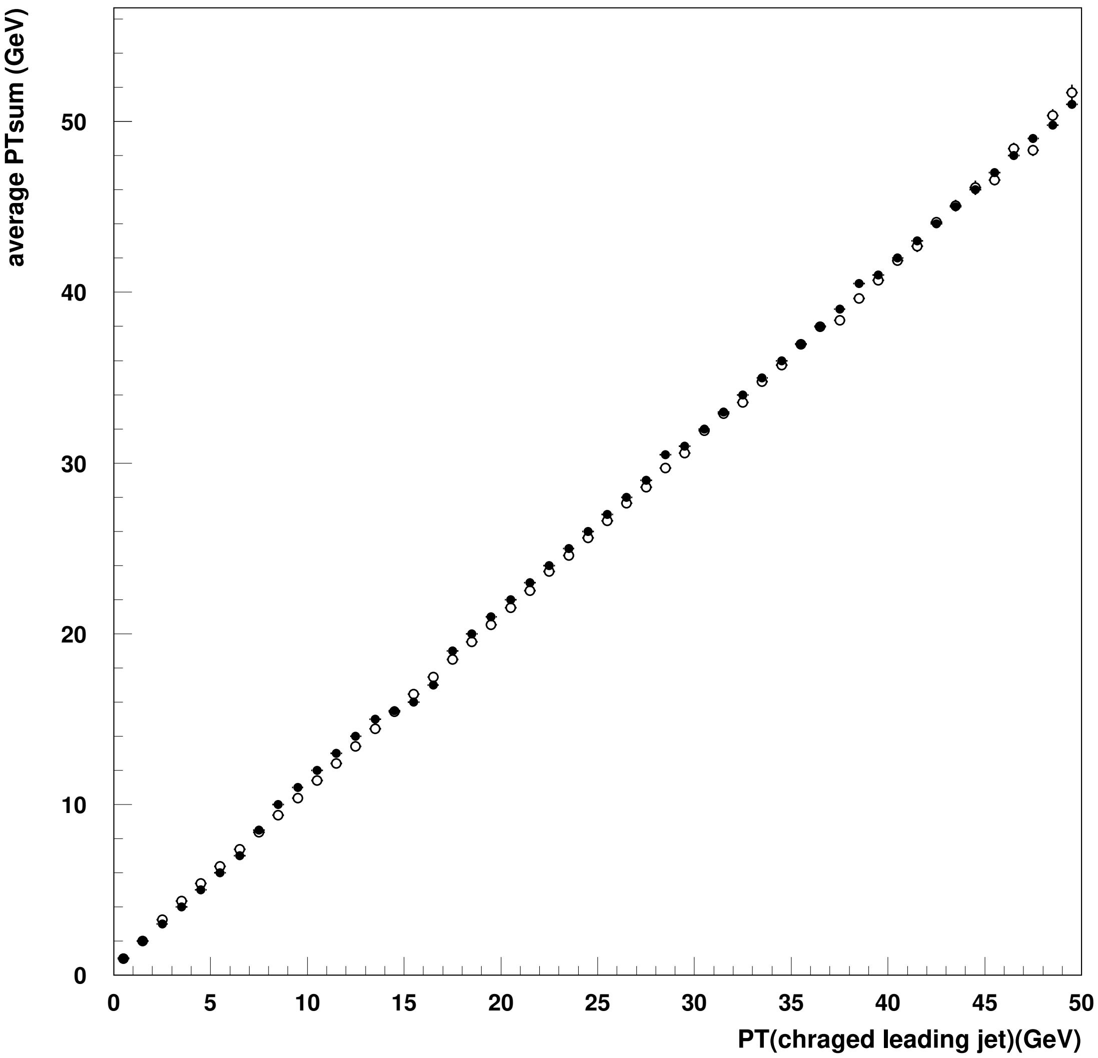

Figure 21: Plots shows the average PTsum of charged particles (PT> 0.5 GeV and $|\eta|<1$) as function of PT(leading charged jet) for the toward region. The solid circles Field and Stuart (corrected) simulated data, hollow circles our (reproduced and corrected) simulated data.

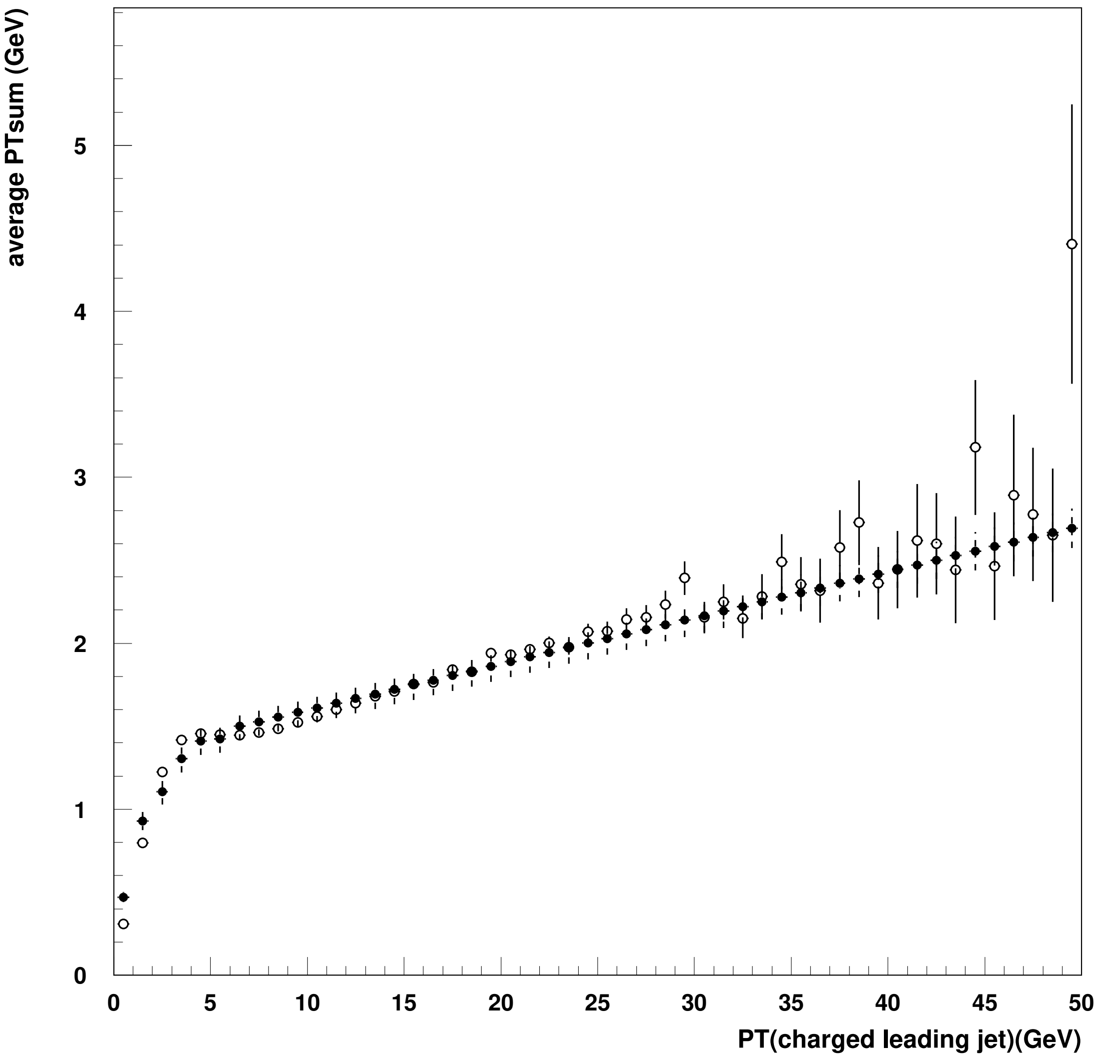

Figure 22: Plots shows the average PTsum of charged particles (PT> 0.5 GeV and $|\eta|$<1) as function of PT(leading charged jet) for the transverse region. The solid circles Field and Stuart (corrected) simulated data, hollow circles our (reproduced and corrected) simulated data.

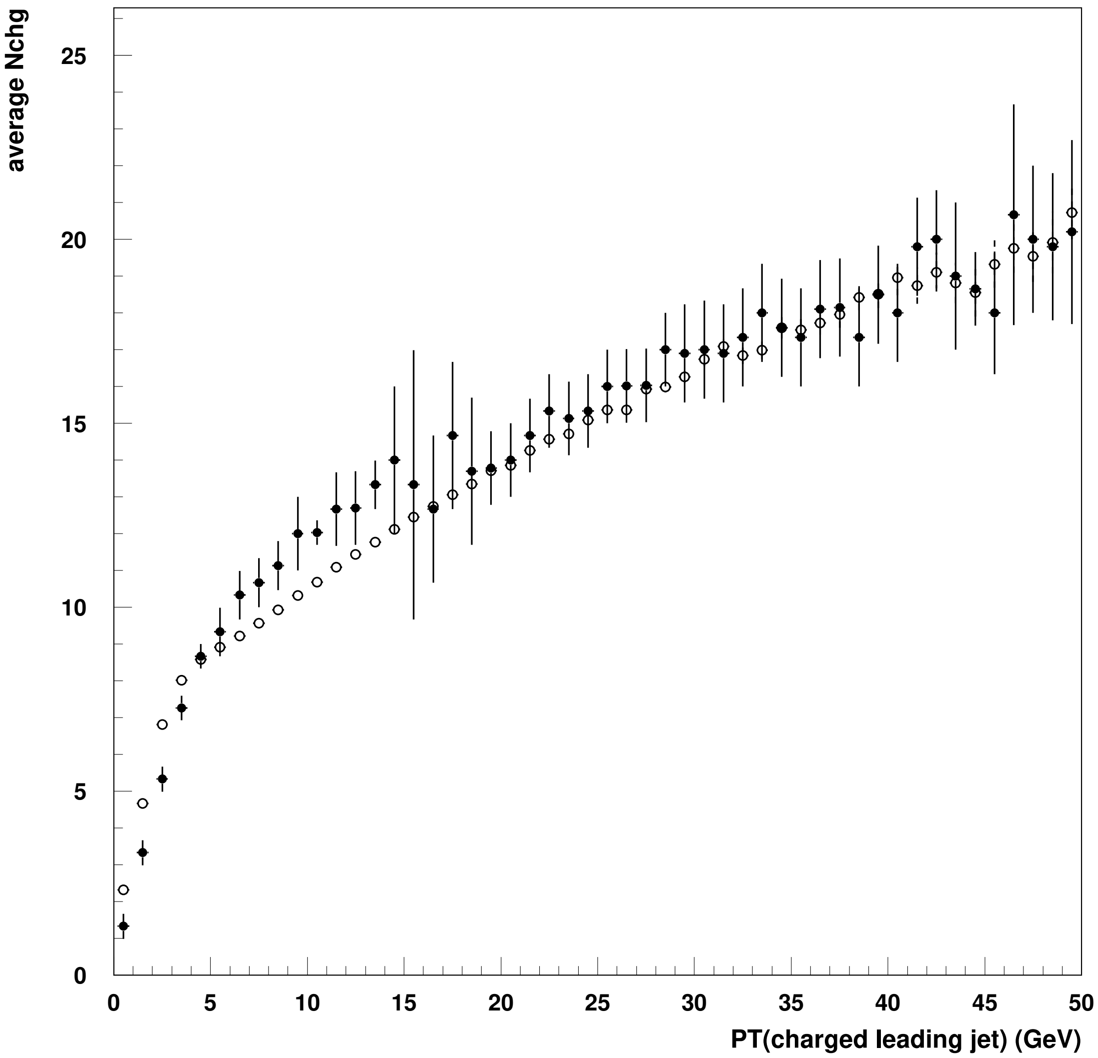

Figure 23: Plots shows the average total number charged particles in the event (PT> 0.5 GeV and $|\eta|$<1 including leading charged jet) as a function of the transverse momentum of the leading charged jet. The solid circles experimental data, hollow circles our (corrected) simulated data.

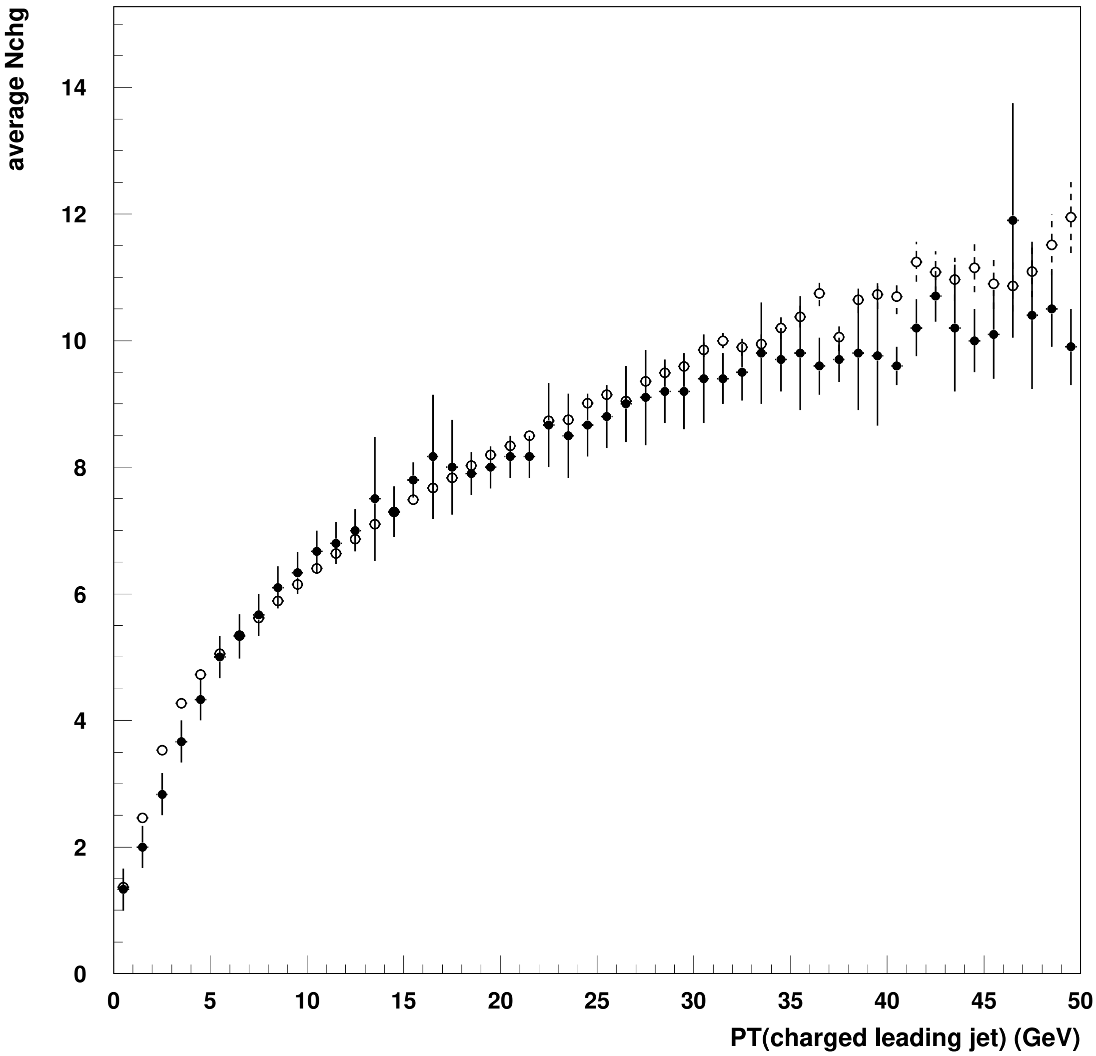

Figure 24: Plots shows the average number of charged particles (PT> 0.5 GeV and $|\eta|$<1) as function of PT(leading charged jet) for the toward region. The solid circles experimental data, hollow circles our (corrected) simulated data.

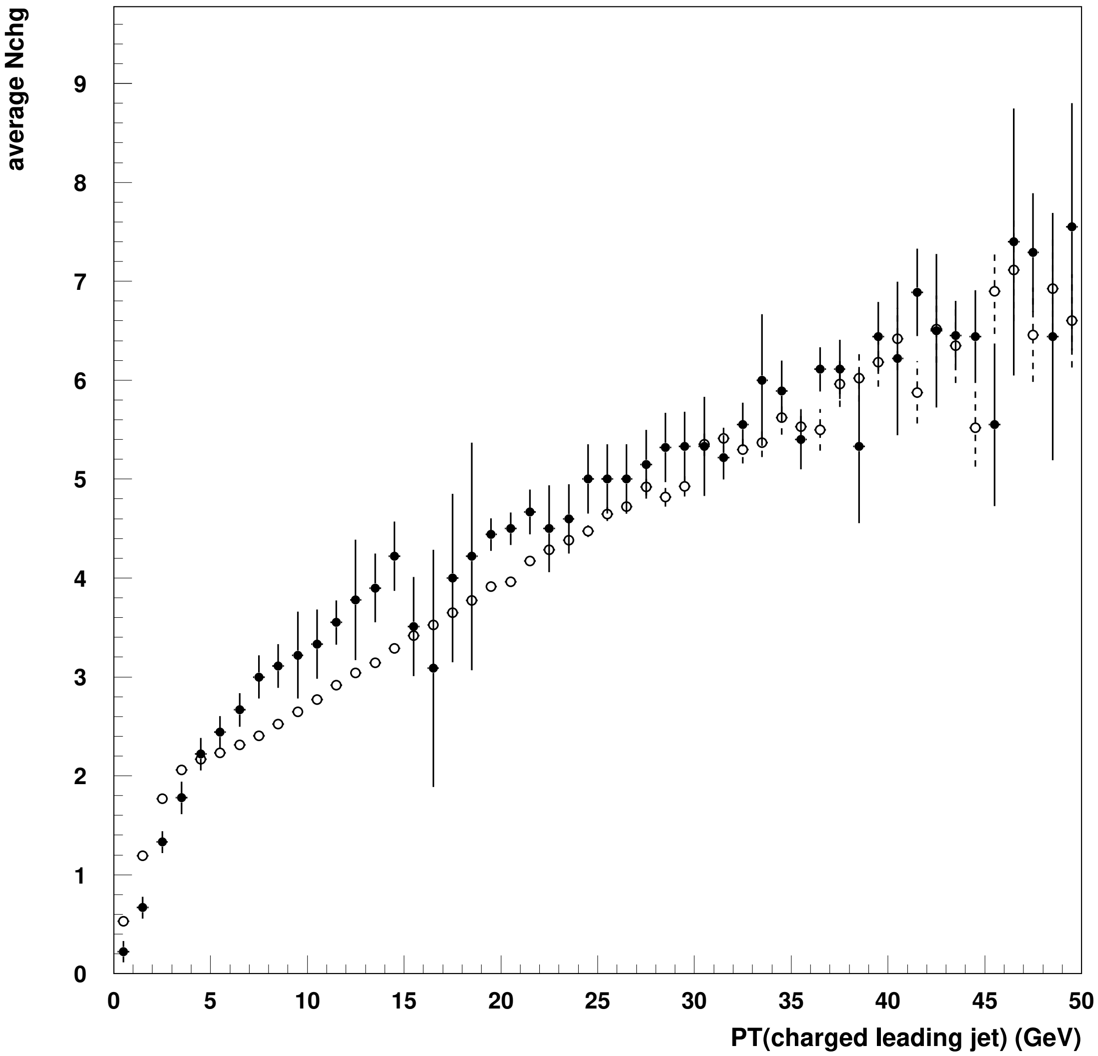

Figure 25: Plots shows the average number of charged particles (PT> 0.5 GeV and $|\eta|$<1) as function of PT(leading charged jet) for the away region. The solid circles experimental data, hollow circles our (corrected) simulated data.

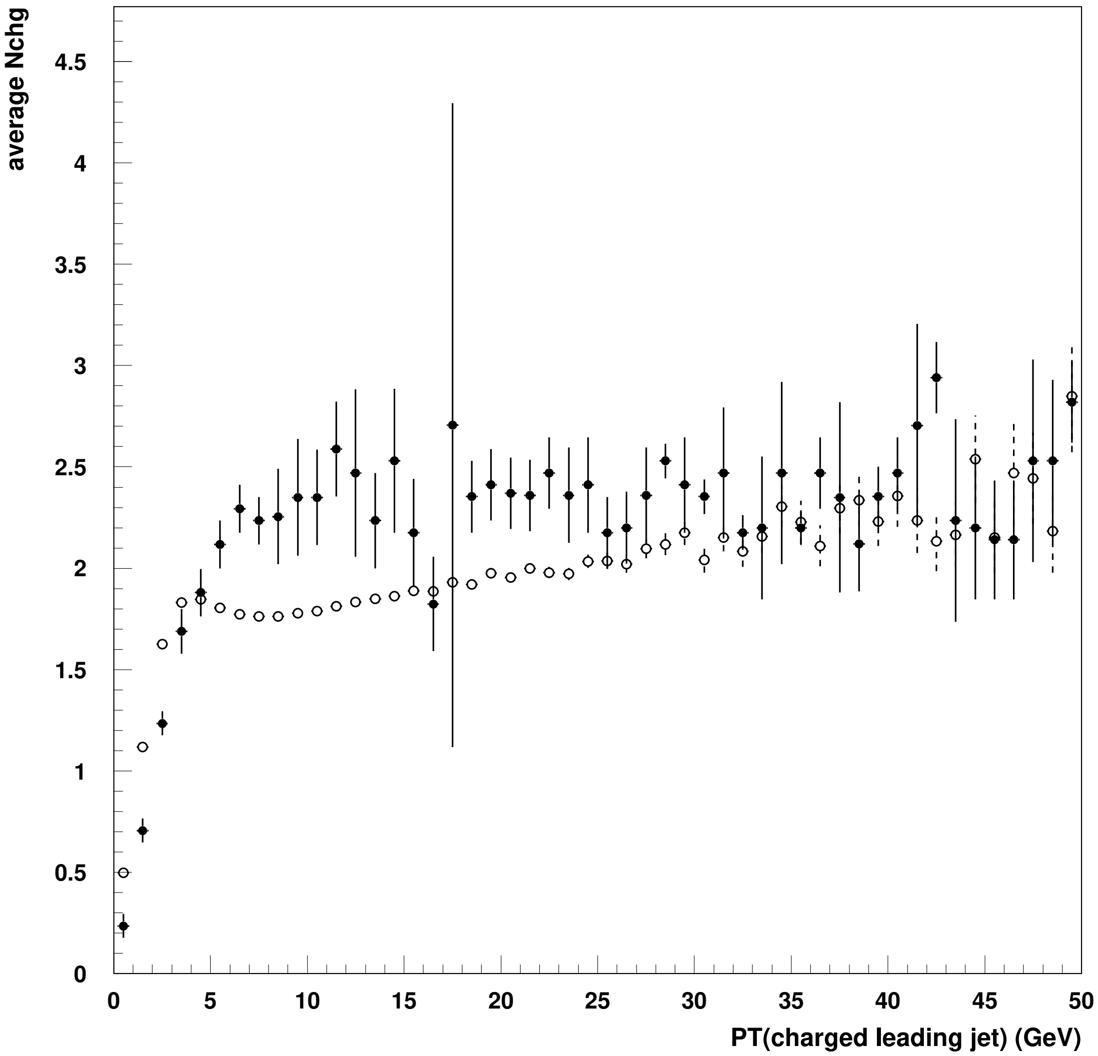

Figure 26: Plots shows the average number of charged particles (PT> 0.5 GeV and $|\eta|$<1) as function of PT(leading charged jet) for the transverse region. The solid circles experimental data, hollow circles our (corrected) simulated data.

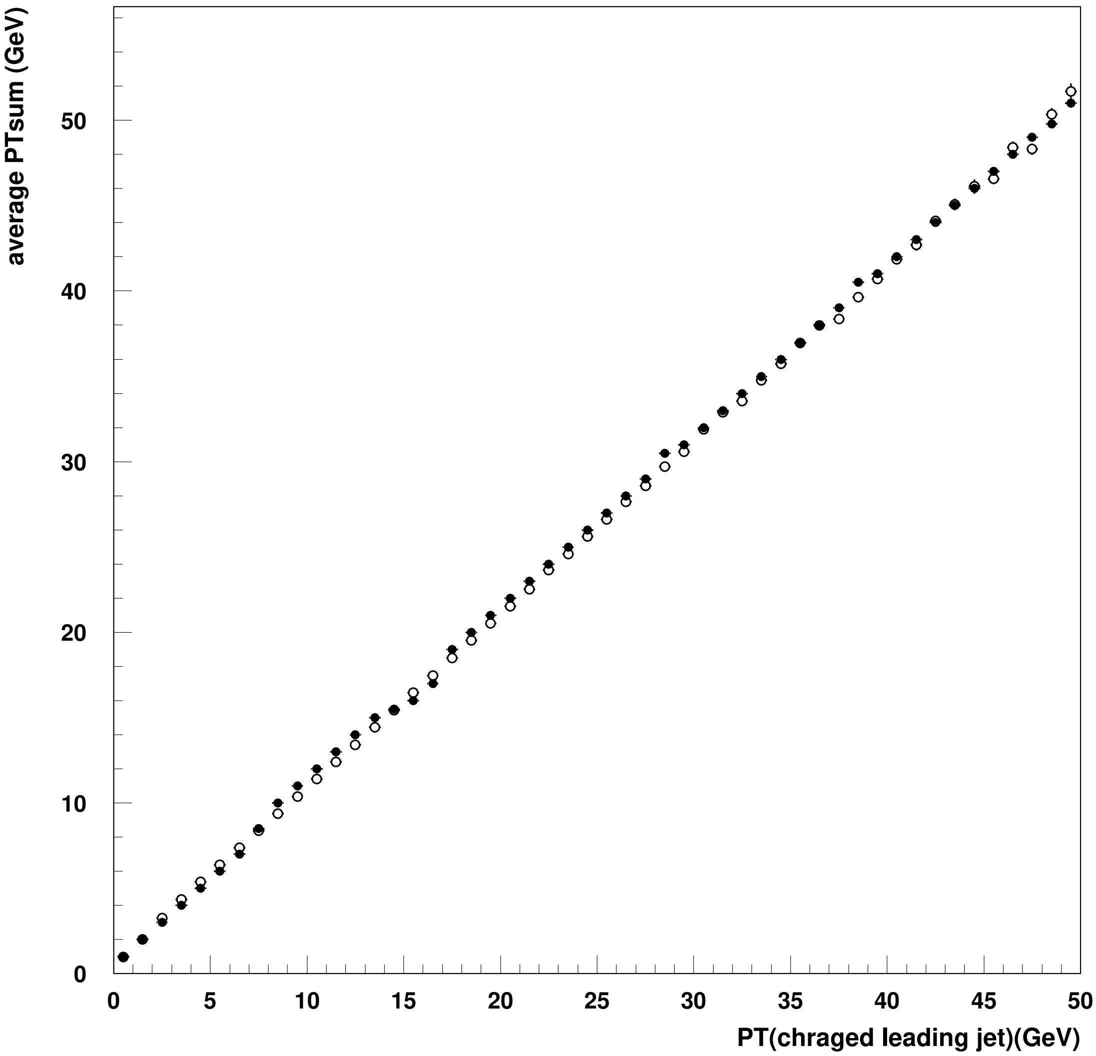

Figure 27: Plots shows the average PTsum of charged particles (PT> 0.5 GeV and $|\eta|<1$) as function of PT(leading charged jet) for the toward region. The solid circles experimental data, hollow circles our (corrected) simulated data.

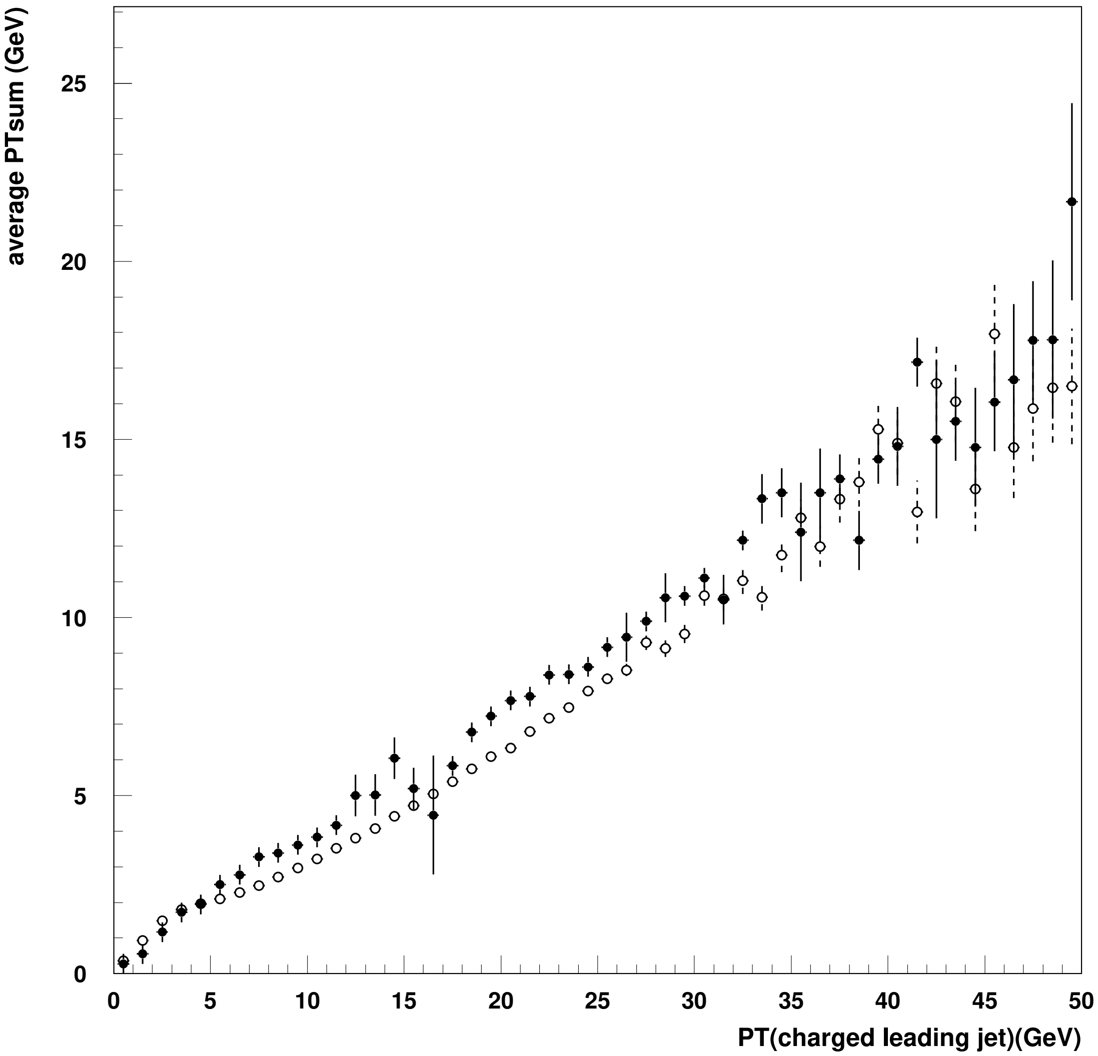

Figure 28: Plots shows the average PTsum of charged particles (PT> 0.5 GeV and $|\eta|<1$) as function of PT(leading charged jet) for the away region. The solid circles experimental data, hollow circles our (corrected) simulated data.

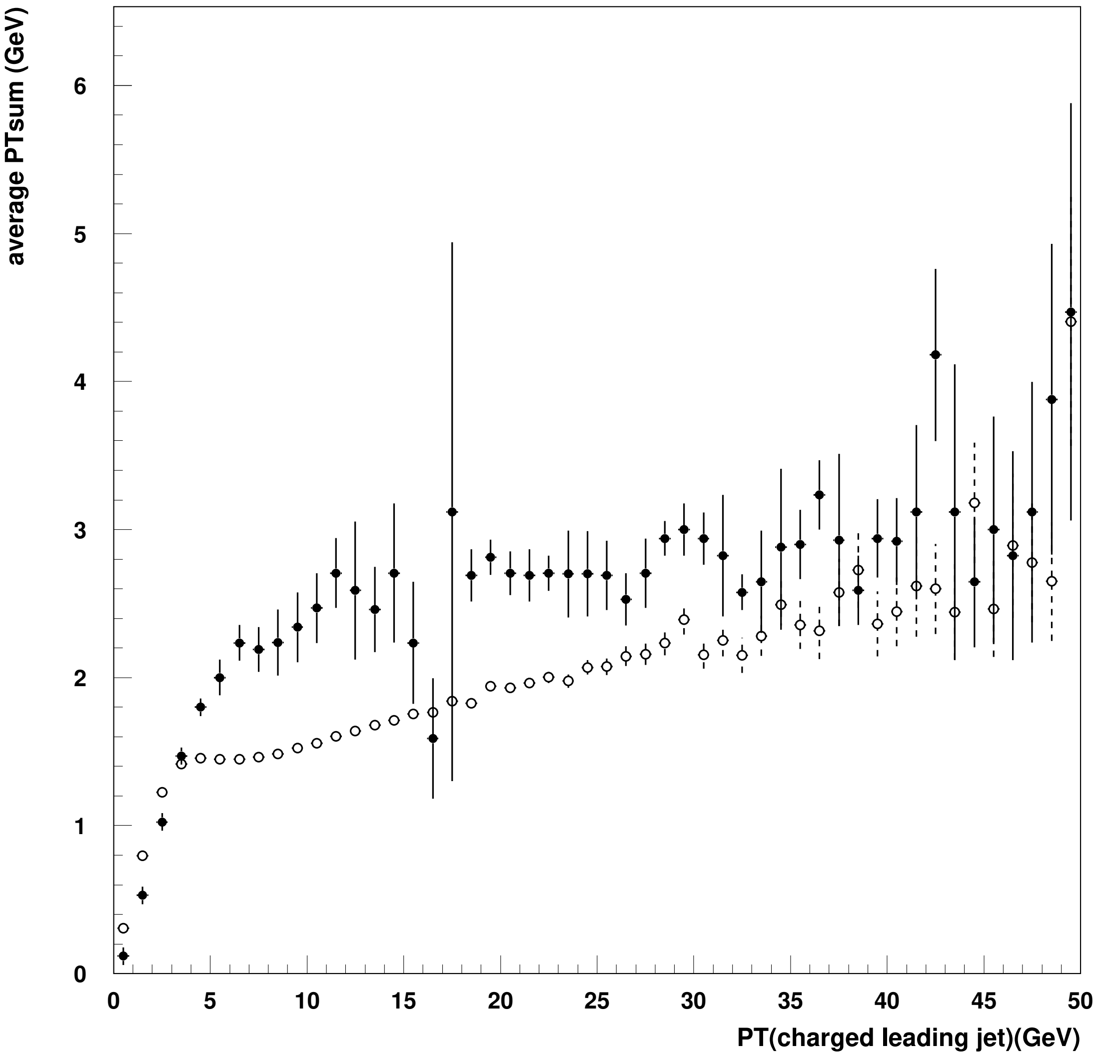

Figure 29: Plots shows the average PTsum of charged particles (PT> 0.5 GeV and $|\eta|$<1) as function of PT(leading charged jet) for the transverse region. The solid circles experimenatal data, hollow circles our (corrected) simulated data.

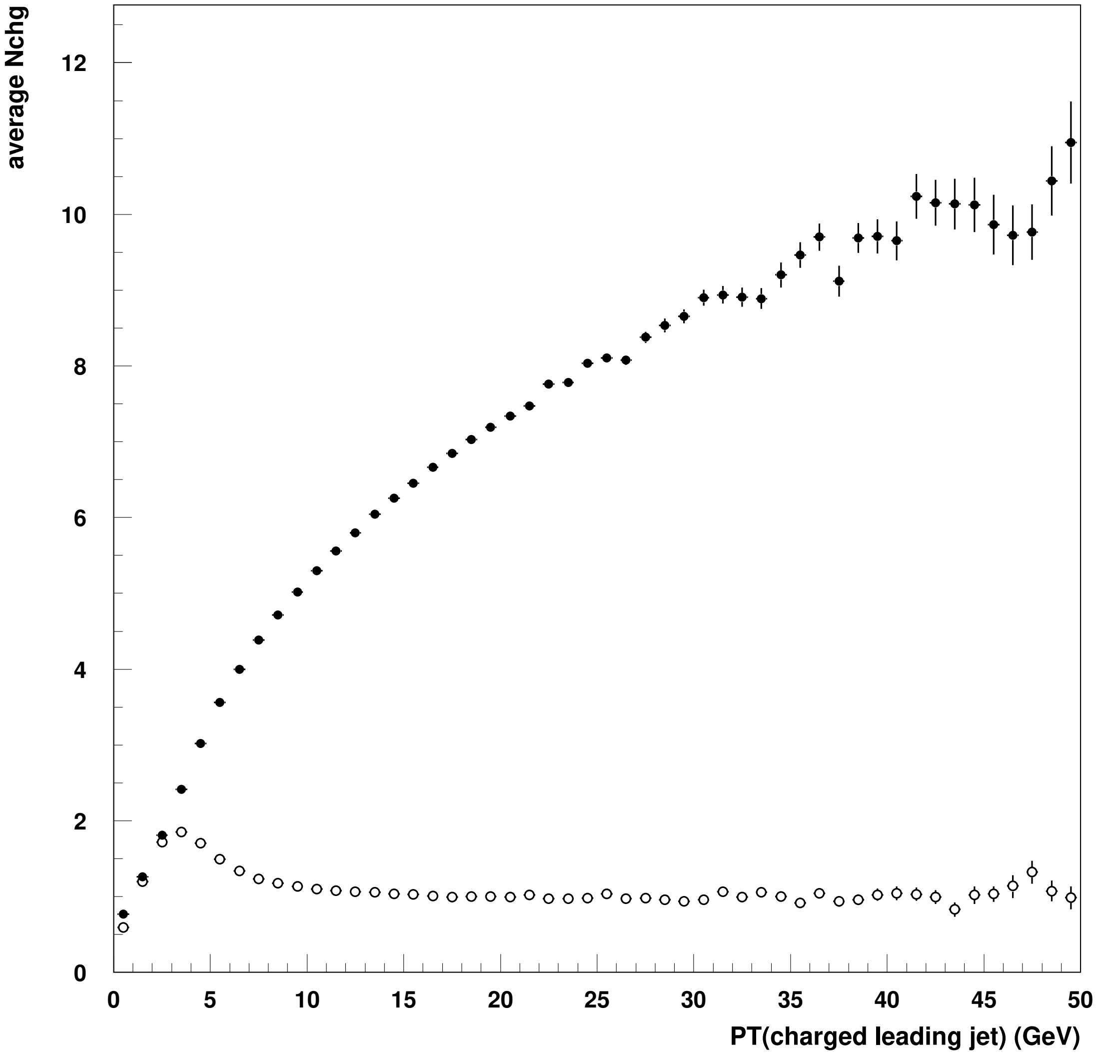

Figure 30: Plots shows the average number of charged particles (PT> 0.5 GeV and $|\eta|$<1) as function of PT(leading charged jet) for the toward region. HERWIG + Underlaying Soft model (PTmin=3.0 GeV, HERWIG parameters set to default). Solid circles particles originating in the hard scattering + (finial and initial state raditaion), hollow circles (particles originating in the beam-beam remnants interactions).

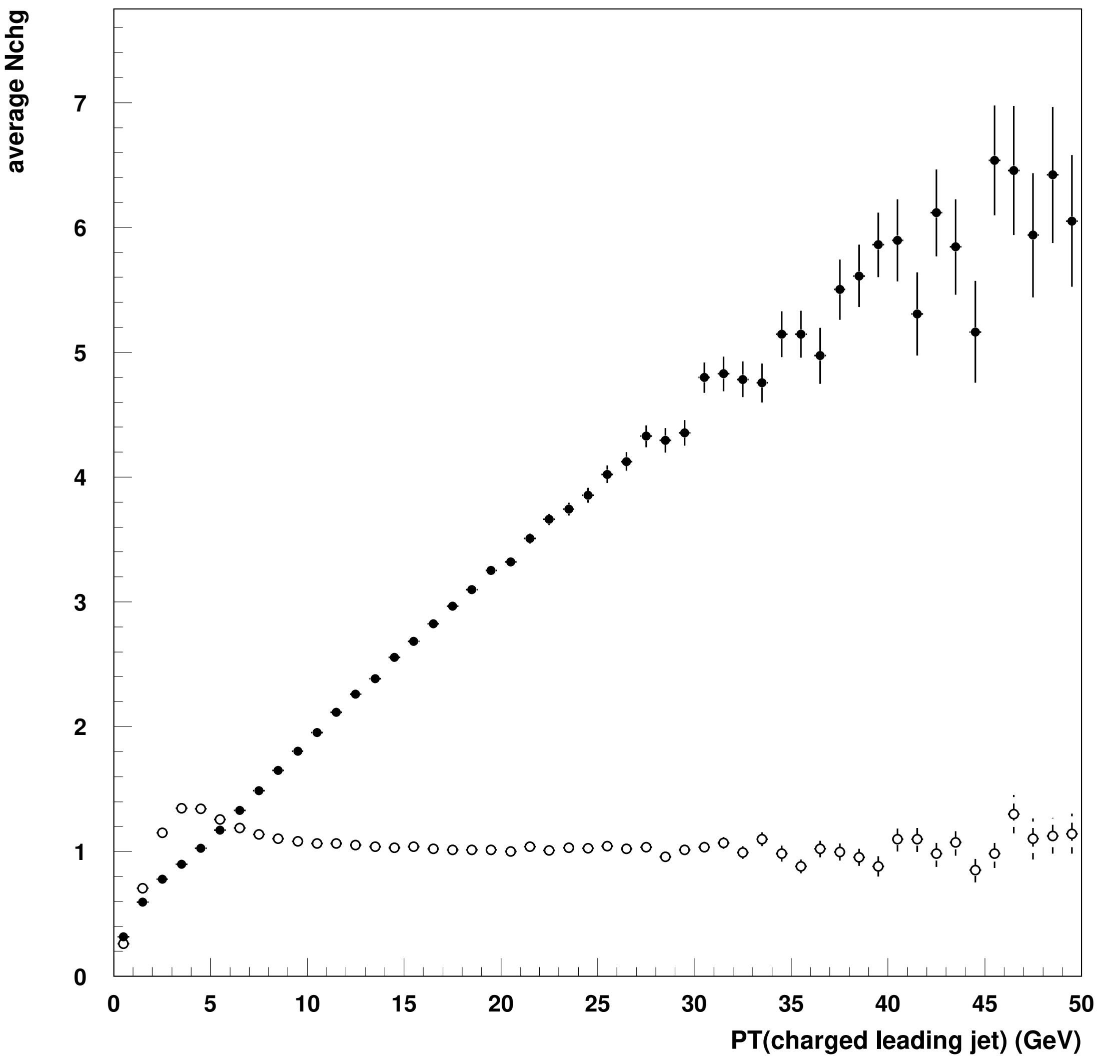

Figure 31: Plots shows the average number of charged particles (PT> 0.5 GeV and $|\eta|<1$) as function of PT(leading charged jet) for the away region. HERWIG + Underlying Soft model (PTmin=3.0 GeV, HERWIG parameters set to default) solid circles (particles originated in the hard scattering + (finial and initial state radiation)), hollow circles (particles originating in the beam-beam remnants interactions).

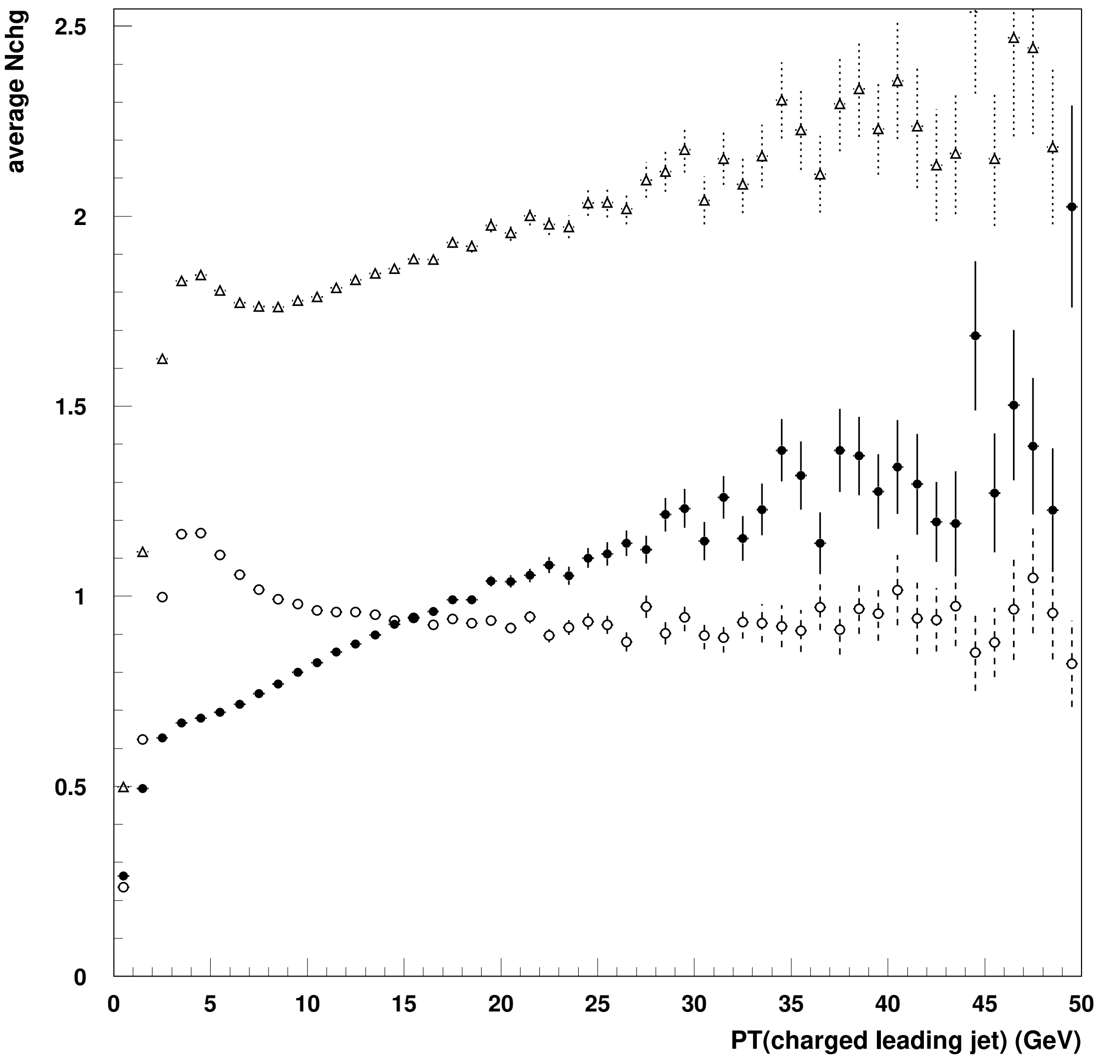

Figure 32: Plots shows the average number of charged particles (PT> 0.5 GeV and $|\eta|$<1) as function of PT(leading charged jet) for the transverse region. HERWIG + Underlying Soft model (PTmin=3.0 GeV, HERWIG parameters set to default) solid circles (particles originated in the hard scattering + (finial and initial state radiation)), hollow circles (particles originating in the beam-beam remnants interactions), triangles total.

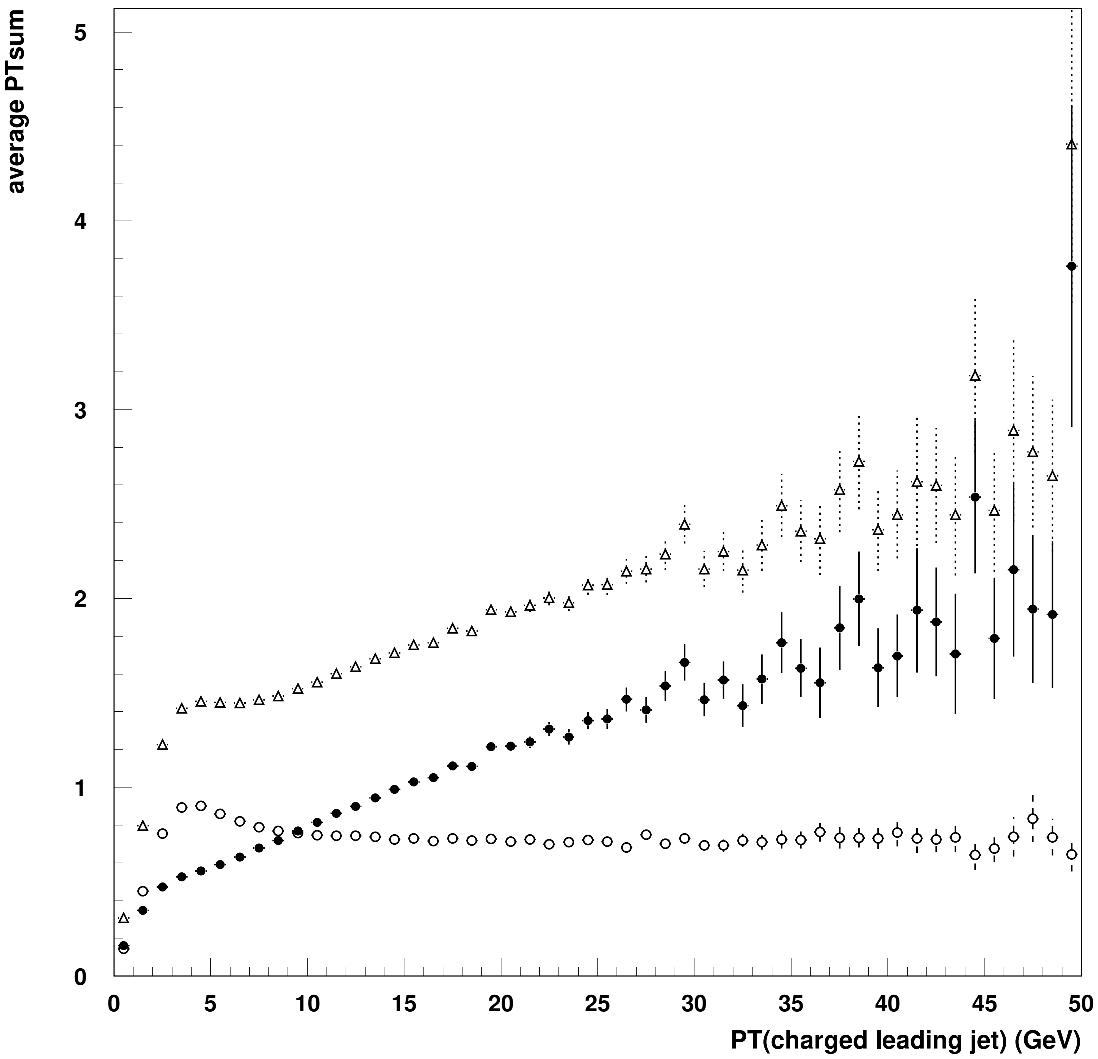

Figure 33: Plots shows the average scalar PTsum of charged particles (PT> 0.5 GeV and $|\eta|<1$) as function of PT(leading charged jet) for the transverse region. HERWIG + Underlying Soft model (PTmin=3.0 GeV, HERWIG parameters set to default) solid circles (particles originated in the hard scattering + (finial and initial state raditaion)), hollow circles (particles originating in the beam-beam remnants interactions), triangles total.

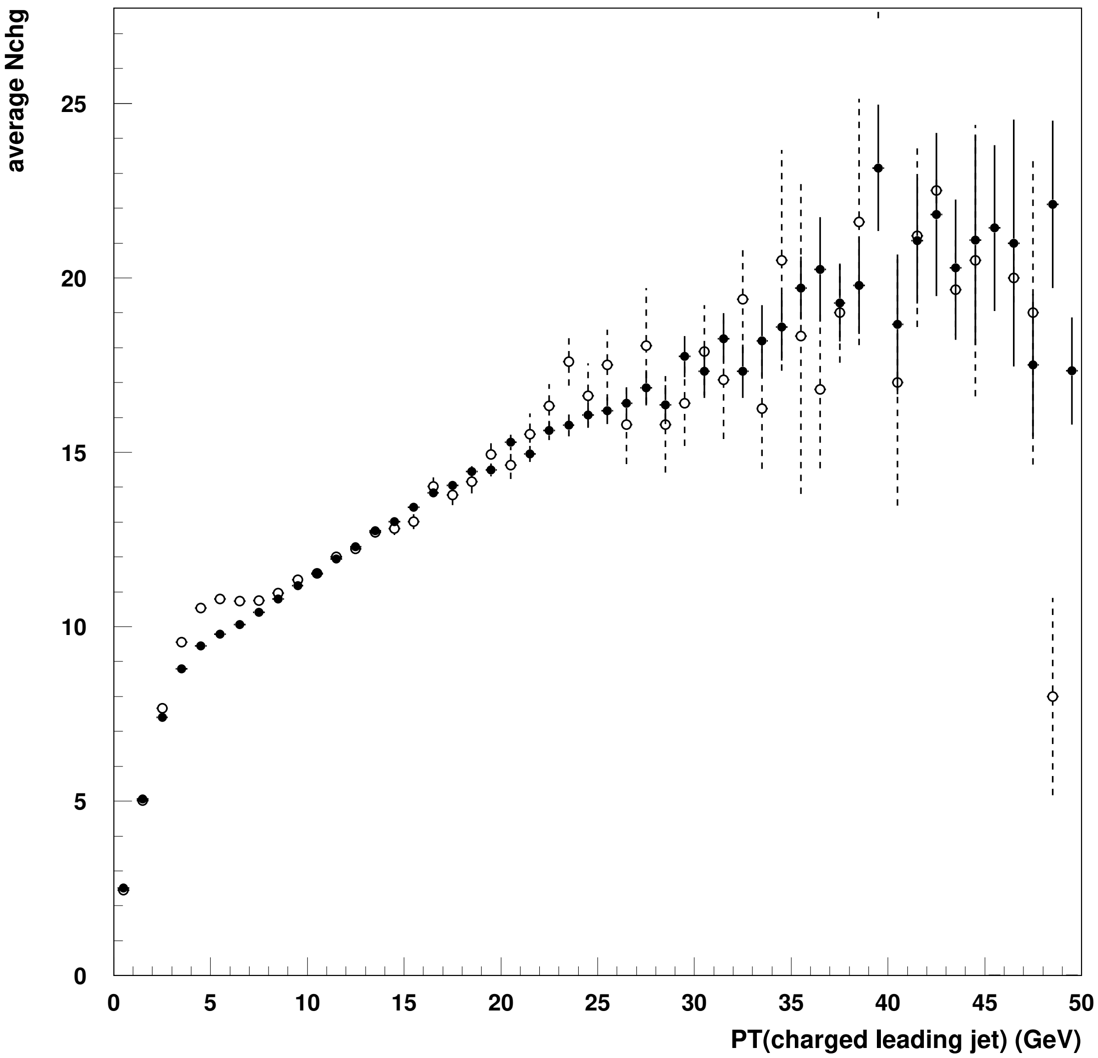

Figure 34: Plots shows the average total number of charged particles in the event (PT> 0.5 GeV and $|\eta|$<1 including leading charged jet) as a function of the transverse momentum of the leading charged jet. HERWIG + Underlying Soft model (PDF=CTEQ4L), solid circles (PTmin=3.0 GeV), hollow circles (PTmin=2.0 GeV).

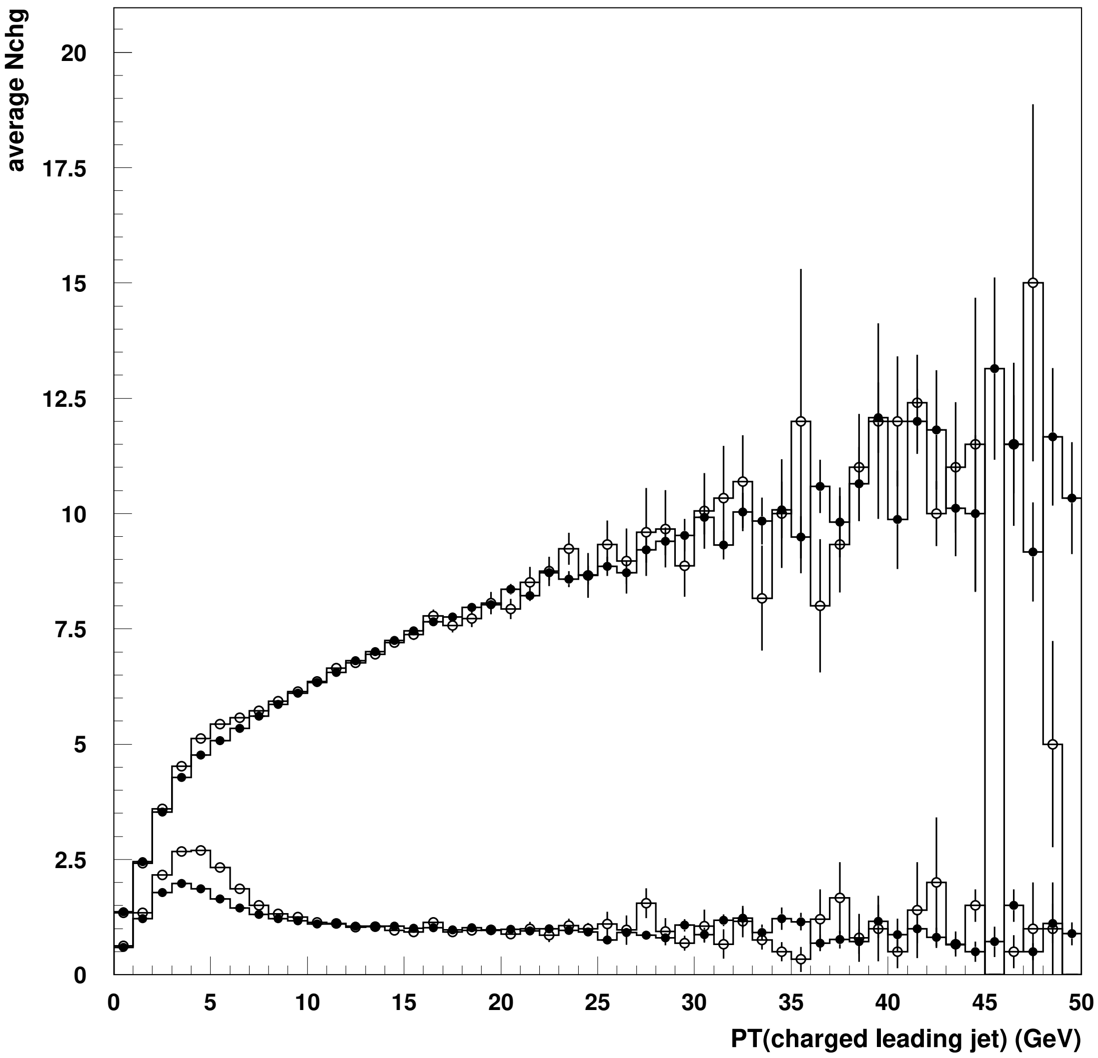

Figure 35: Plots shows the average number of charged particles (PT> 0.5 GeV and $|\eta|<1$) as function of PT(leading charged jet) for the toward region. The two curves below the two total <Nchg> represent the beam-beam remnant contribution. Data simulated with HERWIG + Soft Underlying model (PDF=CTEQ4L), solid circles PTmin=3.0 GeV, hollow circles PTmin=2.0 GeV.

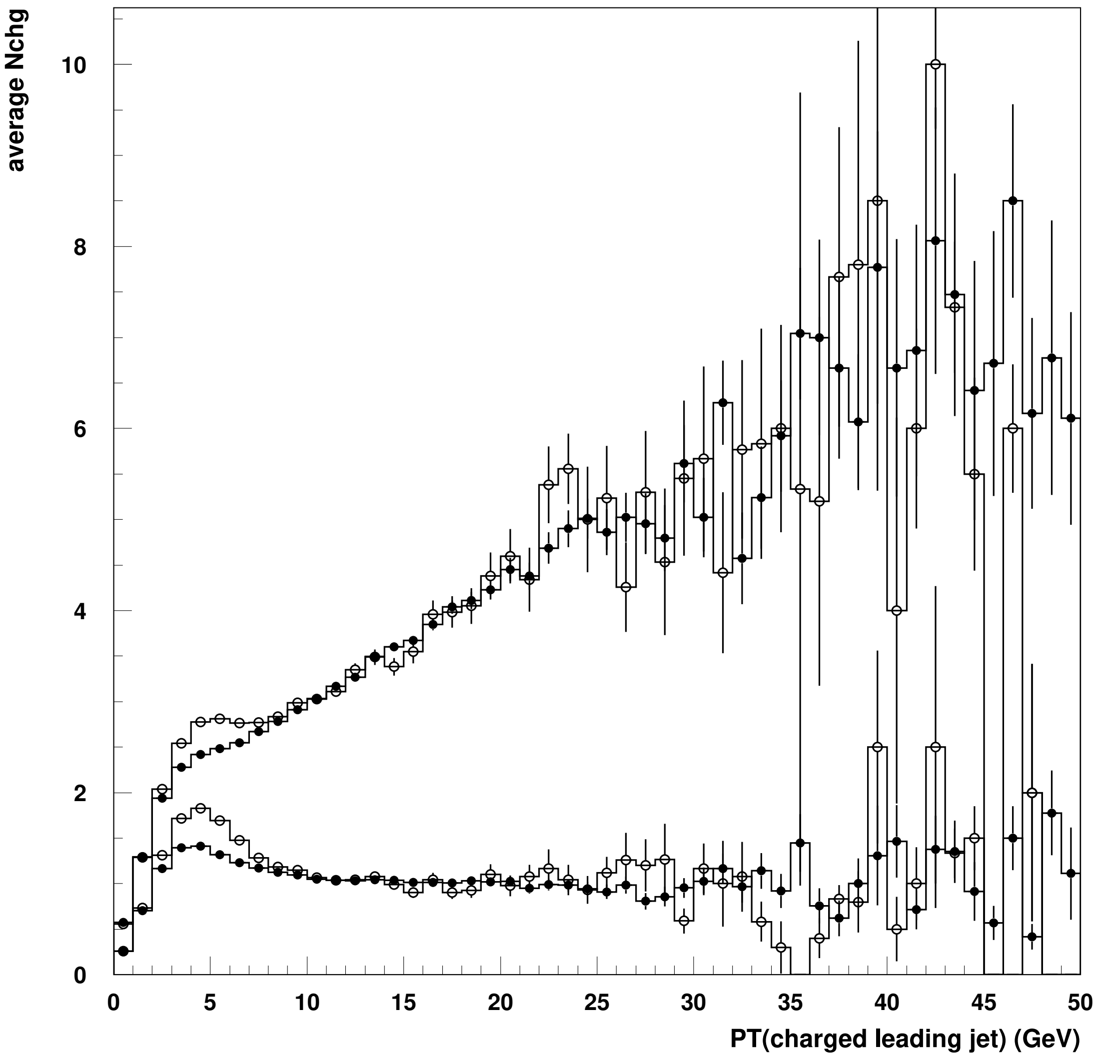

Figure 36: Plots shows the average number of charged particles (PT> 0.5 GeV and $|\eta|$<1) as function of PT(leading charged jet) for the away region. The two curves below the two total <Nchg> represent the beam-beam remnant contribution. Data simulated with HERWIG + Soft Underlying model (PDF=CTEQ4L), the solid circles PTmin=3.0 GeV, hollow circles PTmin=2.0 GeV.

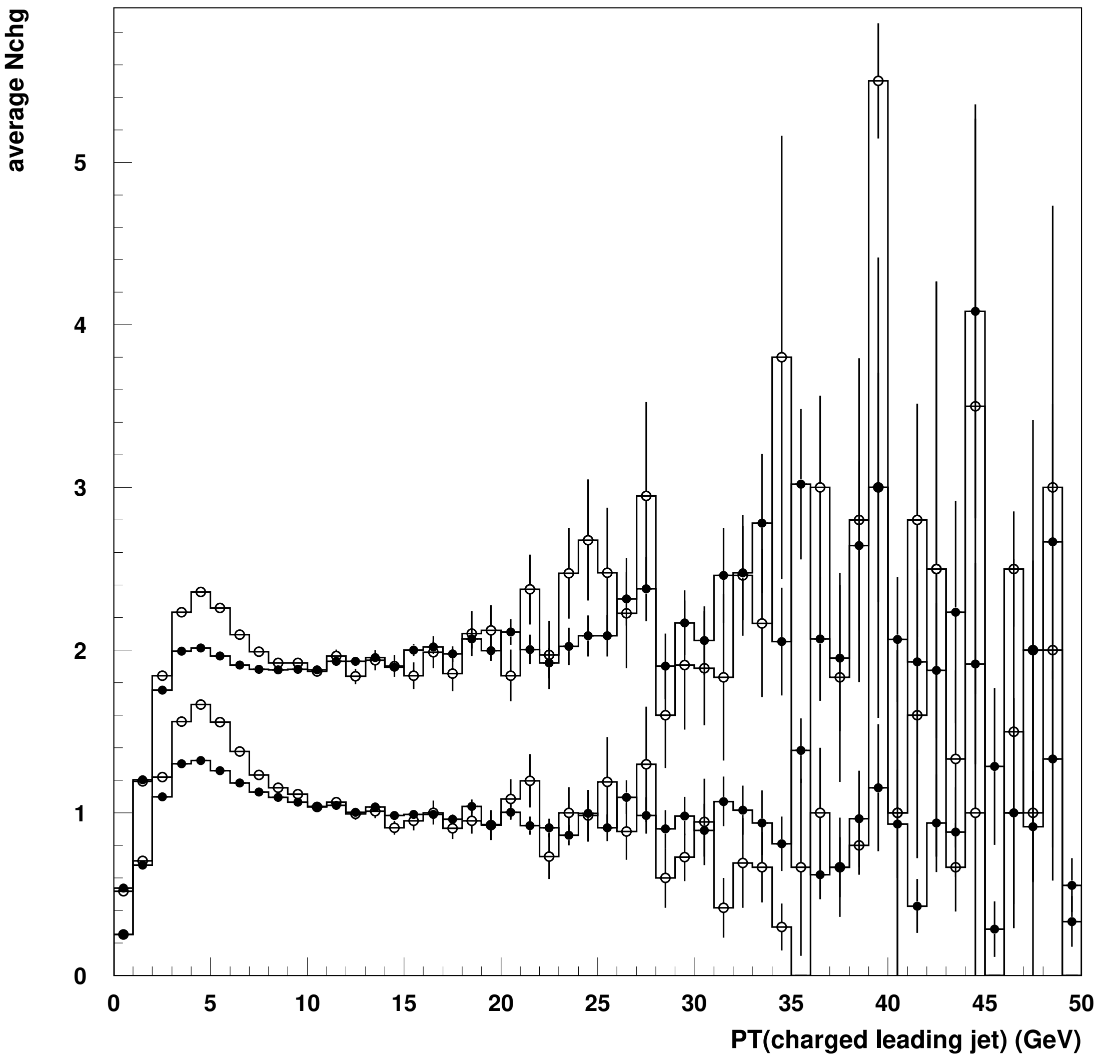

Figure 37: Plots shows the average number of charged particles (PT> 0.5 GeV and $|\eta|$<1) as function of PT(leading charged jet) for the transverse region. The two curves below the two total <Nchg> represent the beam-beam remnant contribution. Data simulated with HERWIG + Soft Underlying model (PDF=CTEQ4L), the solid circles PTmin=3.0 GeV, hollow circles PTmin=2.0 GeV.

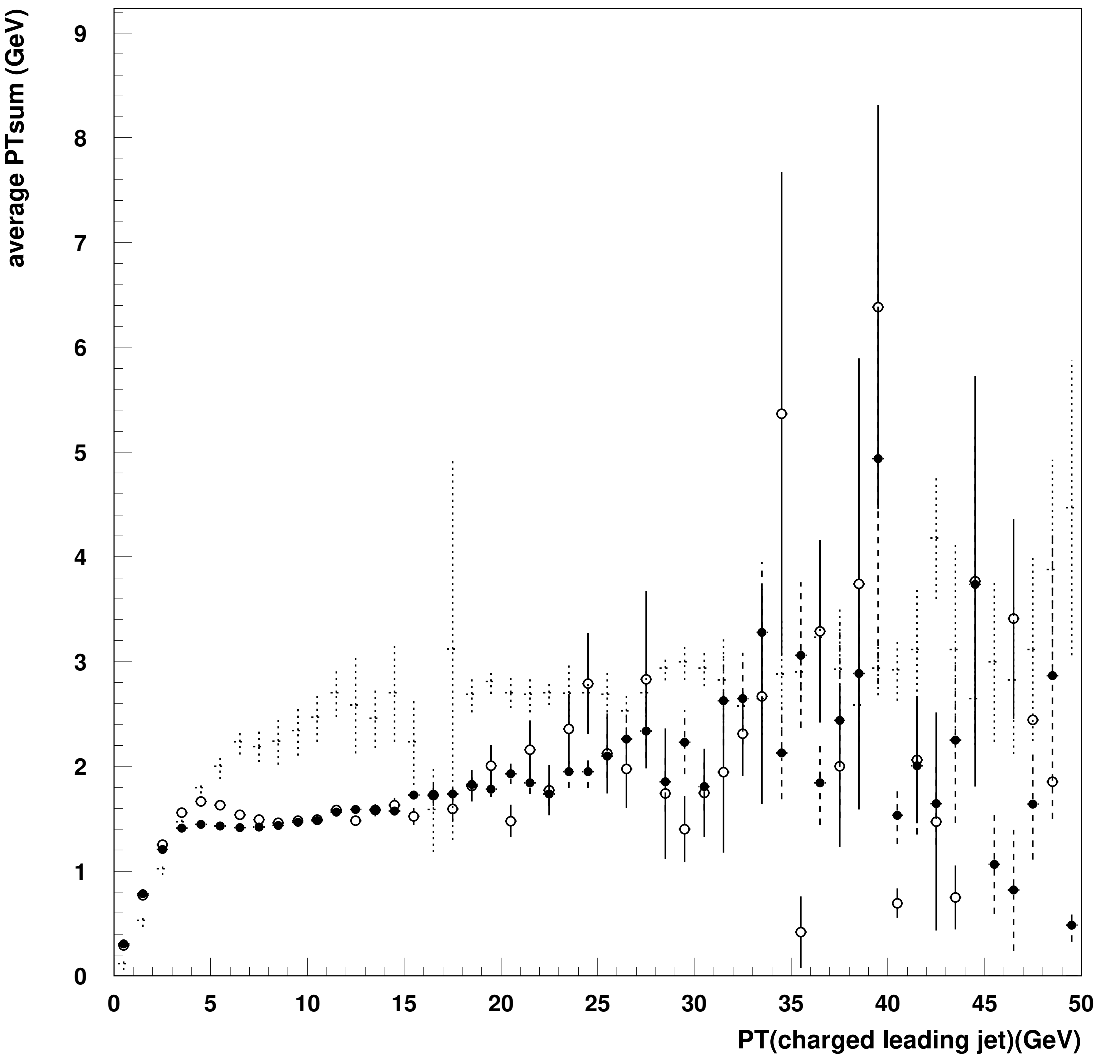

Figure 38: Plots shows the average scalar PTsum of charged particles (PT> 0.5 GeV and $|\eta|<1$) as function of PT(leading charged jet) for the transverse region. Data simulated with HERWIG + Soft Underlying model (PDF=CTEQ4L), the solid circles PTmin=3.0 GeV, hollow circles PTmin=2.0 GeV, dashed line experimental data.

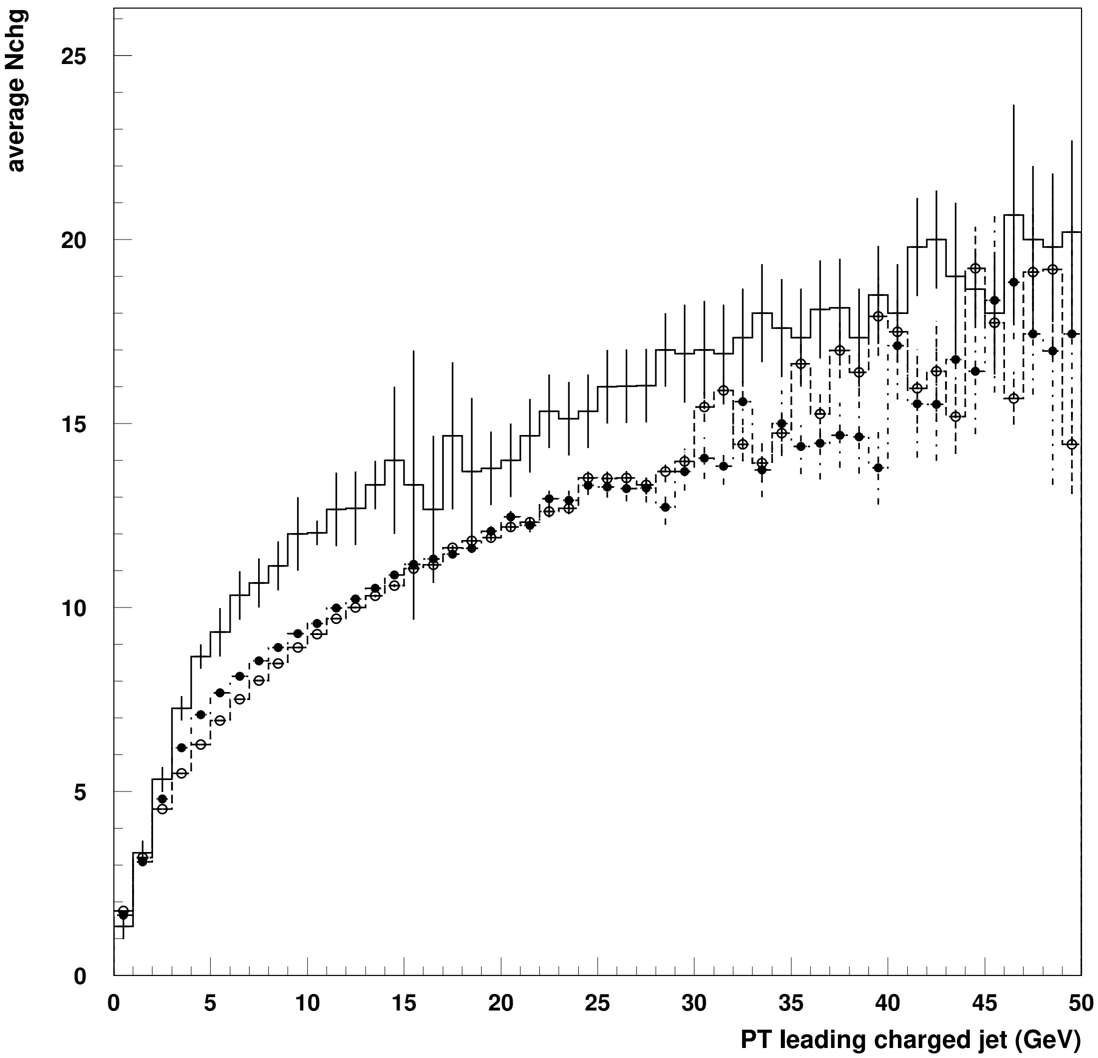

Figure 39: Plots shows the average total number of charged particles in the event (PT> 0.5 GeV and $|\eta|<1$ including leading charged jet) as a function of the transverse momentum of the leading charged jet. HERWIG + Multiparton model, solid circles (PDF=DO(set 1), PTmin=2.0 GeV), hollow circles (PDF=CTEQ4L, PTmin=3.0 GeV).

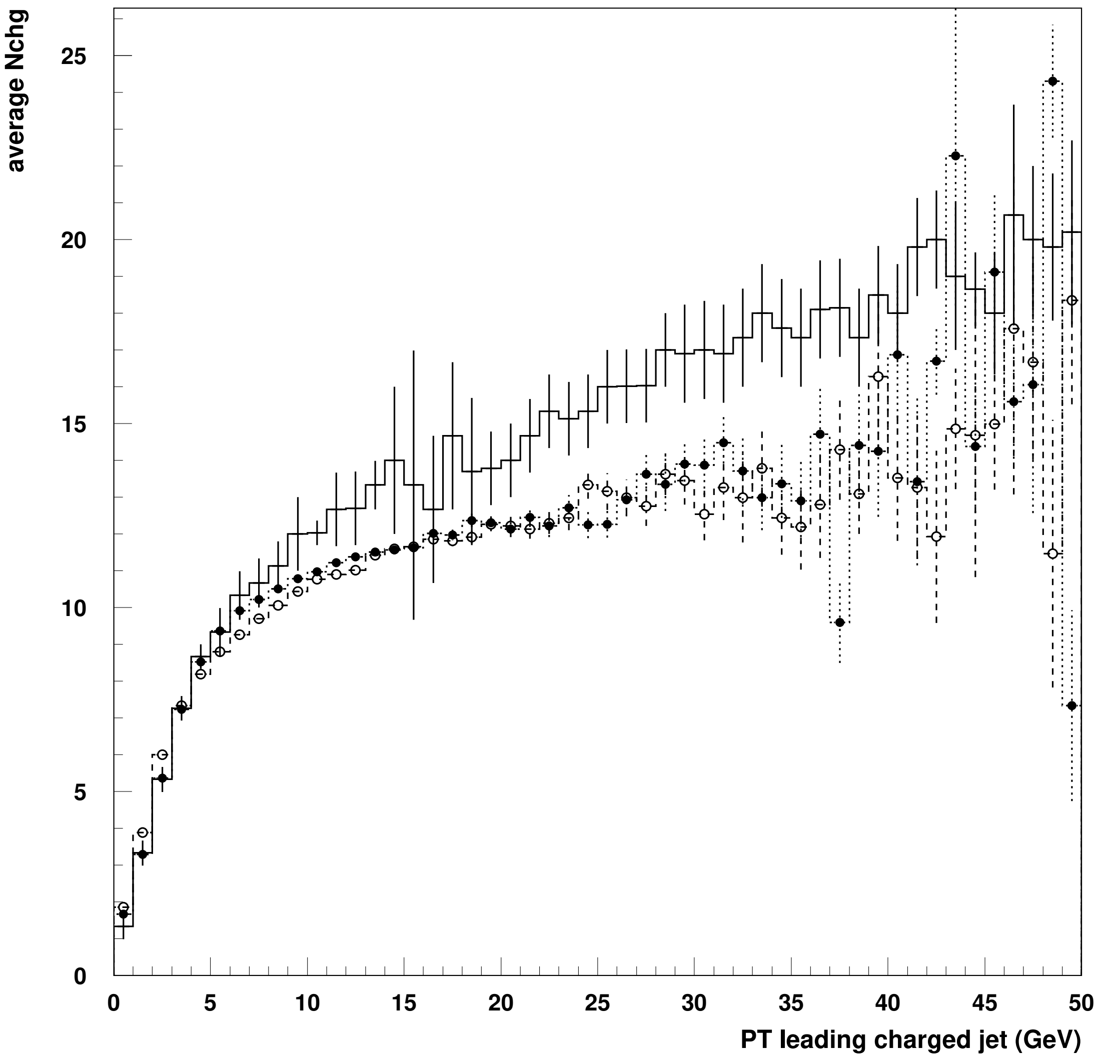

Figure 40: Plots shows the average total number of charged particles in the event (PT> 0.5 GeV and $|\eta|$<1 including leading charged jet) as a function of the transverse momentum of the leading charged jet. HERWIG + Multiparton model, solid circles (PDF=GRV, PTmin=2.2 GeV), hollow circles (PDF=CTEQ4L, PTmin=2.0 GeV).

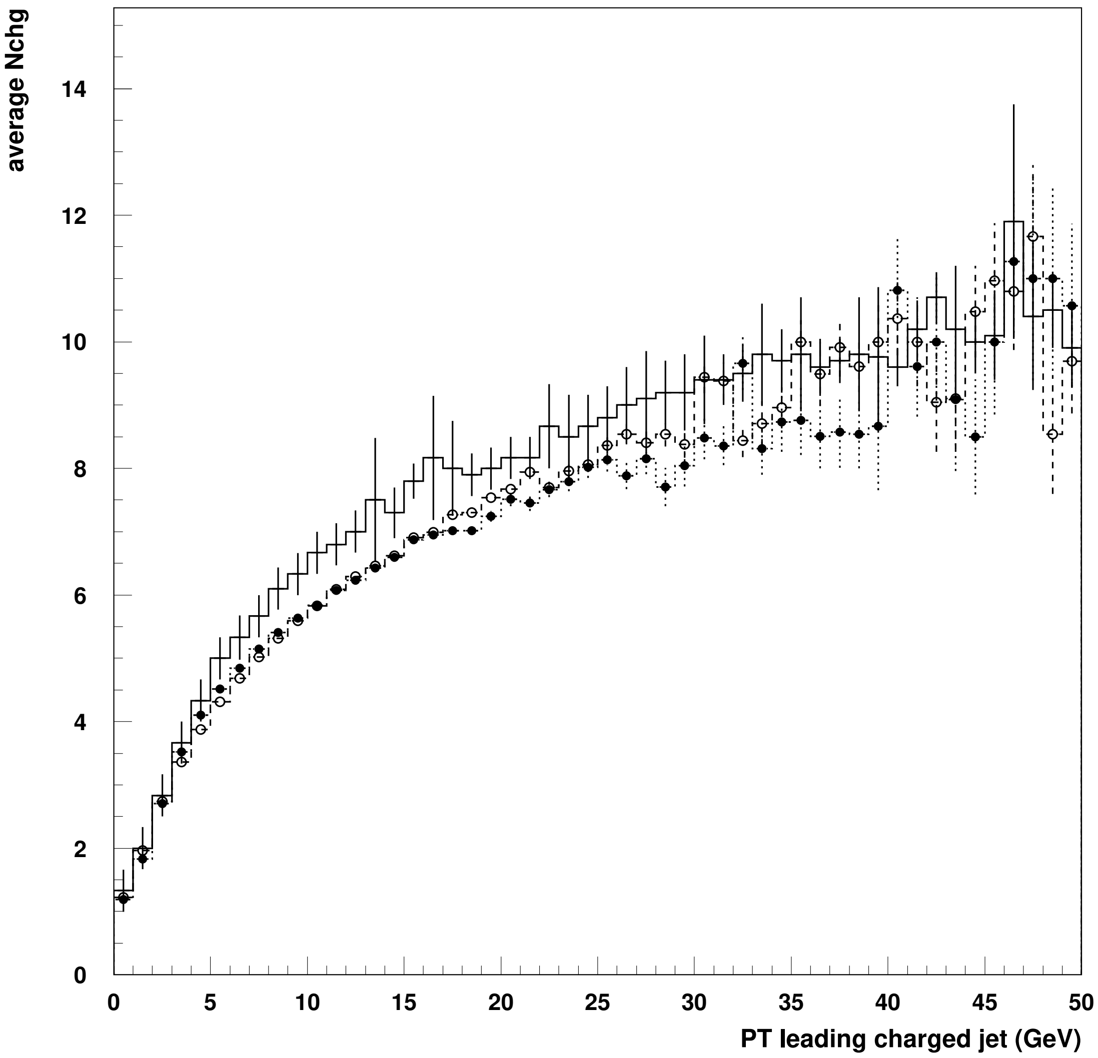

Figure 41: Plots shows the average number of charged particles (PT> 0.5 GeV and $|\eta|$<1) as function of PT(leading charged jet) for the toward region. HERWIG + Multiparton model, solid circles (PDF=DO(set 1), PTmin=2.0 GeV), hollow circles (PDF=CTEQ4L, PTmin=3.0 GeV).

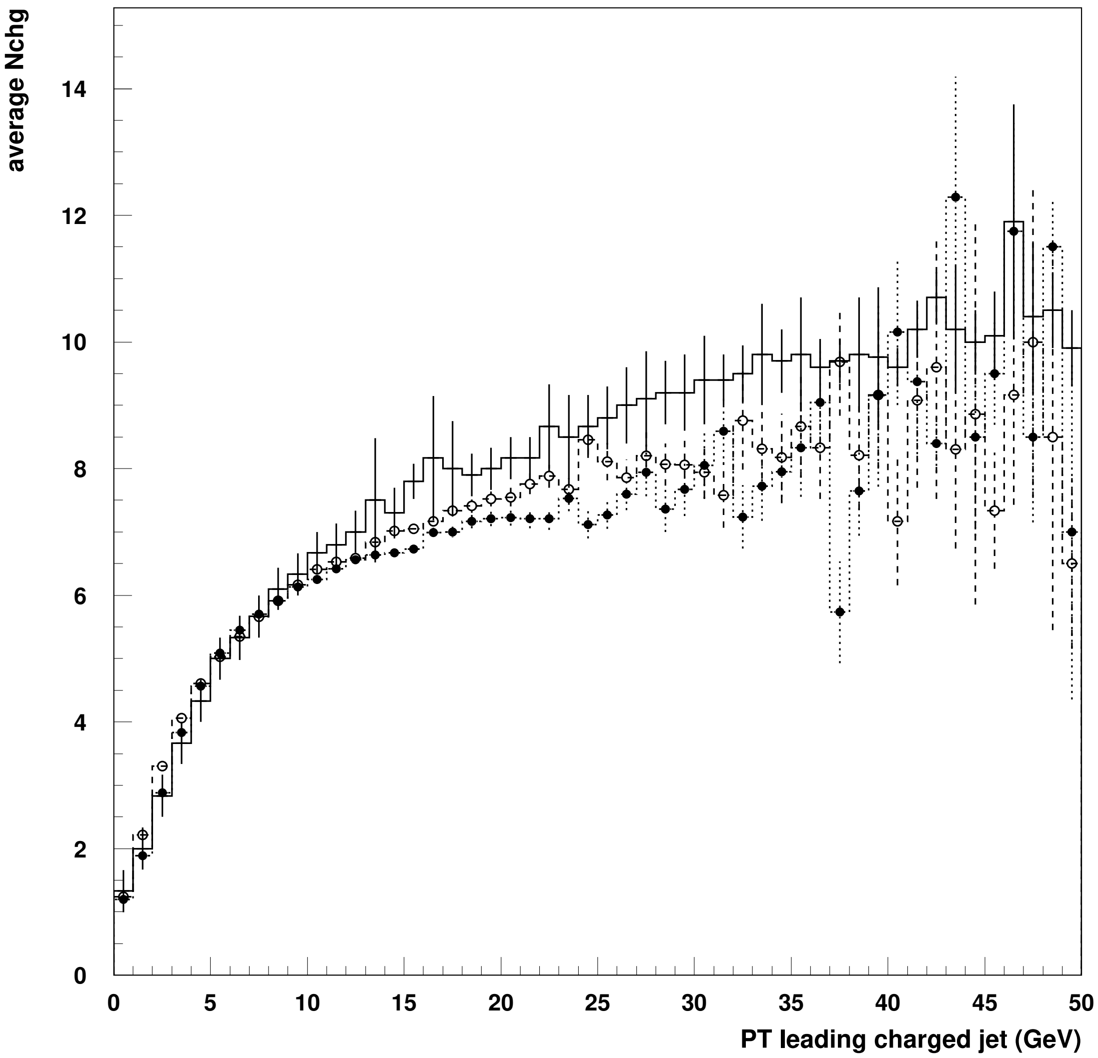

Figure 42: Plots shows the average number of charged particles (PT> 0.5 GeV and $|\eta|<1$) as function of PT(leading charged jet) for the toward region. HERWIG + Multiparton model, solid circles (PDF=GRV, PTmin=2.2 GeV), hollow circles (PDF=CTEQ4L, PTmin=2.0 GeV).

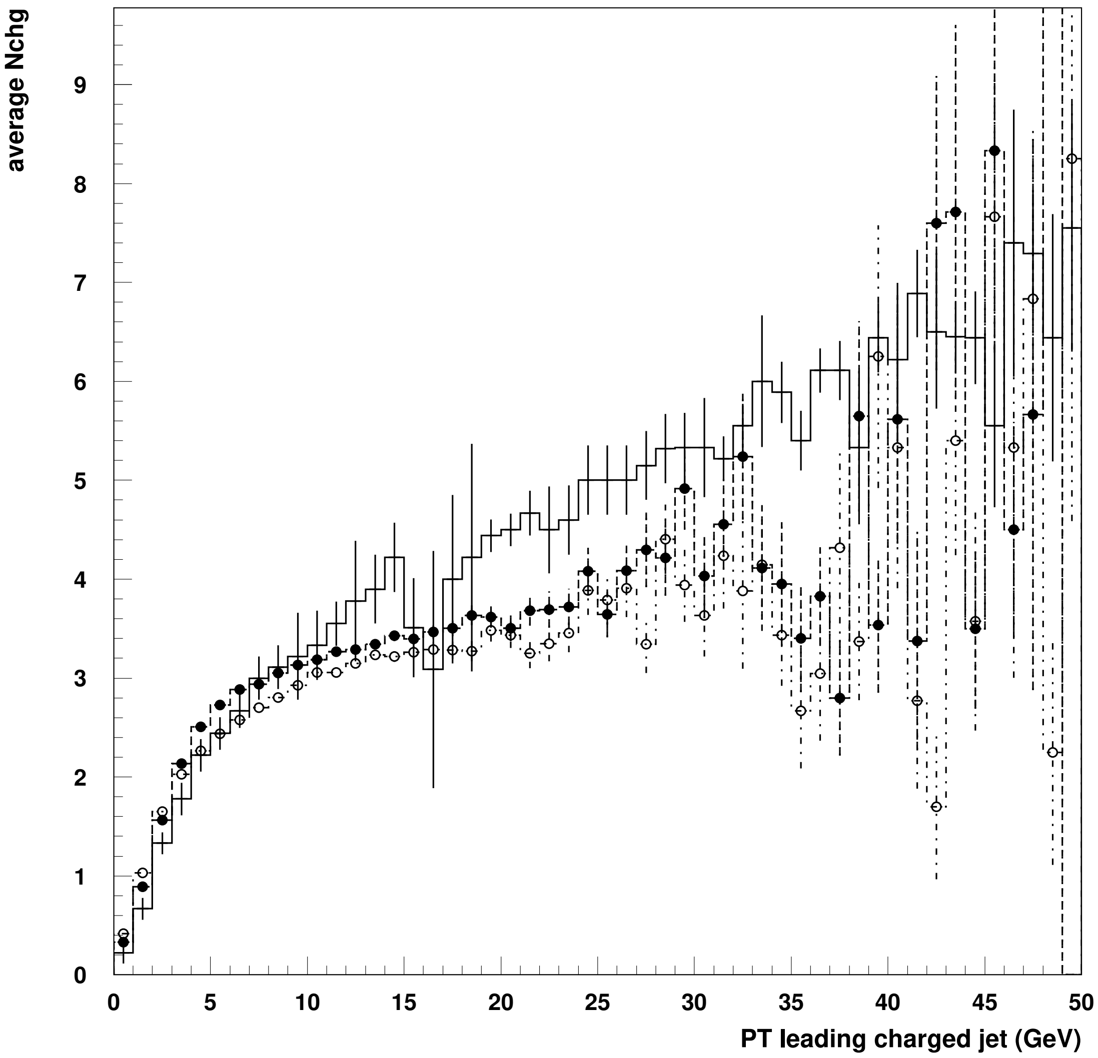

Figure 43: Plots shows the average number of charged particles (PT> 0.5 GeV and $|\eta|$<1) as function of PT(leading charged jet) for the away region. HERWIG + Multiparton model, solid circles (PDF=GRV ,PTmin=2.2 GeV), hollow circles (PDF=CTEQ4L PTmin=2.0 GeV).

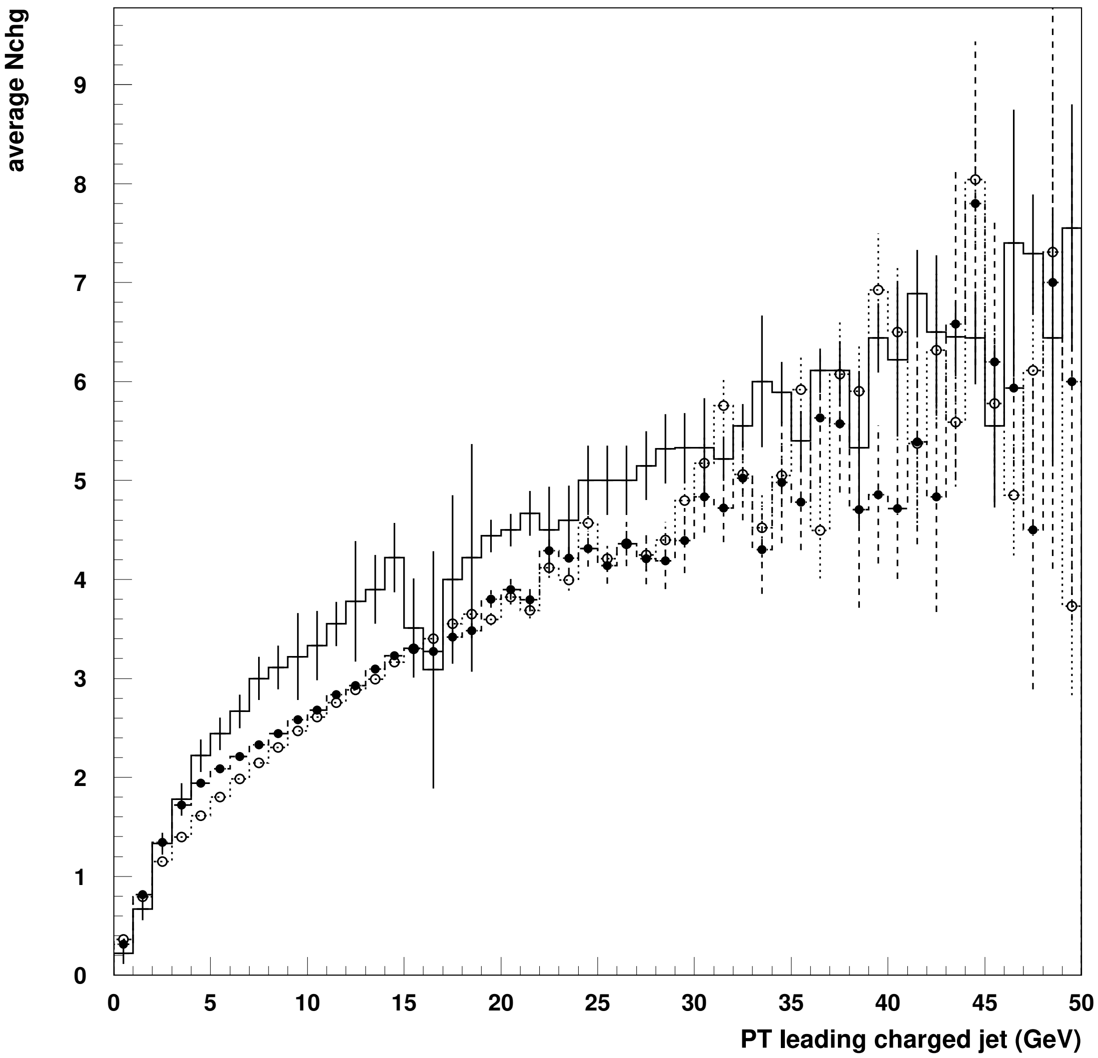

Figure 44: Plots shows the average number of charged particles (PT> 0.5 GeV and $|\eta|<1$) as function of PT(leading charged jet) for the away region. HERWIG + Multiparton model, solid circles (PDF=DO(set 1), PTmin=2.0 GeV), hollow circles (PDF=CTEQ4L, PTmin=3.0 GeV).

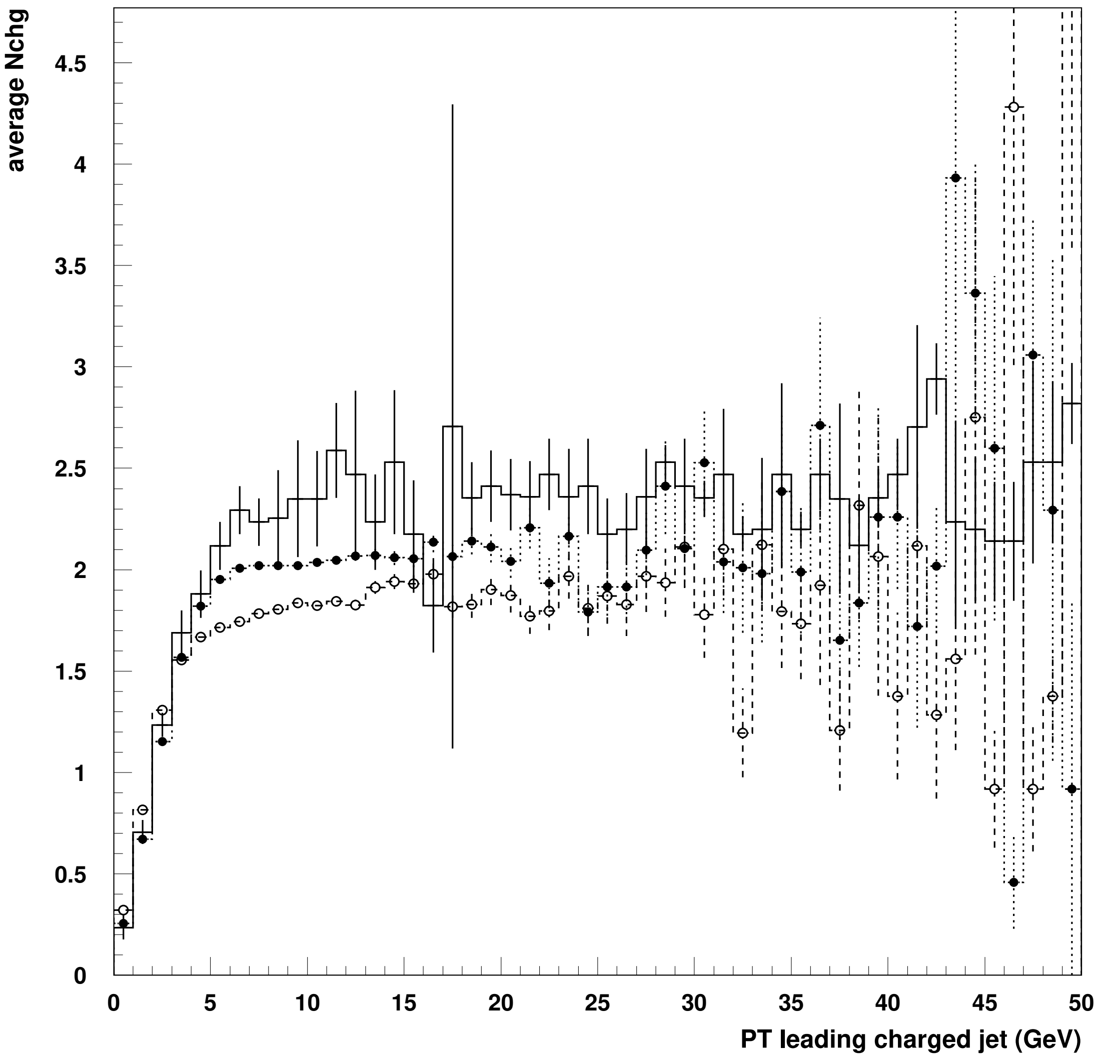

Figure 45: Plots shows the average number of charged particles (PT> 0.5 GeV and $|\eta|<1$) as function of PT(leading charged jet) for the transverse region. HERWIG + Multiparton model solid circles (PDF=GRV, PTmin=2.2 GeV), hollow circles (PDF=CTEQ4L, PTmin=2.0 GeV).

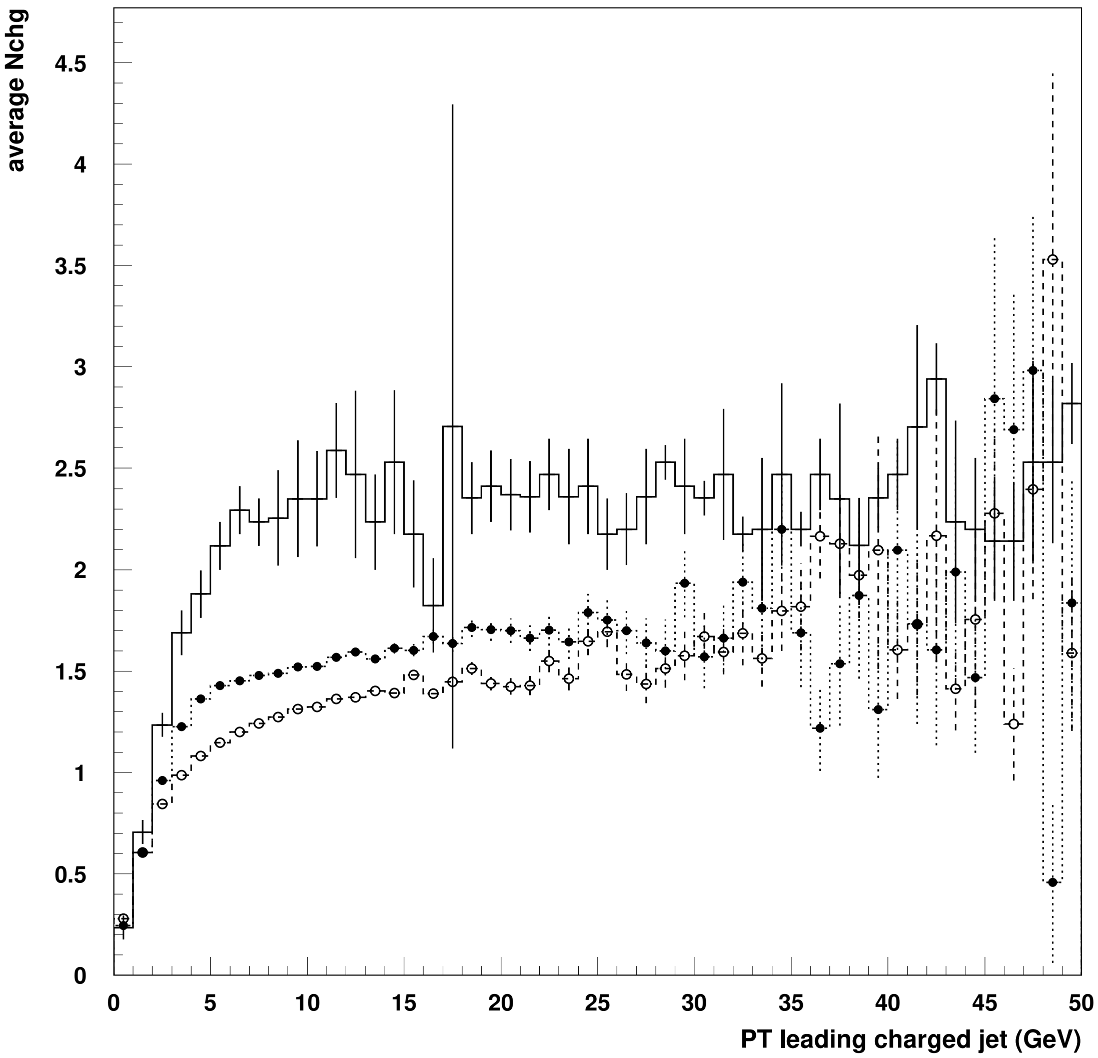

Figure 46: Plots shows the average number of charged particles (PT> 0.5 GeV and $|\eta|$<1) as function of PT(leading charged jet) for the transverse region. HERWIG + Multiparton model solid circles (PDF=DO(set 1), PT-min=2.0 GeV), hollow circles (PDF=CTEQ4L, PTmin=3.0 GeV).

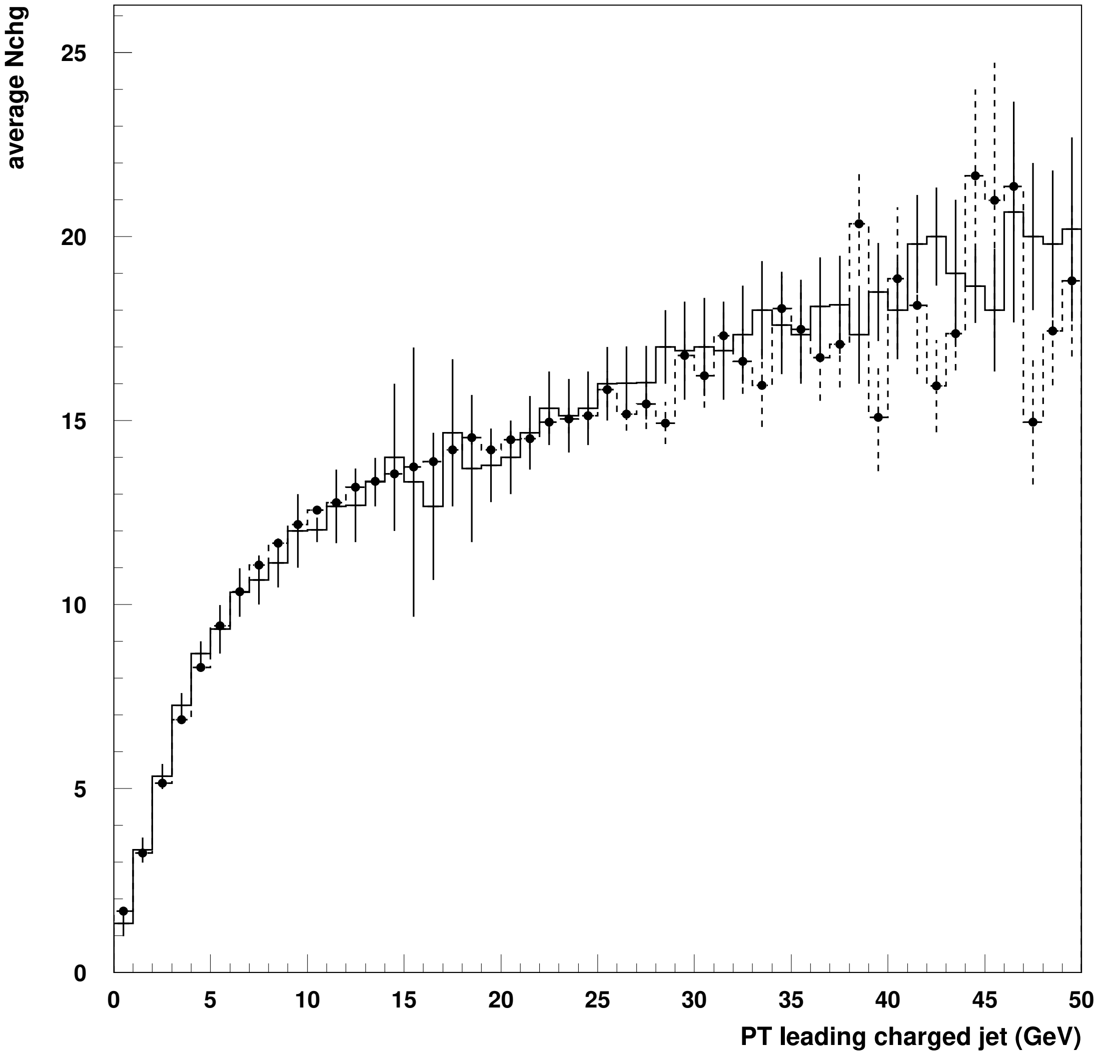

Figure 47: Plots shows the average total number charged particles in the event (PT> 0.5 GeV and $|\eta|$<1 including leading charged jet) as a function of the transverse momentum of the leading charged jet. HERWIG + Multiparton model (PDF=CTEQ4L, PTmin=3.0 GeV, proton radius decreased by a factor of 1.73), solid circles simulated data, solid line experimental data.

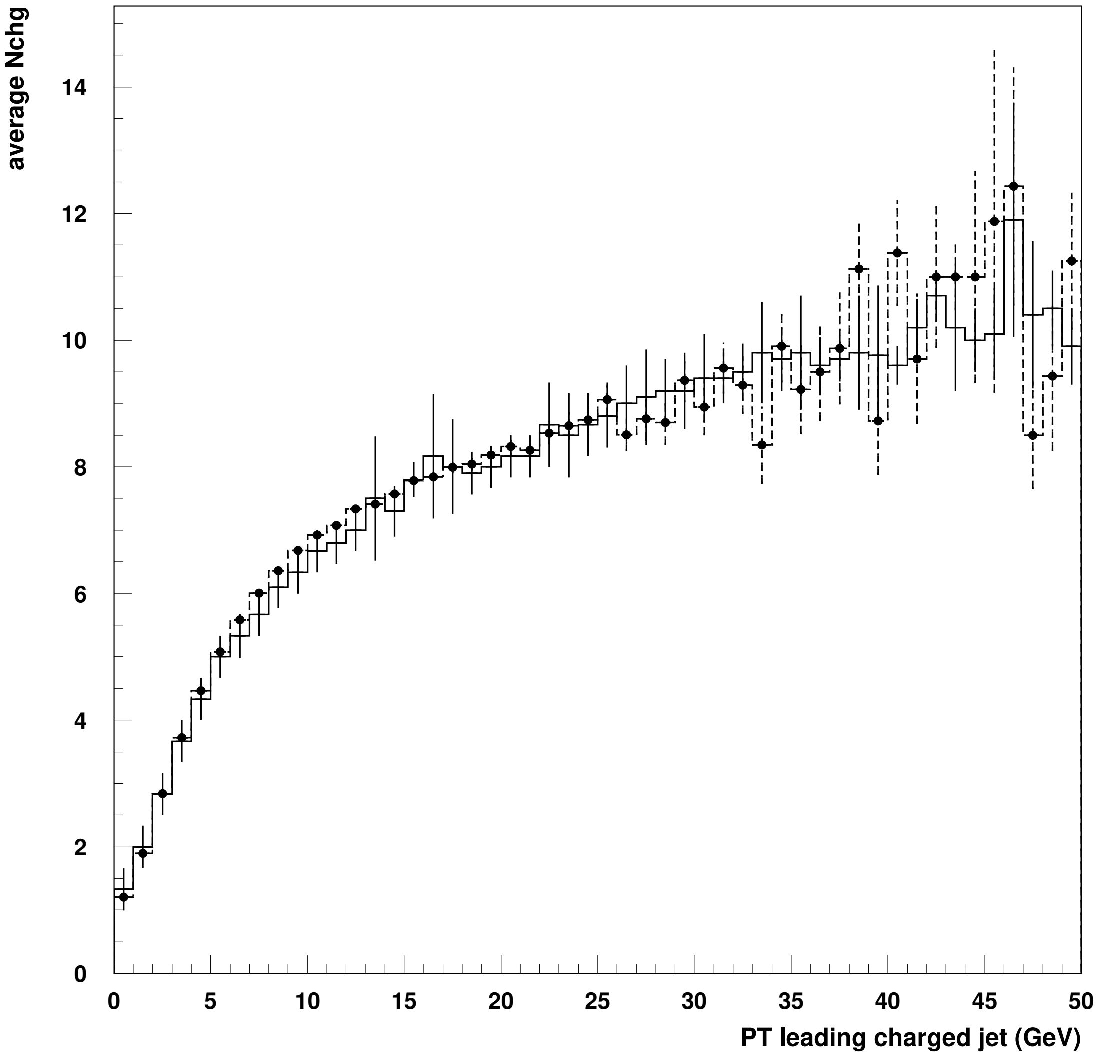

Figure 48: Plots shows the average number of charged particles (PT> 0.5 GeV and $|\eta|$<1) as function of PT(leading charged jet) for the toward region. HERWIG + Multiparton model (PDF=CTEQ4L, PTmin=3.0 GeV, proton radius decreased by a factor of 1.73), solid circles simulated data, solid line experimental data.

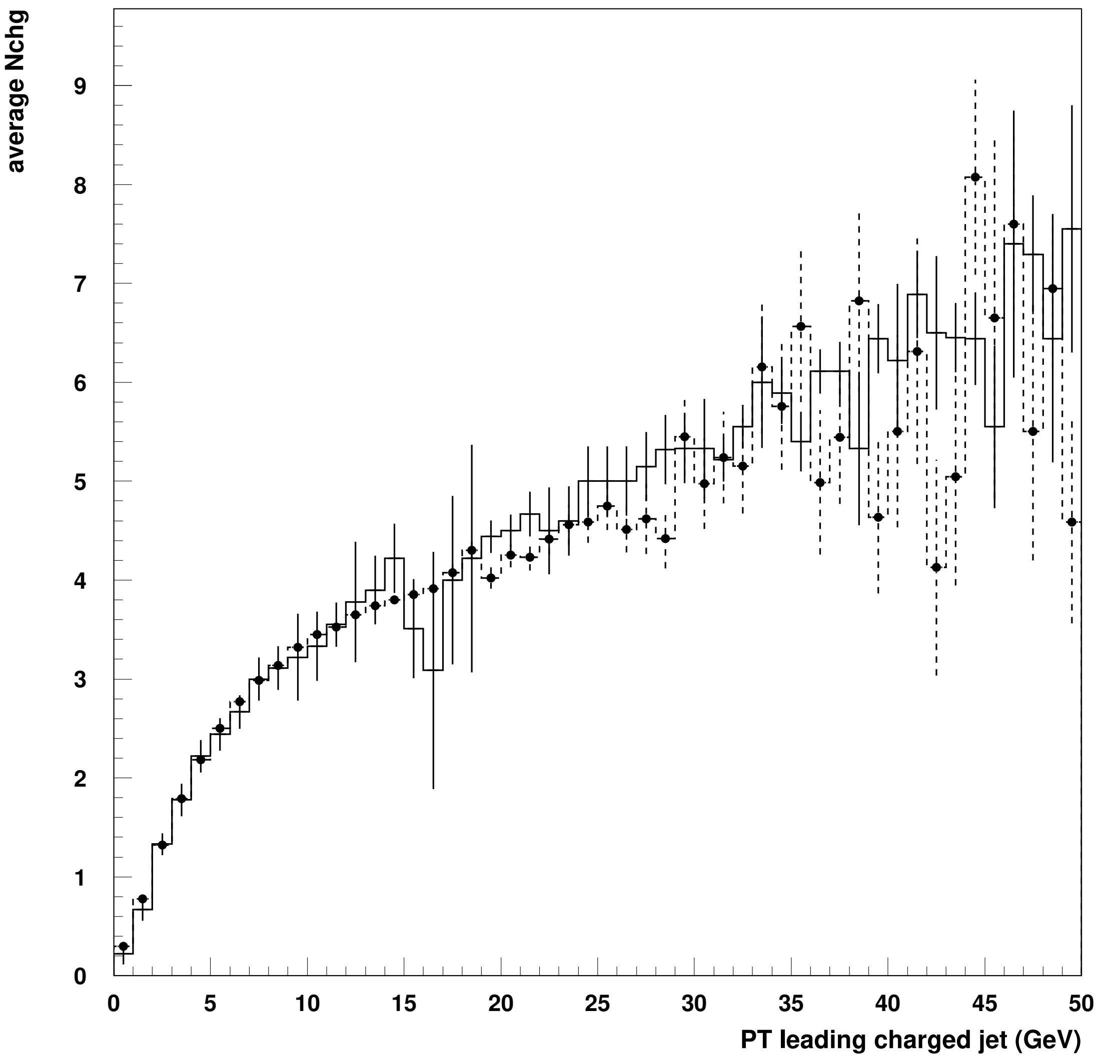

Figure 49: Plots shows the average number of charged particles (PT> 0.5 GeV and $|\eta|$<1) as function of PT(leading charged jet) for the away region. HERWIG + Multiparton model (PDF=CTEQ4L, PTmin=3.0 GeV, proton radius decreased by a factor of 1.73), solid circles simulated data, solid line experimental data.

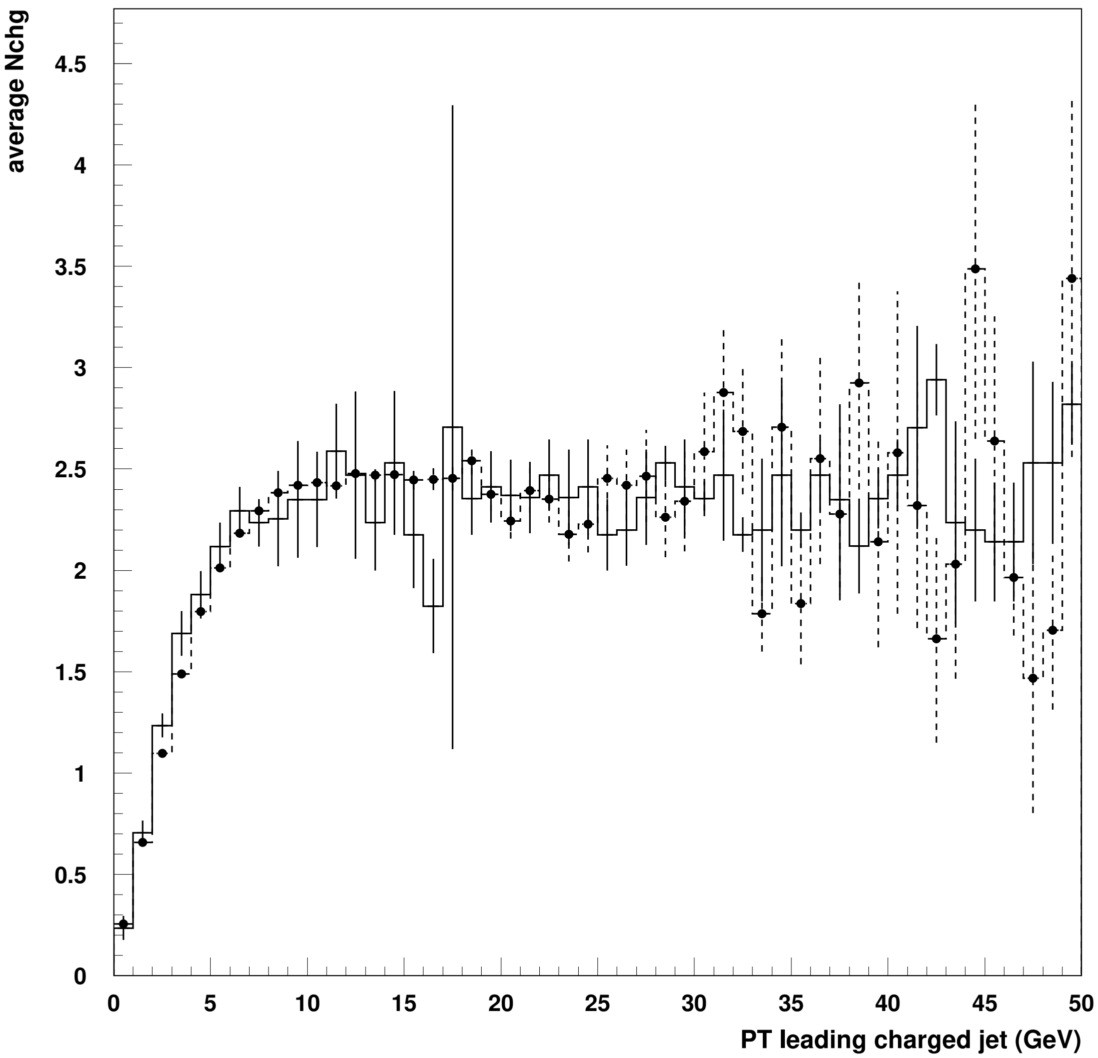

Figure 50: Plots shows the average number of charged particles (PT> 0.5 GeV and $|\eta|$<1) as function of PT(leading charged jet) for the transverse region. HERWIG + Multiparton model (PDF=CTEQ4L, PTmin=3.0 GeV, proton radius decreased by a factor of 1.73), solid circles simulated data, solid line experimental data.

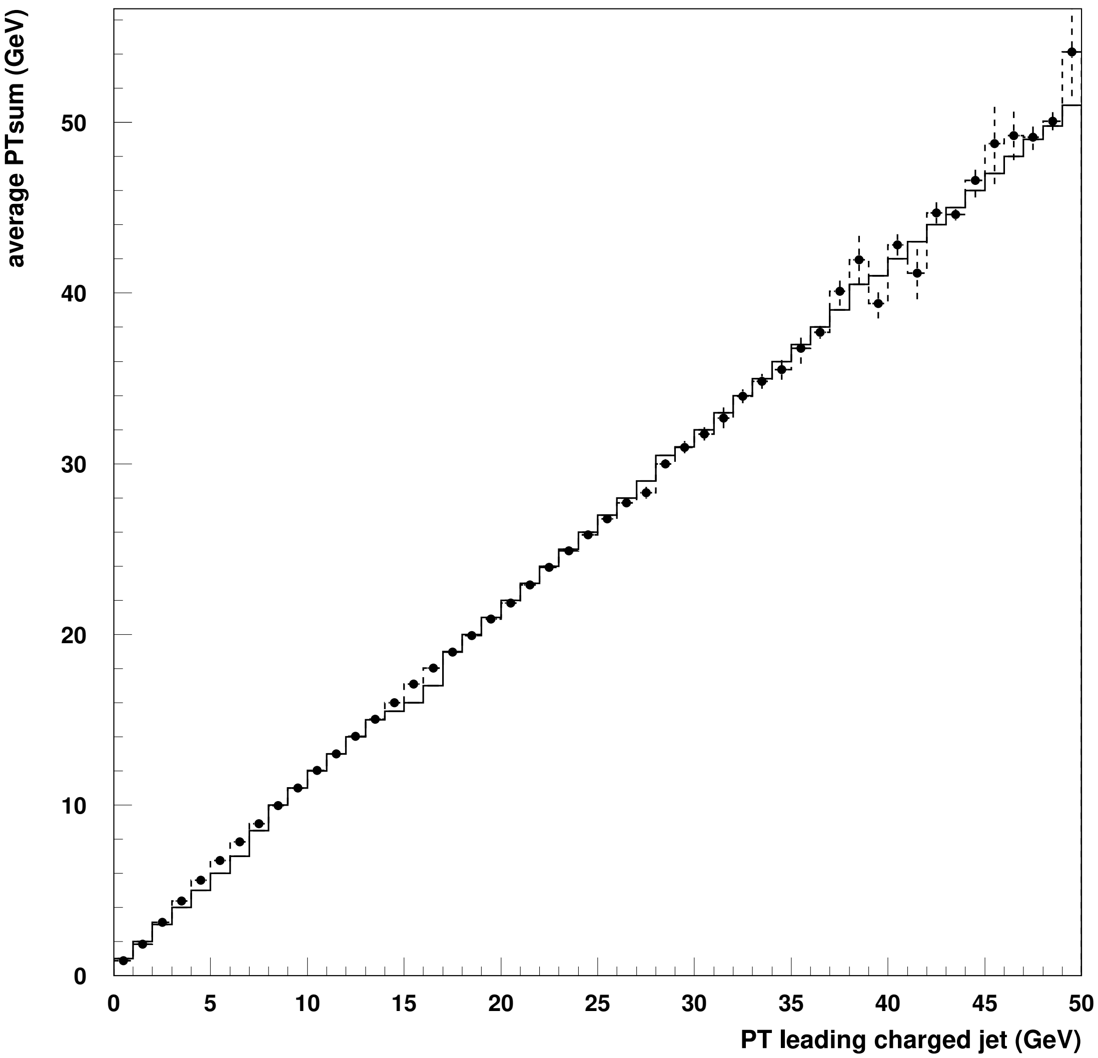

Figure 51: Plots shows the average PTsum of charged particles (PT> 0.5 GeV and $|\eta|<1$) as function of PT(leading charged jet) for the toward region. HERWIG + Multiparton model (PDF=CTEQ4L, PTmin=3.0 GeV, proton radius decreased by a factor of 1.73), solid circles simulated data, solid line experimental data.

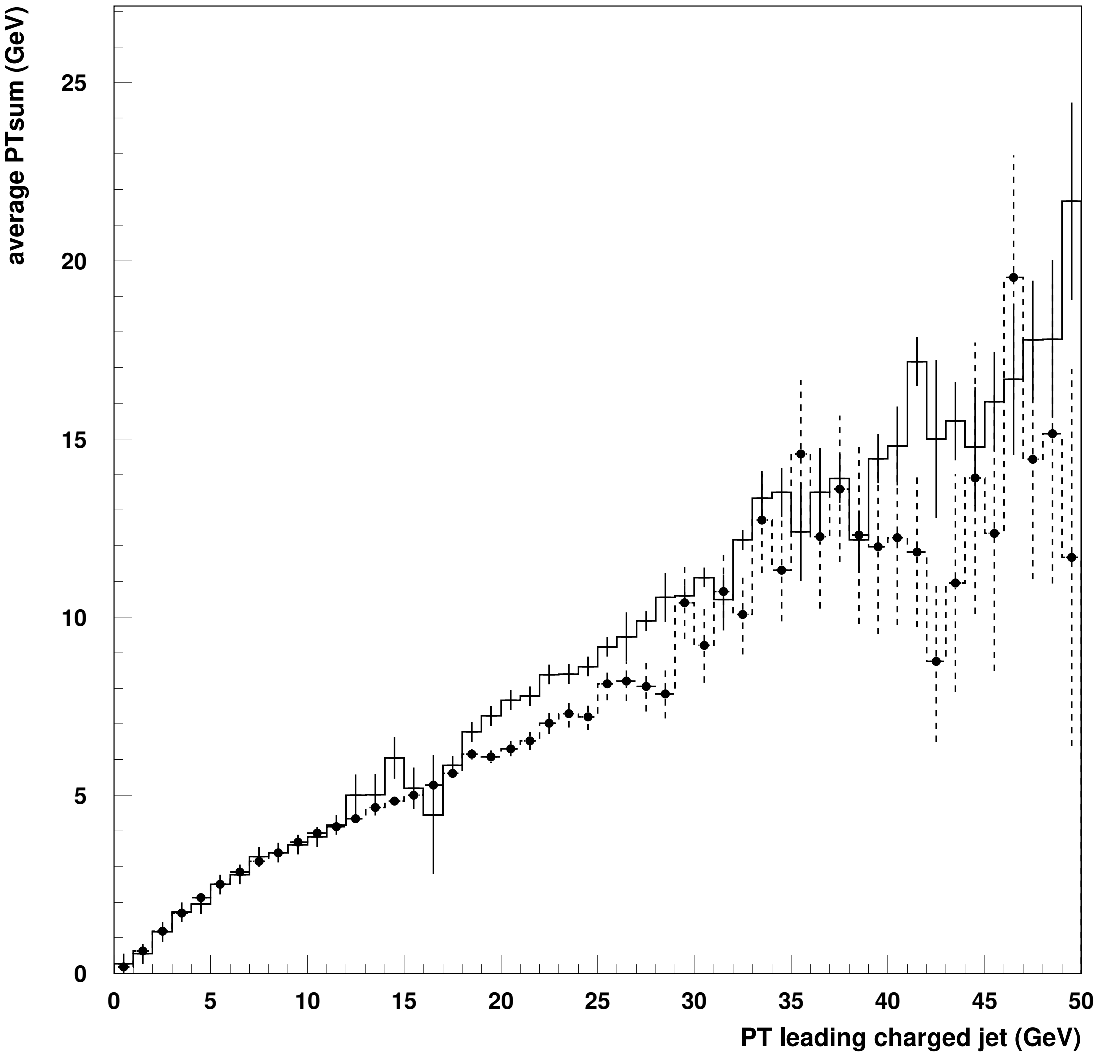

Figure 52: Plots shows the average PTsum of charged particles (PT> 0.5 GeV and $|\eta|$<1)as function of PT(leading charged jet) for the away region. HERWIG + Multiparton model (PDF=CTEQ4L, PTmin=3.0 GeV, proton radius decreased by a factor of 1.73), solid circles simulated data, solid line experimental data.

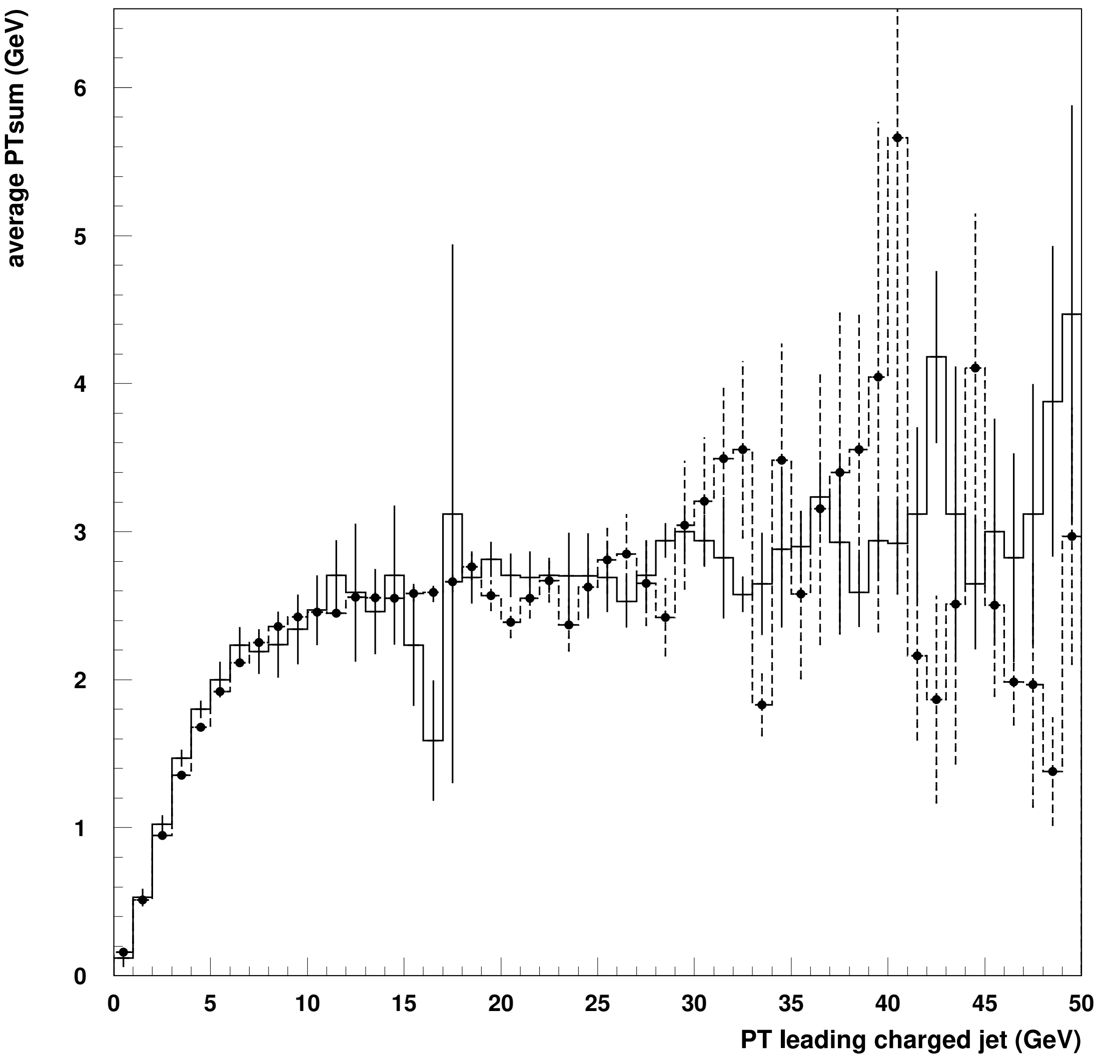

Figure 53: Plots shows the average PTsum of charged particles (PT> 0.5 GeV and $|\eta|<1$) as function of PT(leading charged jet) for the transverse region. HERWIG + Multiparton model (PDF=CTEQ4L, PTmin=3.0 GeV, proton radius decreased by a factor of 1.73), solid circles simulated data, solid line experimental data.

A The strong force and the Quantum-Chromo-Dynamics.

The theoretical and experimental study at high energies of both hadron-hadron, lepton-lepton and lepton-hadron interactions had lead to a description of properties of the strong force. The strong force is responsible for nuclear binding and the interaction between hadrons which are bound states of more fundamental particles called quarks obeying Fermi-Dirac statistics. A brief summary of QCD is presented below.

In quantum field theory known as Quantum Chromodynamics quarks are considered as point like objects with a new quantum number named "color" introduced to explain some bound states of quarks otherwise forbidden by Fermi statistics. This new quantum number can take three different values Red, Green and Blue for quarks and anti-Red, anti-Green and anti-Blue for antiquarks. The quanta of the color gauge field binding quarks together in hadrons and also nucleons into nuclei are called gluons. There is eight different bicolored states of gluons carrying color from one quark to the other. Quarks exist in 6 flavors up, down, charm, strange, top and bottom. While gluons (color field vector bosons) and quarks are colored, hadrons are "colorless" or "white". Because gluons carry theme self a color charge, they can directly interact with other gluons. QCD is called a “non-Abelian” theory because of the direct interaction of it’s field quanta. Both quark and gluons are considered as partons (i.e constituents of hadrons). The strong force exhibit two main properties known as **Asymptotic freedom** and **Confinement**. Both are related to the running of the coupling constant of the strong field α_s. The Asymptotic behavior is exhibited for interactions happening at the very close range (i.e below 1 Fermi) or otherwise at high four momenta exchange q^μ between particles where the coupling constant α_s is below unity and decreases further as the energy of interaction is increased. On the contrary as the range of interaction increases above 1 Fermi and the energy of interaction decreases below 1 GeV the coupling constant α_s increases above unity and the energy stored in the color field increases approximately linearly with the range, producing the second of the above mentioned properties known as the Confinement. The Confinement prevent quarks to be observed as free particles since the energy stored in the field for the range of interaction R$\geq$1 Fermi will be so large that it will favor new quarks being produced. These new quarks will pair together with the one being "stretched“ thus producing new bound states of quarks, only this new bound states, namely hadrons would be observed in the detectors. Because of the Asymptotic Freedom property at large transfered momentum q^μ the perturbative calculations in

QCD may be performed leading to finite results and definite predictions. However in the low energy regime of interaction around and below 1 GeV of transfered momentum the perturbative calculations can not be performed since $\alpha_s \geq 1$ and the interaction is considered as "soft" as opposite to the perturbative called "hard".

A.1 QCD Lagrangian (see Ref.[7])

The QCD is an asymptotically free field theory in four dimensions and only non-Abelian gauge theories exhibit such properties. The gauge group is the SU(3) and the generators of the group may be taken to be any 3^2 - 1 = 8 linearly independent traceless hermitian 3×3 matrices. The fundamental representation of SU(3) symmetry group is a triplet (which are the three color charges of quarks) presented in eq.1

$$R = \begin{pmatrix} 1 \\ 0 \\ 0 \end{pmatrix} G = \begin{pmatrix} 0 \\ 1 \\ 0 \end{pmatrix} B = \begin{pmatrix} 0 \\ 0 \\ 1 \end{pmatrix} \tag{30}$$

In this representation the generators are 3×3 matrices $\lambda^i/2$, with i = 1,....,8. The diagonal matrices are the one having the R, G, B as simultaneous eigenvectors. The λ^i matrices presented below are known as Gell-Mann matrices.

$$\lambda^1 = \begin{pmatrix} 0 & 1 & 0 \\ 1 & 0 & 0 \\ 0 & 0 & 0 \end{pmatrix} \lambda^2 = \begin{pmatrix} 0 & -i & 0 \\ i & 0 & 0 \\ 0 & 0 & 0 \end{pmatrix} \lambda^3 = \begin{pmatrix} 1 & 0 & 0 \\ 0 & -1 & 0 \\ 0 & 0 & 0 \end{pmatrix}$$

$$\lambda^4 = \begin{pmatrix} 0 & 0 & -i \\ 0 & 0 & 0 \\ i & 0 & 0 \end{pmatrix} \lambda^5 = \begin{pmatrix} 0 & 0 & -i \\ 0 & 0 & 0 \\ i & 0 & 0 \end{pmatrix}$$

$$\lambda^6 = \begin{pmatrix} 0 & 0 & 0 \\ 0 & 0 & 1 \\ 0 & 1 & 0 \end{pmatrix} \lambda^7 = \begin{pmatrix} 0 & 0 & 0 \\ 0 & 0 & -i \\ 0 & i & 0 \end{pmatrix} \lambda^8 = \begin{pmatrix} 1 & 0 & 0 \\ 0 & 1 & -i \\ 0 & 0 & -2 \end{pmatrix}$$

T_A=$\lambda_i/2$ are the generators of the color special unitary SU(3) group where A = 1,...8. The commutation relation between the color generators is given below :

$$[T^A, T^B] = if_{ABC} T_C \tag{31}$$

The f_{ABC} are real constants, called the structure constants of the group. They are fully antisymmetric under interchange of any pair of indices and the non vanishing values are permutations of : $f_{123} = 1$, $f_{458} = f_{678} = \sqrt{3}/2$,

$f_{147} = f_{165} = f_{246} = f_{257} = f_{345} = f_{376} = \frac{1}{2}$ By convention the normalization of the SU(N) matrices is chosen to be

$$Tr\,T_A T_B = T_R \delta_{AB},\, T_R = 1/2. \tag{32}$$

With this convention the color matrices obey the following relations:

$$\sum_A T^A_{ab} T^A_{bc} = C_F \delta_{ac}, C_F = \frac{N^2-1}{2N} \tag{33}$$

where the a,b,c indices runs over quark flavors.

$$TrT^C T^D = \sum_{A,B} f^{ABC} f^{ABD} = C_A \delta^{CD}, C_A = N. \tag{34}$$

Thus for SU(3)

$$C_F = \frac{4}{3}, C_A = 3. \tag{35}$$

The expression of the Lagrangian density Ref.[7] invariant under the SU(3) local gauge phase transformation is given in eq.36[2].

$$\mathcal{L}_{classical} + \mathcal{L}_{gauge-fixing} + \mathcal{L}_{ghost}. \tag{36}$$

where

$$\mathcal{L}_{classical} = -\frac{1}{4} G^A_{\mu\nu} G^{\mu\nu}_A + \sum_{flaviours} \overline{q}_a (i\gamma^\mu D_\mu - m)_{ab} q_b \tag{37}$$

and

$$G^A_{\mu\nu} = [\partial_\mu G^A_\nu - \partial_\nu G^A_\mu - g f^{ABC} G^B_\mu G^C_\nu] \tag{38}$$

where G^A_μ are eight color gauge fields representing 8 bicolored gluons : R$\overline{G}$, R$\overline{B}$,G$\overline{R}$,G$\overline{B}$,B$\overline{R}$,B$\overline{G}$,$\sqrt{\frac{1}{2}}$(R$\overline{R}$ - G$\overline{G}$),$\sqrt{\frac{1}{6}}$(R$\overline{R}$ + G$\overline{G}$ - 2B$\overline{B}$). The first term in eq.37 is called the kinetic term and it is gauge invariant. The inclusion of the third term in the gauge color field (see eq.38) insures the gauge invariance of the QCD Lagrangian under local color phase transformation. The third non-Abelian term in eq.38 on the right give rise to triplet and quadratic gluon self interaction-term and to the property of the asymptotic freedom, g is the coupling constant which determines the strength of the interaction between colored quanta. On the right of eq.37 there is no mass term for the gluons since such term will not be gauge invariant Ref.[7]. Only the mass term for the quarks exist. D_μ is defined in eq.49.

[2]The invariance of the free Lagrangian under the local SU(3) phase transformation is presented in more detail in appendix.D.

$$\mathcal{L}_{gauge-fixing} = -\frac{1}{2\lambda}(\partial^{\alpha} G_{\mu}^{A})^{2} \quad (39)$$

Without the gauge fixing term it would be impossible to define the propagator for the gluon field without making a choice of the gauge. The eq.39 fixes the class of covariant gauges with gauge parameter λ. In a non-Abelian QCD theory this gauge fixing term must be supplemented by a ghost Lagrangian which expression is given in eq.40 Ref.[7].

$$\mathcal{L}_{ghost} = \partial_{\alpha}\eta^{A^{\dagger}}(D_{AB}^{\alpha}\eta^{\beta}). \quad (40)$$

The η^{A} is a complex scalar field which obeys Fermi statistics. The ghost fields cancel unphysical degrees of freedom which would otherwise propagate in covariant gauges.

B Hard scattering process between two hadrons(see Ref.[7])

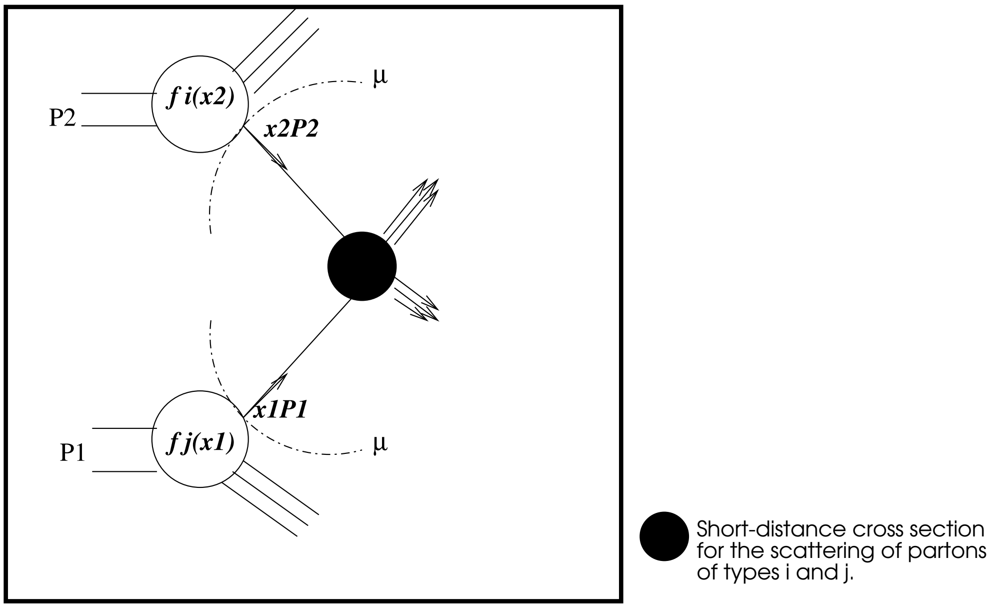

Figure 54: The parton model description of a hard scattering process

In the Fig.54 is pictured a hard scattering process between two hadrons. The scattering is the outcome of interaction between the quarks and gluons (partons), constituents of the incoming hadrons. The cross section for a hard scattering process between two hadrons with four-momenta P_1 and P_2 is given in eq.41. Ref.[7]

$$\sigma(P_1, P_2) = \sum_{i,j} dx_1 dx_2 f_i(x_1, \mu) f_j(x_2, \mu) \hat{\sigma}_{ij}(p_1, p_2, \alpha_s(\mu^2), Q^2/\mu^2) \tag{41}$$

The coupling $\alpha_s(\mu^2)$ is the value of the strong coupling at the renormalization scale μ^2 . The $\alpha_s(Q^2)$ (where Q^2 is the typical hard interaction scale) running coupling is defined in eq.42.

$$\alpha_s(Q^2) = \frac{\alpha_s(\mu^2)}{1 + \frac{\alpha_s(\mu^2)}{12\pi}(33 - 2n_f)log(Q^2/\mu^2)} \tag{42}$$

which also can be written as

$$\alpha_s = \frac{g_s^2}{4\pi} \tag{43}$$

As mentioned in Sec.A $\alpha_s(Q^2)$ decreases with increasing Q^2 and therefore becomes small for short distance interactions and thus present the properties of asymptotic freedom. By defining Λ^2 as the scale at which for sufficiently low Q^2 the coupling becomes large

$$\Lambda = \mu^2 exp\left[\frac{-12\pi}{(33 - 2n_f)\alpha_s(\mu^2)}\right] \tag{44}$$

$\alpha_s(Q^2)$ can be expressed as function of Λ thus we obtain for $\alpha_s(Q^2)$ the following expression

$$\alpha_s(Q^2) = \frac{12\pi}{(33 - 2n_f)log(Q^2/\Lambda^2)} \tag{45}$$

The momenta of the partons participating in the hard process are $x_1 P_1$ and $x_2 P_2$. $Q(\approx E_T^{jet})$ is the characteristic scale of the hard scttering. The momenta of partons (inside hadrons) are distributed according to the parton distribution functions $f_i(x_1, \mu)$ and $f_i(x_1, \mu)$ defined at the factorisation scale μ. The short distance cross section for the scattering of partons of types i and j is denoted by $\hat{\sigma}$. Since the coupling is small at high energy the short-distance cross section can be calculated as a perturbation series in the running coupling α_s. The factorisation scale μ in eq.41 and eq.42 is an arbitrary parameter. It is the scale which separates the long-distance and short-distance physics. A parton emitted with a transvers momentum less then the scale μ, is considered as part of the hadron structure and is absorbed into the parton distribution. A parton emited with a transvers momentum superior to μ is part of the short-distance cross section. The scale μ should be chosen to be of the order of the hard scale Q which characterizes the parton-parton interaction.

C Jet physics and jet cross sections (see Ref.[7])

When the energy of scattering of two incoming partons is high enough to produce two outgoing partons with high enough p_T then this outgoing partons will be observed as jets of particles. For a 2→2 parton scattering process the differential cross section at the parton level for two jets is given bellow in eq.46.

$$d^6\hat{\sigma} = \frac{1}{2\hat{s}}\frac{1}{16\pi^2}\overline{\sum}\|\mathcal{M}\|^2\delta^4(p_1+p_2-p_3-p_4)\frac{d^3p_3}{E_3}\frac{d^3p_4}{E_4} \tag{46}$$

where $\overline{\sum}$ denotes the average and the sum over the initial-state and final-state spins and colors respectively; $\hat{s} = (p_1+p_2)^2$. To obtain the single-jet inclusive differential cross section the eq.46 may be integrated over the momentum of one of the jets and then convoluted with the parton distribution functions.

D Non-Abelian Gauge Invariance (see Ref.[18])

The free Lagrangian in QCD is given in eq.47.

$$\mathcal{L}_0 = \overline{q_j}(i\gamma^\mu\partial_\mu - m)q_j \tag{47}$$

where q_1,q_2,q_3 are the three color fields. In eq.47 just one quark flavor is considered. $\mathcal{L}_0$ is required to be invariant under the local phase transformation given in eq.48.

$$q(x) \rightarrow Uq(x) \equiv exp^{i\alpha_A(x)T_A}q(x) \tag{48}$$

Where U in eq.48 is a 3×3 unitary matrix The expression for the covariant derivative which transforms under the local phase transformation like $q(x)$ is given in eq.49.

$$D_\mu = \partial_\mu + igT_AG^A_\mu \tag{49}$$

Replacing the $\partial_\mu \rightarrow D_\mu$ in the Lagrangian eq.47, a new expression for the Lagrangian is obtained eq.50

$$\mathcal{L} = \overline{q_j}(i\gamma^\mu\partial_\mu - m)q_j - g(\overline{q_j}\gamma^\mu T_A q)G^A_\mu \tag{50}$$

For the Lagrangian to be invariant then G_μ^A is required to have the following expression given in eq.51.

$$G_\mu^A \rightarrow G_\mu^A - \frac{1}{g}\partial_\mu \alpha_A - f_{ABC}\alpha_A G_\mu^C. \tag{51}$$

To the Lagrangian in eq.51 is then added an invariant kinetic energy term for each of the G_μ^A color fields, this complete the expression for the gauge invariant QCD Lagrangian given in eq.52.

$$\mathcal{L} = \overline{q_j}(i\gamma^\mu \partial_\mu - m)q_j - g(\overline{q_j}\gamma^\mu T_A q)G_\mu^A - \frac{1}{4}G_{\mu\nu}^A G_A^{\mu\nu} \tag{52}$$

E Collider Luminosities (see Ref.[7])

At a particle collider the rate N at which events of a given type occur is determined by the luminosity of the machine, L, multiplied by the cross section for the relevant scattering process, σ:

$$N = L\sigma \tag{53}$$

The Luminosity of the collider in a p$\overline{p}$ collision is defined as :

$$L = \frac{f}{\pi}\frac{N_p N_{\overline{p}}}{n_b}\frac{\gamma}{\sqrt{\beta_x \beta_y E_x E_y}} \tag{54}$$

where f is the revolution frequency, n_b is the number of bunches and $\gamma =$ E/m is the normal relativistic factor, E_x and E_y are the transverse emittance of the beams, β_x and β_y are the betatron oscillations of the beams. We notice that the parton luminosity factor is not the same as the hadron luminosity since the parton luminosity is determined by the parton distribution functions (see eq.41). Since the parton only carry a fraction of their parent hadron's momentum, the available center-of-mass-energy-squared of the parton parton collision, $\hat{s}$, is less then the overall hadron-hadron collision energy, s, by a factor of $x_1 x_2$ (see eq.41).

References

[1] J. M. Butterworth, J. R. Forshaw and M. H. Seymour, [hep-ph/9601371].

[2] B. Abbott *et al.* [D0 Collaboration], Phys. Rev. Lett. **82** (1999) 2451 [hep-ex/9807018].

[3] B. Abbott *et al.* [D0 Collaboration], Phys. Rev. Lett. **82** (1999) 2457 [hep-ex/9807014].

[4] T. Affolder *et al.* [CDF Collaboration], Phys. Rev. **D61** (2000) 091101 [hep-ex/9912022].

[5] G.Marchesini and B.R.Webber,Nucl.Phys.B328(1984) 1,Nucl.Phys.B310(1988)461.

[6] M.H. Seymour, Jet Shapes in Hadron Collisions: Higher Orders, Resummation and Hadronisation. [hep-ph/9707338].

[7] R.K.Ellis,W.J.Stirling and B.R.Weber, QCD and Collider Physics.

[8] M.H.Seymour,PhD thesis.

[9] J.Huth *et al.*, in proceedings of Research Directions for the Decade, Snowmass 1990, Editor E.L.Berger,(World Scientific,Singapour,1992).

[10] T.Sjöstrand,Phys.Lett.157B (1985) 321.

[11] F.Abe *et al.*,Phys.ReV.**45**,1448(1992)

[12] B. Abbott *et al.* [D0 Collaboration], Nucl. Instrum. Meth. **A424** (1999) 352 [hep-ex/9805009].

[13] B. Abbott, M. Bhattacharjee, D. Elvira, F. Nang and H. Weerts [D0 Collaboration], FERMILAB-PUB-97-242-E.

[14] The Underlying Event in Hard Scattering Processes. Rick Field and David Stuart "Contribution to the Run 2 Workshop on QCD and Weak Boson Physics" February 1, 2000.

[15] M.Glück,E.Reya and A.Vogt,Z.Phys.C53(1992) 127;
M.Glück and E.Reya,Dortmund DO-TH 93/27 (1993);
M.Glück,E.Reya and A.Vogt,Phys. Lett B306 (1993) 391;
M.Glück,E.Reya and A.Vogt,Z. Phys. C67 (1995) 433.

[16] HERWIG v5.9, hep-ph/9912396; G. Marchesini, B.R. Webber, G. Abbiendi, I.G. Knowles, M.H. Seymour and L. Stanco, Computer Phys. Commun. 67 (1992) 465.

[17] Zeit. für Phys. C72 (1996) 637-646

[18] Quarks and Leptons : Introductory Course in Modern Particle Physics, Francis Halzen, Alan D.Martin.